Measurement of the *CP*-violating phase ϕ_s in $B_s^0 \rightarrow J/\psi\phi$ decays in ATLAS at 13 TeV

The ATLAS Collaboration

A measurement of the $B_s^0 \rightarrow J/\psi\phi$ decay parameters using $80.5\,\mathrm{fb}^{-1}$ of integrated luminosity collected with the ATLAS detector from 13 TeV proton–proton collisions at the LHC is presented. The measured parameters include the *CP*-violating phase ϕ_s, the width difference $\Delta\Gamma_s$ between the B_s^0 meson mass eigenstates and the average decay width Γ_s. The values measured for the physical parameters are combined with those from $19.2\,\mathrm{fb}^{-1}$ of 7 TeV and 8 TeV data, leading to the following:

$$
\begin{aligned}
\phi_s &= -0.087 \pm 0.036 \ \text{(stat.)} \pm 0.021 \ \text{(syst.) rad} \\
\Delta\Gamma_s &= 0.0657 \pm 0.0043 \ \text{(stat.)} \pm 0.0037 \ \text{(syst.) ps}^{-1} \\
\Gamma_s &= 0.6703 \pm 0.0014 \ \text{(stat.)} \pm 0.0018 \ \text{(syst.) ps}^{-1}
\end{aligned}
$$

Results for ϕ_s and $\Delta\Gamma_s$ are also presented as 68% confidence level contours in the ϕ_s–$\Delta\Gamma_s$ plane. Furthermore the transversity amplitudes and corresponding strong phases are measured. ϕ_s and $\Delta\Gamma_s$ measurements are in agreement with the Standard Model predictions.

1 Introduction

In the presence of new physics (NP) phenomena, sources of *CP* violation in *b*-hadron decays can arise in addition to those predicted by the Standard Model (SM) [1]. In the $B_s^0 \to J/\psi\phi$ decay, *CP* violation occurs due to interference between a direct decay and a decay with B_s^0–$\bar{B}_s^0$ mixing. The oscillation frequency of B_s^0 meson mixing is characterised by the mass difference, Δm_s, of the heavy (B_H) and light (B_L) mass eigenstates. The *CP*-violating phase ϕ_s is defined as the weak phase difference between the B_s^0–$\bar{B}_s^0$ mixing amplitude and the $b \to c\bar{c}s$ decay amplitude. In the SM the phase ϕ_s is small and is related to the Cabibbo–Kobayashi–Maskawa (CKM) quark mixing matrix elements via the relation $\phi_s \simeq -2\beta_s$, with $\beta_s = \arg[-(V_{ts}V_{tb}^*)/(V_{cs}V_{cb}^*)]$. By combining beauty and kaon physics observables, and assuming no NP contributions to B_s^0 mixing and decays, a value of $-2\beta_s = -0.03696^{+0.00072}_{-0.00082}$ rad was predicted by the CKMFitter group [2] and $-2\beta_s = -0.03700 \pm 0.00104$ rad according to the UTfit Collaboration [3]. While large NP enhancements of the mixing amplitude have been excluded by the precise measurement of the oscillation frequency [4], the NP couplings involved in the mixing may still increase the size of the observed *CP* violation by enhancing the mixing phase ϕ_s with respect to the SM value.

Other physical quantities involved in B_s^0–$\bar{B}_s^0$ mixing are the decay width $\Gamma_s = (\Gamma_L + \Gamma_H)/2$ and the width difference $\Delta\Gamma_s = \Gamma_L - \Gamma_H$, where Γ_L and Γ_H are the decay widths of the light and heavy mass eigenstates, respectively. The latest predictions for the width difference in the SM are $\Delta\Gamma_s = 0.091 \pm 0.013$ ps^{-1} [5] and $\Delta\Gamma_s = 0.092 \pm 0.014$ ps^{-1} [6]. A potential NP enhancement of ϕ_s would also decrease the size of $\Delta\Gamma_s$, but it is not expected to be affected as significantly as ϕ_s [7]. Nevertheless, extracting $\Delta\Gamma_s$ from the data is an important test of theoretical predictions [7].

Theory predictions have been made for the lifetime ratios $\tau(B_s^0)/\tau(B_d)$ and $\tau(B_s^0)/\tau(B^+)$, with the latest update Ref. [8]. The lifetime $\tau(B_s^0)$ has not been calculated in theory yet at a precision comparable with those obtained by experiments. The current world combined value of the decay width, Γ_s, obtained from experimental results is $\Gamma_s = 0.6600 \pm 0.0016$ ps^{-1} [9].

The analysis of the time evolution of the $B_s^0 \to J/\psi\phi$ decay provides the most precise determination of ϕ_s and $\Delta\Gamma_s$. Previous measurements of these quantities have been reported by the D0, CDF, LHCb, ATLAS and CMS Collaborations [10–17]. Additional improvements in measuring ϕ_s from $B_s^0 \to \psi(2S)\phi$, $B_s^0 \to D_s^+D_s^-$ and $B_s^0 \to J/\psi\pi^+\pi^-$ decays have been achieved by the LHCb Collaboration [18–21].

The analysis presented here introduces a measurement of the $B_s^0 \to J/\psi\phi$ decay parameters using 80.5 fb^{-1} of the LHC proton–proton (pp) data collected by the ATLAS detector during 2015–2017, at a centre-of-mass energy, $\sqrt{s}$, equal to 13 TeV. The analysis closely follows a previous ATLAS measurement [13] that was performed using 19.2 fb^{-1} of the data collected at 7 TeV and 8 TeV, and introduces more precise signal and background models.

2 ATLAS detector and Monte Carlo simulation

The ATLAS detector[1] consists of three main components: an inner detector (ID) tracking system immersed in a 2 T axial magnetic field, electromagnetic and hadronic calorimeters, and a muon spectrometer (MS).

---

[1] ATLAS uses a right-handed coordinate system with its origin at the nominal interaction point. The *z*-axis is along the beam pipe, the *x*-axis points to the centre of the LHC ring and the *y*-axis points upward. Cylindrical coordinates (r, ϕ) are used in the transverse plane, *r* being the distance from the origin and ϕ being the azimuthal angle around the beam pipe. The pseudorapidity η is defined as $\eta = -\ln[\tan(\theta/2)]$ where θ is the polar angle.

The inner tracking detector covers the pseudorapidity range $|\eta| < 2.5$, and consists of silicon pixel, silicon microstrip, and transition radiation tracking detectors. The ID is surrounded by a high-granularity liquid-argon (LAr) sampling electromagnetic calorimeter. A steel/scintillator tile calorimeter provides hadronic coverage in the central rapidity range. The endcap and forward regions are equipped with LAr calorimeters for electromagnetic and hadronic measurements. The MS surrounds the calorimeters and provides a system of tracking chambers and detectors for triggering. A full description can be found in Refs. [22–24].

The data were collected during periods with different instantaneous luminosity, so several triggers were used in the analysis. All triggers were based on the identification of a $J/\psi \to \mu^+\mu^-$ decay, with transverse momentum (p_T) thresholds of either 4 GeV or 6 GeV for the muons. Data quality requirements are imposed on the data, notably on the performance of the MS, ID and calorimeter systems. The measurement uses 80.5 fb^{-1} of pp collision data. The uncertainty in the combined 2015–2017 integrated luminosity is 2.0% [25], obtained using the LUCID-2 detector [26] for the primary luminosity measurements.

To study the detector response, estimate backgrounds, and model systematic effects, 100M Monte Carlo (MC) simulated $B_s^0 \to J/\psi\phi$ events were generated using Pythia 8.210 [27] tuned with ATLAS data, using the A14 set of parameter values [28] together with the CTEQ6L1 set of parton distribution functions [29]. The detector response was simulated using the ATLAS simulation framework based on Geant4 [30, 31]. In order to account for the varying number of proton–proton interactions per bunch crossing (pile-up) and trigger configurations during data-taking, the MC events were weighted to reproduce the same pile-up and trigger conditions as in the data. Additionally, background samples of both the exclusive ($B_d^0 \to J/\psi K^{0*}$ and $\Lambda_b \to J/\psi pK^-$) and inclusive ($b\bar{b} \to J/\psi X$ and $pp \to J/\psi X$) decays were simulated, using the same simulation tools as in the case of the signal events. For validation studies related to flavour tagging, detailed in Section 4, events with $B^\pm \to J/\psi K^\pm$ exclusive decays were also simulated.

3 Reconstruction and candidate selection

The reconstruction and candidate selection for the decay $B_s^0 \to J/\psi(\mu^+\mu^-)\phi(K^+K^-)$ is described here. Events must pass the trigger selections described in Section 2. In addition, each event must contain at least one reconstructed primary vertex, formed from at least four ID tracks, and at least one pair of oppositely charged muon candidates that are reconstructed using information from the MS and the ID. The muons used in the analysis are required to meet the *Tight*[2] or *Low-p_T*[3] working point identification criteria. The muon track parameters are determined from the ID measurement alone, since the precision of the measured track parameters is dominated by the ID track reconstruction in the p_T range of interest for this analysis. Pairs of oppositely charged muon tracks are re-fitted to a common vertex and the pair is accepted if the quality of the fit meets the requirement $\chi^2/\text{ndof} < 10$. In order to account for varying mass resolution in different parts of the detector, the J/ψ candidates are divided into three subsets according to the pseudorapidity η of the muons. In the first subset, both muons have $|\eta| < 1.05$, where the values $\eta = \pm 1.05$ correspond to the edges of the barrel part of the MS. In the second subset, one muon has $1.05 < |\eta| < 2.5$ and the

---

[2] Tight muon reconstruction is optimised to maximise the purity of muons at the cost of some efficiency, requiring combined muons with hits in at least two stations of the MS and additional criteria, described in Ref. [32].

[3] This working point is optimised to provide good muon reconstruction efficiency down to a p_T of ≈ 3 GeV, while controlling the fake-muon rate. It allows ≥ 1 (≥ 2) MDT station tracks up to $|\eta| < 1.3$ ($1.3 < |\eta| < 1.55$) for candidates reconstructed by algorithms utilising inside-out combined reconstruction [32]. Additional cuts on the number of precision stations and on variables very sensitive to the decays in flight of hadrons are also applied to suppress fake muons.

other muon $|\eta| < 1.05$. The third subset contains candidates where both muons have $1.05 < |\eta| < 2.5$. A maximum likelihood fit is used to extract the J/ψ mass and the corresponding mass resolution for these three subsets, and in each case the signal region is defined symmetrically around the fitted mass, so as to retain 99.7% of the J/ψ candidates identified in the fits.

The candidates for the decay $\phi \to K^+K^-$ are reconstructed from all pairs of oppositely charged tracks, with $p_T > 1$ GeV and $|\eta| < 2.5$, that are not identified as muons. Candidate events for $B_s^0 \to J/\psi(\mu^+\mu^-)\phi(K^+K^-)$ decays are selected by fitting the tracks for each combination of $J/\psi \to \mu^+\mu^-$ and $\phi \to K^+K^-$ to a common vertex. The fit is also constrained by fixing the invariant mass calculated from the two muon tracks to the J/ψ mass [33]. A quadruplet of tracks is accepted for further analysis if the vertex fit has $\chi^2/\text{ndof} < 3$. For the $\phi \to K^+K^-$ candidate, the invariant mass of the track pairs (using a charged kaon mass hypothesis) must fall within the interval 1.0085 GeV $< m(K^+K^-) < 1.0305$ GeV. The interval, chosen using MC simulation, is selected to retain 98% of true $\phi \to K^+K^-$ decays. The B_s^0 candidate with the lowest χ^2/ndof is selected in events where more than one candidate passes all selections. In total, $2\,977\,526$ B_s^0 candidates are collected within the mass range of 5.150–5.650 GeV. This range is chosen to give enough background events in the sidebands of the mass distributions to allow precise determination of the properties of the background events.

The mean number of interactions per bunch crossing is 30, necessitating a choice of the best candidate for the primary vertex at which the B_s^0 meson is produced. Primary vertex positions are recalculated after removing any tracks used in the B_s^0 meson reconstruction. The variable used to select the best candidate for the primary vertex is the three-dimensional impact parameter, a_0, which is calculated as the minimum distance between each primary vertex candidate and the line extrapolated from the reconstructed B_s^0 meson vertex in the direction of the B_s^0 momentum. The chosen primary vertex is the one with the smallest a_0. A simulated dataset is used to estimate the fraction of B_s^0 candidates where the incorrect production vertex is selected (12%) and demostrates that the mis-selection of reconstructed primary vertex does not bias the reconstructed proper decay time.

For each B_s^0 meson candidate the proper decay time t is estimated using:

$$t = \frac{L_{xy}\, m_B}{p_{T_B}},$$

where p_{T_B} is the reconstructed transverse momentum of the B_s^0 meson candidate and m_B denotes the mass of the B_s^0 meson, taken from Ref. [33]. The transverse decay length, L_{xy}, is the displacement in the transverse plane of the B_s^0 meson decay vertex relative to the primary vertex, projected onto the direction of the B_s^0 transverse momentum.

4 Flavour tagging

To identify, or *tag*, the flavour of a neutral B meson at the point of production, information is extracted using the decay of the other (or *opposite*) b-hadron that is produced from the pair production of b and $\bar{b}$ quarks. This method is called opposite-side tagging (OST).

The OST algorithms each define a discriminating variable, based on charge information, which is sensitive to the flavour (i.e. b- or $\bar{b}$-quark) of the opposite-side b-hadron. The algorithms thus provide a probability that a signal B meson in a given event is produced in a given flavour. The calibration of the OST algorithms proceeds using data containing $B^\pm \to J/\psi K^\pm$ candidate decays, where the charge of the kaon determines

the flavour of the B meson, providing a self-tagging sample of events. These OST algorithms are calibrated as a function of the discriminating variable, using yields of signal $B^{\pm}$ mesons extracted from fits to the data. Once calibrated, the OST algorithms are applied to $B_s^0 \to J/\psi(\mu^+\mu^-)\phi(K^+K^-)$ candidate events to provide a probability that each candidate was produced in a B_s^0 or $\bar{B}_s^0$ meson state, which is used in the maximum likelihood fit (described in Section 5). This approach assumes invariance of the OST algorithm with respect to the specific signal b-hadron type (i.e $B^{\pm}$ meson or B_s^0 meson), which is tested and the difference is considered as a systematic uncertainty.

4.1 $B^{\pm} \to J/\psi K^{\pm}$ event selection

Candidate $B^{\pm} \to J/\psi K^{\pm}$ decays are identified in a series of steps. First, J/ψ candidates are selected from oppositely charged muon pairs forming a good vertex, as described in Section 3. Each muon is required to have $p_T > 4$ GeV and $|\eta| < 2.5$. Dimuon candidates with invariant mass $2.8 < m(\mu^+\mu^-) < 3.4$ GeV, as determined from the re-fitted track parameters of the vertex, are retained for further analysis. To form the $B^{\pm}$ candidate, an additional track is required, which is not identified as an electron or muon. The track is assigned the charged-kaon mass hypothesis and combined with the dimuon candidate using a vertex fit, performed with the mass of the dimuon pair constrained to the J/ψ mass. Prompt background contributions are suppressed by a requirement on the proper decay time of the $B^{\pm}$ candidate of $t > 0.2$ ps.

The tagging probabilities are determined from B^+ and B^- signal events. These signal yields are derived from fits to the invariant mass distribution, $m(J/\psi K^{\pm})$, and performed in intervals of the discriminating variables. To describe the $B^{\pm} \to J/\psi K^{\pm}$ signal, two Gaussian functions with a common mean are used. An exponential function is used to describe the combinatorial background and a hyperbolic tangent function to parameterise the low-mass contribution from incorrectly or partially reconstructed b-hadron decays. A Gaussian function is used to describe the $B^{\pm} \to J/\psi \pi^{\pm}$ contribution, with fixed parameters taken from simulation except for the normalisation, which is a free parameter. A fit to the overall mass distribution is used to define the shapes of signal and backgrounds. Subsequent fits are performed in the intervals of the tagging discriminating variables, separately for B^+ and B^- candidate events, with the normalisations and also the slope of the exponential function left free. The B^+ and B^- signal yields are extracted from these fits. Figure 1 shows the invariant mass distribution of $B^{\pm}$ candidates overlaid with a fit to all selected candidates, and including the individual fit components for the signal and backgrounds.

4.2 Flavour tagging methods

The flavour of the signal B meson at the point of production is inferred using several methods, which differ in their efficiency and discrimination power. The measured charge of a lepton (electron or muon) from the semileptonic decay of a B meson provides strong discrimination; however, the ATLAS sensitivity to $b \to \ell$ transitions are diluted through processes that can change the charge of the observed lepton, such as through neutral B meson oscillations, or through the cascade decays $b \to c \to \ell$. The separation power of lepton tagging is enhanced by considering a weighted sum of the charge of the tracks in a cone around the lepton. If no lepton is present, a weighted sum of the charge of the tracks in a jet associated with the opposite-side b-hadron decay is used to provide discrimination. This weighted sum, or *cone charge*, is defined as:

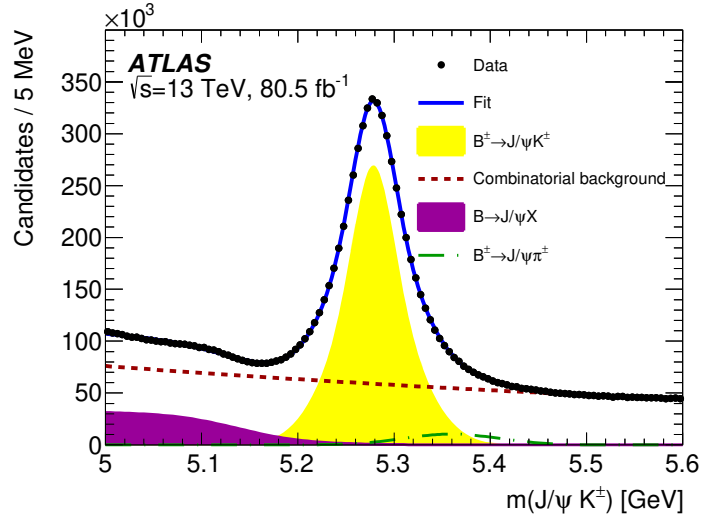$$Q_x = \frac{\sum_i^{N \text{ tracks}} q_i \cdot (p_{Ti})^{\kappa}}{\sum_i^{N \text{ tracks}} (p_{Ti})^{\kappa}}, \tag{1}$$

Figure 1: The invariant mass distribution for selected $B^\pm \to J/\psi K^\pm$ candidates. Data are shown as points, and the overall result of the fit is given by the blue curve. The contributions from the combinatorial background component are indicated by the red dotted line, partially reconstructed b-hadron decays by the purple shaded area, and decays of $B^\pm \to J/\psi \pi^\pm$, where the pion is misassigned as a kaon, by the green dashed line.

where $x = \{\mu, e, \text{jet}\}$ refers to muon, electron, or jet charge, respectively, and the summation is made using the charge of the track, q_i, and its $p_{\mathrm{T}i}$, over a selected set of tracks, including the lepton, in a cone of size $\Delta R = \sqrt{(\Delta\phi)^2 + (\Delta\eta)^2}$, around the lepton or jet direction. The value of the parameter κ is optimised on each OST method, by determining the value of κ that maximises the *tagging power* (defined in Section 4.3). The requirements on the tracks and ΔR are described below, dependent on the OST method.

Two subcategories of Q_x are considered: the first *discrete* category is used in the case where the cone charge is formed either from only one track or from more than one track of the same charge; this results in a cone charge of $Q_x = \pm 1$. The second *continuous* category is used when more than one track is considered, and the sum contains tracks of both negative and positive charge. In the continuous case, Q_x is divided into intervals within the range $-1 < Q_x < 1$ for each OST algorithm.

A probability $P(B|Q_x)$ is constructed, which is defined as the probability that a B meson is produced in a state containing a $\bar{b}$-quark, given the value of the cone charge Q_x. Since Q_x is evaluated on the opposite side, a large, negative value of Q_x tends to correspond to a higher value of $P(B|Q_x)$. An equivalent probability for the b-quark case is defined as $P(\bar{B}|Q_x)$. Using the $B^\pm$ calibration samples, $P(Q_x|B^\pm)$ for each tagging method used can be defined. The probability to tag a B_s^0 meson as containing a $\bar{b}$-quark is therefore given as $P(B|Q_x) = P(Q_x|B^+)/(P(Q_x|B^+) + P(Q_x|B^-))$, and correspondingly $P(\bar{B}|Q_x) = 1 - P(B|Q_x)$. If there is no OST information available for a given B_s^0 meson, a probability of 0.5 is assigned to that candidate.

Muon tagging

For muon-based tagging, at least one additional muon is required in the event, with $p_{\mathrm{T}} > 2.5$ GeV, $|\eta| < 2.5$ and $|\Delta z| < 5$ mm, where $|\Delta z|$ is the difference in z between the primary vertex and the longitudinal impact parameter of the ID track associated with the muon. Muons are classified and kept if their identification

quality selection working point is either Tight or Low-p_T; these categories are subsequently treated as distinct flavour tagging methods. For muons with $p_T > 4$ GeV, Tight muons are the dominant category, with the Low-p_T requirement typically identifying muons of $p_T < 4$ GeV. In the case of multiple muons satisfying selection criteria in one event, Tight muons are chosen over Low-p_T muons. Within the same muon category, the muon with the highest p_T that passes the selections is used.

A muon cone charge variable, Q_μ, is constructed according to Eq. (1), with $\kappa = 1.1$ and the sum over the reconstructed ID tracks within a cone of size $\Delta R = 0.5$ around the muon direction. These tracks must have $p_T > 0.5$ GeV, $|\eta| < 2.5$, and $|\Delta z| < 5$ mm. Tracks associated with the decay of a B meson signal candidate are excluded from the sum. In each interval of Q_μ, a fit to the $J/\psi K^\pm$ invariant mass spectrum is performed and the number of signal events extracted. The fit model used is described in Section 4.1. Figure 2 shows the distributions of the muon cone charge using $B^\pm$ signal candidates for Tight muons, and includes the tagging probability as a function of the cone charge variable. The corresponding distributions for Low-p_T muons are shown in Figure 3.
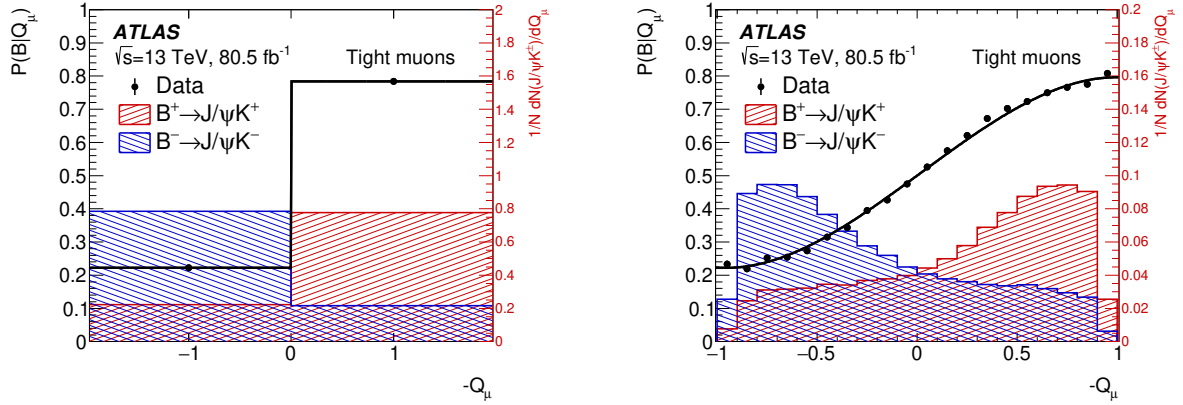

Figure 2: Cone charge distributions, $-Q_\mu$, for Tight muons, shown for cases of discrete charge (left), and for the continuous distribution (right). For each plot, in red (blue), the normalised B^+ (B^-) cone charge distribution is shown (corresponding to the right axis scale). A B^+ (B^-) candidate is more likely to have a large negative (positive) value of Q_μ. Superimposed is the distribution of the tagging probability, $P(B|Q_\mu)$, as a function of the cone charge, derived from a data sample of $B^\pm \rightarrow J/\psi K^\pm$ decays, and defined as the probability to have a B^+ meson (on the signal-side) given a particular cone charge Q_μ. The fitted parameterisation, shown in black, is used as the calibration curve to infer the probability to have a B_s^0 or $\bar{B}_s^0$ meson at production in the decays to $J/\psi\phi$.

Electron tagging

Electrons are identified using ID and calorimeter information, and must satisfy the *Medium* electron quality criteria [34]. The ID track associated with the electron is required to have $p_T > 0.5$ GeV, $|\eta| < 2.5$, and $|\Delta z| < 5$ mm. To reject electrons from the signal-side of the decay, electrons with $\cos(\zeta_b) > 0.93$, where ζ_b is the opening angle between the momentum of the signal B meson candidate and the electron momentum, are not considered. In the case of more than one electron passing the selection, the electron with the highest p_T is chosen. Charged particle tracks within a cone of size $\Delta R = 0.5$ are used to form the electron cone charge Q_e, constructed according to Eq. (1), with $\kappa = 1.0$. The resulting electron cone charge distributions are shown in Figure 4, together with the corresponding tagging probability.
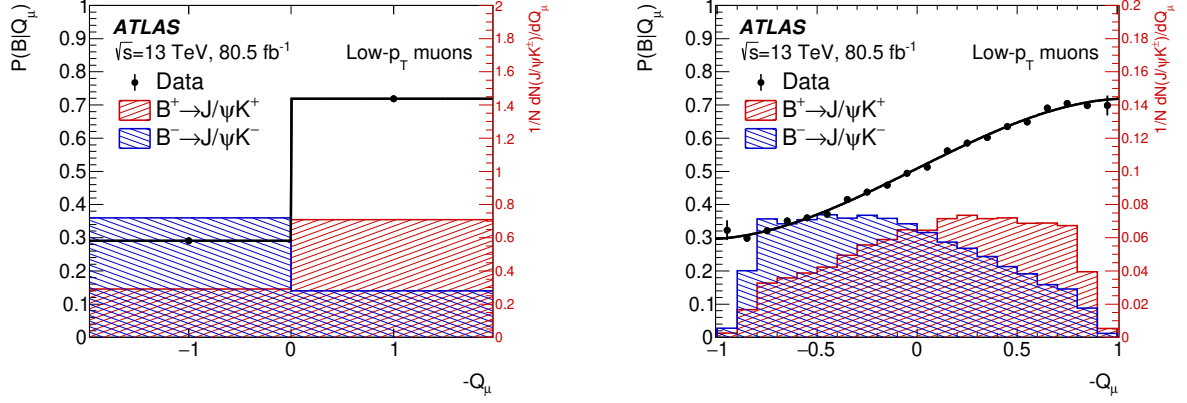
Figure 3: Normalised cone charge distributions (shown against the right axis scale), $-Q_\mu$, for B^+ (B^-) events shown in red (blue) for Low-p_T muons, for cases of discrete charge (left), and for the continuous distribution (right). Superimposed is the distribution of the tagging probability, $P(B|Q_\mu)$.
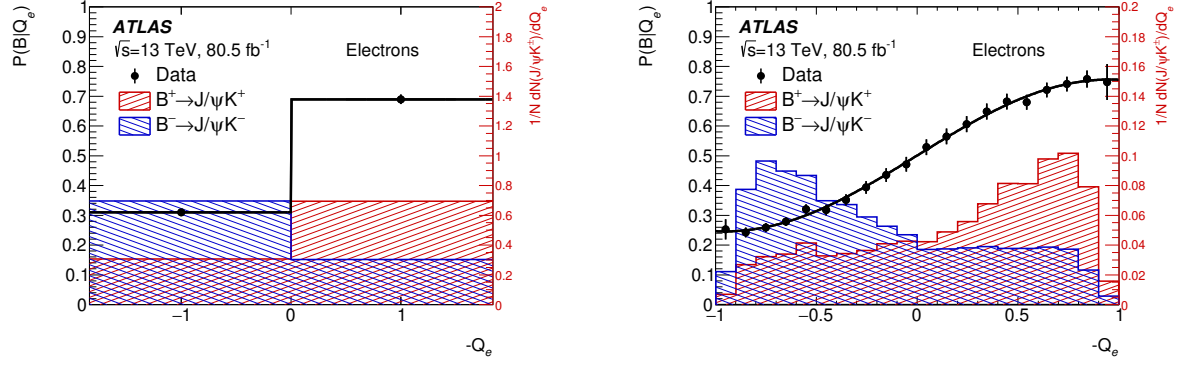

Figure 4: Normalised cone charge distributions (shown against the right axis scale), $-Q_e$, for B^+ (B^-) events shown in red (blue) for electrons, for cases of discrete charge (left), and the continuous distribution (right). Superimposed is the distribution of the tagging probabilities, $P(B|Q_e)$.

Jet tagging

In the absence of a muon or electron, a jet identified as containing a b-hadron is required. Jets are reconstructed from calorimetric information [35] using the anti-k_t algorithm [36, 37] with a radius parameter $R = 0.4$. The identification of a b-tagged jet uses a multivariate algorithm *MV2c10* [38], utilising boosted decision trees (BDT), which output a classifier value. Jets are selected if this value exceeds 0.56. This value is chosen to maximise the tagging power of the calibration sample. In the case of multiple selected jets, the jet with the highest value of the BDT output classifier is used. Jets associated with the signal decay are not considered in this selection.

Tracks within a cone of size $\Delta R = 0.5$ around the jet axis are used to define a jet cone charge, Q_{jet}, constructed according to Eq. (1), where $\kappa = 1.1$ and the sum is over the tracks associated with the jet, with $|\Delta z| < 5$ mm, and excluding tracks from the decay of the signal B meson candidate. Figure 5 shows the distribution of the opposite-side jet cone charge for $B^\pm$ signal candidates.
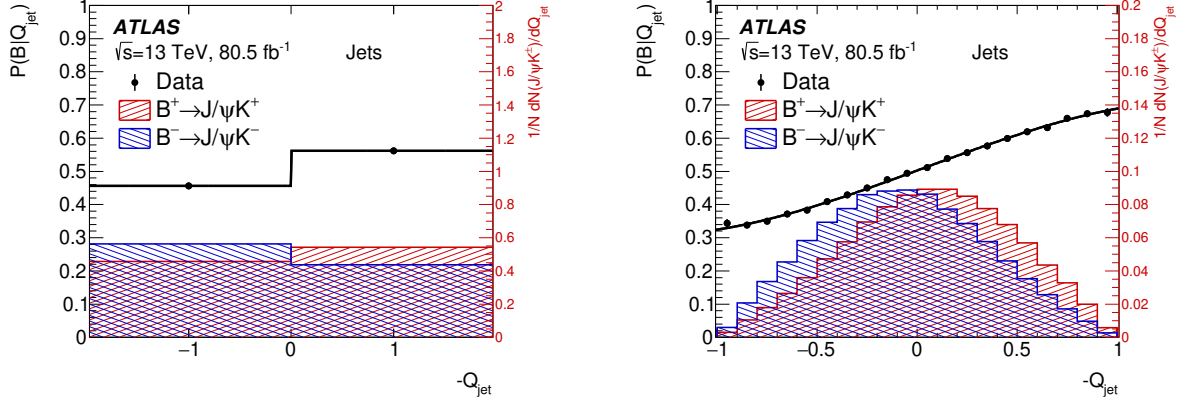
8

Figure 5: Normalised cone charge distributions (shown against the right axis scale), $-Q_{\text{jet}}$, for B^+ (B^-) events shown in red (blue) for jets, for cases of discrete charge (left), and the continuous distribution (right). Superimposed is the distribution of the tag probability, $P(B|Q_{\text{jet}})$.

4.3 Flavour tagging performance

In order to quantify and compare the performance of the various tagging methods, three figure-of-merit terms are constructed, which describe: the fraction of events used by a given tagging method, the purity of the method, and the overall power of the tagging method in the sample. The efficiency, ϵ_x, of an individual tagging method is defined as the number of signal events tagged by that method divided by the total number of signal events in the sample. The purity of a particular flavour tagging method, called the dilution, is defined as $\mathcal{D}(Q_x) = 2P(B|Q_x) - 1$. The tagging power of a particular tagging method is then defined as $T_x = \sum_i \epsilon_{xi} \cdot \mathcal{D}^2(Q_{xi})$, where the sum is over the probability distribution in intervals of the cone charge variable. An effective dilution, $D_x = \sqrt{T_x/\epsilon_x}$, is calculated from the measured tagging power and efficiency.

By definition, there is no overlap between lepton-tagged and jet-charge-tagged events. The overlap between events with a muon (either Tight or Low-p_{T}) and events with an electron corresponds to around 0.6% of all tagged events. In the case of multiply tagged events, the OST method is selected in the following order: Tight muon, electron, Low-p_{T} muon, jet. However, the ordering of muon- and electron-tagged events is shown to have negligible impact on the final results. A summary of the tagging performance for each method and the overall performance on the $B^\pm$ sample is given in Table 1.

4.4 Using tag information in the B_s^0 fit

For the maximum likelihood fit performed on the B_s^0 data, and described in detail in Section 5, the per-candidate probability, $P(B|Q_x)$, that the B meson candidate was produced in a state B_s^0 (versus a $\bar{B}_s^0$) is provided by the calibrations derived from the $B^\pm \rightarrow J/\psi K^\pm$ sample, described above, and shown in Figures 2–5. Since the distributions of $P(B|Q_x)$ from signal B_s^0 mesons and backgrounds can be expected to be different, separate probability density functions (PDFs) are necessary to describe these distributions in the likelihood function. These PDFs are defined as $P_{\text{s}}(P(B|Q_x))$ and $P_{\text{b}}(P(B|Q_x))$, describing the probability distributions for signal and background, respectively, and are derived from the sample of B_s^0 candidates. For the exclusive decays $B_d \rightarrow J/\psi K^{0*}$ and $\Lambda_b \rightarrow J/\psi p K^-$ that are present in the sample

Table 1: Summary of tagging performances for the different flavour tagging methods on the sample of $B^\pm$ signal candidates, as described in the text. Uncertainties shown are statistical only. The efficiency (ϵ_x) and tagging power (T_x) are each determined by summing over the individual bins of the cone charge distribution. The effective dilution (D_x) is obtained from the measured efficiency and tagging power. For the efficiency, effective dilution, and tagging power, the corresponding uncertainty is determined by combining the appropriate uncertainties in the individual bins of each charge distribution.

Tag method	ϵ_x [%]	D_x [%]	T_x [%]
Tight muon	4.50 ± 0.01	43.8 ± 0.2	0.862 ± 0.009
Electron	1.57 ± 0.01	41.8 ± 0.2	0.274 ± 0.004
Low-p_T muon	3.12 ± 0.01	29.9 ± 0.2	0.278 ± 0.006
Jet	12.04 ± 0.02	16.6 ± 0.1	0.334 ± 0.006
Total	21.23 ± 0.03	28.7 ± 0.1	$1.75 \ \pm 0.01$

of B_s^0 candidates, $P_s(P(B|Q_x))$ is used to model the probability distributions for these contributions (described further in Section 5.2). The PDFs consist of the fraction of events that are tagged with a particular method (or are untagged), the fractions of those events categorised as discrete or continuous, and for those that are continuous, a PDF of the corresponding probability distribution.

Continuous PDF

The parameterisations of the continuous PDF components of $P_{s,b}(P(B|Q_x))$ for each OST method are defined as follows. In the sideband regions, $5.150 < m(J/\psi KK) < 5.317$ GeV and $5.417 < m(J/\psi KK) < 5.650$ GeV, unbinned maximum likelihood fits to the $P(B|Q_x)$ distributions are performed to extract the background (continuous category) PDFs for $P_b(P(B|Q_x))$. For the Tight muon and electron methods, the parameterisation has the form of the sum of a second-order polynomial and two exponential functions. A Gaussian function is used for the Low-p_T muons. For the jet tagging algorithm an eighth-order polynomial is used.

For the signal, fits are performed to the $P(B|Q_x)$ distributions, using all events in the $m(J/\psi KK)$ distributions to extract the signal (continuous category) PDFs for $P_s(P(B|Q_x))$. In these fits, the parameters describing the background PDFs are fixed to their previously extracted values, as is the relative normalisation of signal and background, extracted from a fit to the $m(J/\psi KK)$ distribution. For the signal PDFs, the Tight muon tagging method uses the sum of two exponential functions and a constant function to describe the signal. For the electron tagging method, the signal function has the form of the sum of a second-order polynomial and two exponential functions, and for the Low-p_T muon and jet tagging methods a Gaussian function is used.

Discrete PDF

In the case where the cone charge is discrete, the fractions of events f_{+1} (f_{-1}) with cone charges +1 (−1) are determined separately for signal and background using events from the signal and sideband regions of the B_s^0 mass distribution (as defined in Section 3). The remaining fraction of events, $1 - f_{+1} - f_{-1}$, corresponds to the continuous parts of the distribution. Positive and negative charges are equally probable for background candidates formed from a random combination of a J/ψ and a pair of tracks, but this is not

necessarily the case for background candidates formed from a partially reconstructed b-hadron. Table 2 summarises the fractions f_{+1} and f_{-1} obtained from each tagging method for signal and background events.

Table 2: Fractions f_{+1} and f_{-1} of events with cone charges of +1 and -1, respectively, for signal and background events and for the different tagging methods. Only statistical uncertainties are given.

Tag method	Signal		Background	
	f_{+1} [%]	f_{-1} [%]	f_{+1} [%]	f_{-1} [%]
Tight muon	6.9 ± 0.3	7.5 ± 0.3	4.7 ± 0.1	4.9 ± 0.1
Electron	20 ± 1	19 ± 1	16.8 ± 0.2	17.3 ± 0.2
Low-p_T muon	10.9 ± 0.5	11.6 ± 0.5	7.0 ± 0.1	7.5 ± 0.1
Jet	3.60 ± 0.15	3.54 ± 0.15	3.05 ± 0.03	3.17 ± 0.03

The fractions of signal and background events tagged using the different OST methods are found using a similar sideband-subtraction method, and are summarised in Table 3.

Table 3: Fractions of signal and background events tagged using the different methods. The efficiencies include both the continuous and discrete contributions. Only statistical uncertainties are quoted.

Tag method	Signal efficiency [%]	Background efficiency [%]
Tight muon	4.06 ± 0.06	3.21 ± 0.01
Electron	1.86 ± 0.04	1.48 ± 0.01
Low-p_T muon	2.95 ± 0.05	2.70 ± 0.01
Jet	12.1 ± 0.1	9.41 ± 0.02
Untagged	79.1 ± 0.3	83.20 ± 0.05

To account for possible deviations of the data from the selected fit models, variations of the procedure described here are used to determine systematic uncertainties, as described in Section 6.

5 Maximum likelihood fit

An unbinned maximum likelihood fit is performed on the selected events to extract the parameter values of the $B_s^0 \rightarrow J/\psi(\mu^+\mu^-)\phi(K^+K^-)$ decay. The fit uses information about the reconstructed mass, m, the measured proper decay time, t, the measured mass uncertainty, σ_m, the measured proper decay time uncertainty, σ_t, the measured transverse momentum, p_T, the tagging probability, $P(B|Q_x)$, and the transversity angles, Ω, of each $B_s^0 \rightarrow J/\psi\phi$ decay candidate. The measured value of the proper decay time uncertainty, σ_t, is calculated from the covariance matrix associated with the vertex fit for each candidate event. The transversity angles $\Omega = (\theta_T, \psi_T, \phi_T)$ are defined in Section 5.1. The likelihood function is

defined as a combination of the signal and background PDFs as follows:

$$\ln \mathcal{L} = \sum_{i=1}^{N} w_i \cdot \ln[f_\text{s} \cdot \mathcal{F}_\text{s}(m_i, t_i, \sigma_{m_i}, \sigma_{t_i}, \Omega_i, P_i(B|Q_x), p_{\text{T}_i}) + f_\text{s} \cdot f_{B^0} \cdot \mathcal{F}_{B^0}(m_i, t_i, \sigma_{m_i}, \sigma_{t_i}, \Omega_i, P_i(B|Q_x), p_{\text{T}_i})$$

$$+ f_\text{s} \cdot f_{\Lambda_b} \cdot \mathcal{F}_{\Lambda_b}(m_i, t_i, \sigma_{m_i}, \sigma_{t_i}, \Omega_i, P_i(B|Q_x), p_{\text{T}_i})$$

$$+ (1 - f_\text{s} \cdot (1 + f_{B^0} + f_{\Lambda_b}))\mathcal{F}_\text{bkg}(m_i, t_i, \sigma_{m_i}, \sigma_{t_i}, \Omega_i, P_i(B|Q_x), p_{\text{T}_i})],$$

(2)

where N is the number of selected candidates, w_i is a weighting factor to account for the trigger efficiency (described in Section 5.3). The terms $\mathcal{F}_\text{s}$, $\mathcal{F}_{B^0}$, $\mathcal{F}_{\Lambda_b}$ and $\mathcal{F}_\text{bkg}$ are the PDFs modelling the signal, B^0 background, Λ_b background, and the other background distributions, respectively. The term f_s is the fraction of signal candidates and f_{B^0} and f_{Λ_b} are the background fractions of B^0 mesons and Λ_b baryons misidentified as B_s^0 candidates, calculated relative to the number of signal events. These background fractions are fixed to their expectation from the MC simulation, and variations are applied as part of the evaluation of the effects of systematic uncertainties. The mass m_i, the proper decay time t_i and the decay angles Ω_i are the values measured from the data for each event i. A detailed description of the signal PDF terms in Eq. (2) is given in Section 5.1. The three background functions are described in Section 5.2.

5.1 Signal PDF

The PDF used to describe the signal events, $\mathcal{F}_\text{s}$, has the following composition:

$$\mathcal{F}_\text{s}(m_i, t_i, \sigma_{m_i}, \sigma_{t_i}, \Omega_i, P_i(B|Q_x), p_{\text{T}_i}) = P_\text{s}(m_i|\sigma_{m_i}) \cdot P_\text{s}(\sigma_{m_i}|p_{\text{T}_i}) \cdot P_\text{s}(t_i, \Omega_i|\sigma_{t_i}, P_i(B|Q_x))$$
$$\cdot P_\text{s}(\sigma_{t_i}|p_{\text{T}_i}) \cdot P_\text{s}(P_i(B|Q_x)) \cdot A(\Omega_i, p_{\text{T}_i}) \cdot P_\text{s}(p_{\text{T}_i}).$$

The mass term $P_\text{s}(m_i|\sigma_{m_i})$ is modelled in the following way:

$$P_\text{s}(m_i|\sigma_{m_i}) \equiv \frac{1}{\sqrt{2\pi}S_m\sigma_{m_i}} \cdot e^{\frac{-(m_i - m_{B_s})^2}{2(S_m\sigma_{m_i})^2}}.$$

(3)

The term $P_\text{s}(m_i|\sigma_{m_i})$ uses per-candidate mass errors, σ_{m_i}, calculated for each $J/\psi\phi$ candidate from the covariance matrix associated with the four-track vertex fit. Each measured candidate mass is convolved with a Gaussian function with a width equal to σ_{m_i} multiplied by a scale factor S_m, introduced to account for any mismeasurements. Both S_m and the mean value m_{B_s}, which is the B_s^0 meson mass, are free parameters determined in the fit.

The PDF term $P_\text{s}(t_i, \Omega_i|\sigma_{t_i}, P_i(B|Q_x))$ takes into account the lifetime resolution, so each time element in Table 4 is convolved with a Gaussian function defined as:

$$R(t^{'} - t_i, \sigma_{t_i}) \equiv \frac{1}{\sqrt{2\pi}\ S_t\ \sigma_{t_i}} \cdot e^{\frac{-(t_i^{'} - t_i)^2}{2(S_t\sigma_{t_i})^2}}.$$

(4)

S_t is a scale factor (a parameter of the fit) and σ_{t_i} is the per-candidate uncertainty on proper decay time t_i. This convolution is performed numerically on an event-by-event basis and the value σ_{t_i} is measured for

each B_s^0 candidate, based on the tracking error matrix of the four final state particles. The probability term $P_s(\sigma_{t_i}|p_{\mathrm{T}_i})$ is introduced to account for differences between signal and background events for the values of the per-candidate time errors. Distributions of this variable for signal and background described by gamma functions are shown in Figure 6. The average value of the time error for signal events is 69 fs.
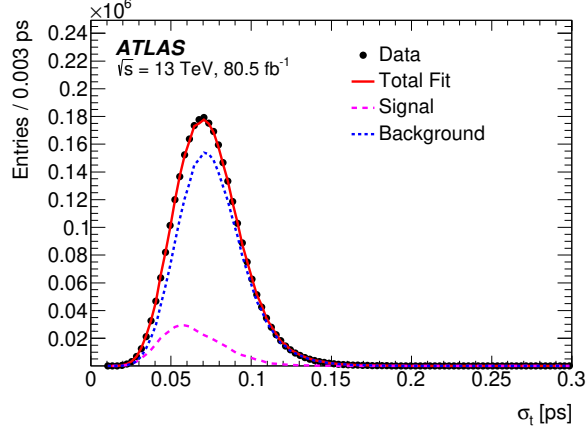

Figure 6: The proper decay time uncertainty distribution for data (black), and the fits to the background (blue) and the signal (purple) contributions. The total fit is shown as a red curve.

The same approach was applied for the probability terms $P_s(\sigma_{m_i}|p_{\mathrm{T}_i})$ and $P_s(p_{\mathrm{T}_i})$ accounting for differences between signal and background events for the values of the per-candidate mass error and p_{T_i} values, respectively. The tagging probability term for signal $P_s(P_i(B|Q_x))$ is described in Section 4.4.

The term $P_s(t_i, \Omega_i|\sigma_{t_i}, P_i(B|Q_x))$ is a joint PDF for the decay time t and the transversity angles Ω for the $B_s^0 \rightarrow J/\psi(\mu^+\mu^-)\phi(K^+K^-)$ decay. Ignoring detector effects, the distribution for the time t and the angles Ω is given by the differential decay rate [39]:

$$\frac{\mathrm{d}^4\Gamma}{\mathrm{d}t\,\mathrm{d}\Omega} = \sum_{k=1}^{10} O^{(k)}(t)g^{(k)}(\theta_T, \psi_T, \phi_T),$$

where $O^{(k)}(t)$ are the time-dependent functions corresponding to the contributions of the four different amplitudes (A_0, $A_{||}$, $A_\perp$, and A_S) and their interference terms, and $g^{(k)}(\theta_T, \psi_T, \phi_T)$ are the angular functions. Table 4 shows the time-dependent and the angular functions of the transversity angles. The formulae for the time-dependent functions have the same structure for B_s^0 and $\bar{B}_s^0$ but with a sign reversal in the terms containing Δm_s, which is a fixed parameter of the fit (using Ref. [33]). The formalism used throughout this analysis assumes no direct CP violation, i.e. $\lambda = (q/p)(\bar{A}/A) = 1$. In Table 4, the parameter $A_\perp(t)$ is the time-dependent amplitude for the CP-odd final-state configuration while $A_0(t)$ and $A_{||}(t)$ correspond to CP-even final-state configurations. The amplitude $A_S(t)$ gives the contribution from the CP-odd non-resonant $B_s^0 \rightarrow J/\psi K^+K^-$ S-wave state [40] (which includes the f_0 meson). The corresponding functions are given in the last four lines of Table 4 ($k = 7$–10). The amplitudes are parameterised by $|A_i|e^{i\delta_i}$, where $i = \{0, ||, \perp, S\}$, $\delta_0 = 0$ and are normalised such that $|A_0(0)|^2 + |A_\perp(0)|^2 + |A_{||}(0)|^2 = 1$. The amplitude $|A_\perp(0)|$ is determined according to this condition, while the remaining three amplitudes are parameters of the fit. The value $|A_S|^2$ is the ratio of the S-wave yield to the $\phi \rightarrow K^+K^-$ yield in the interval of $m(K^+K^-)$ used in the analysis. In the sum over the mass interval, the interference terms (lines 8–10 in Table 4) are corrected by a factor α that takes into account the mass-dependent differences in absolute amplitude and phase between the $\phi \rightarrow K^+K^-$ and the S-wave amplitudes. The correction is based on the

Breit–Wigner description of the ϕ and on model assumptions for the shape and the phase variations of the S-wave amplitude. The phase δ_S is the phase difference between $A_0(0)$ and the S-wave amplitudes at the $\phi \to K^+K^-$ peak. The values of α and the related systematic uncertainty are discussed in Section 6.

The angles $(\theta_T, \psi_T, \phi_T)$, are defined in the rest frames of the final-state particles. The x-axis is determined by the direction of the ϕ meson in the J/ψ rest frame, and the K^+K^- system defines the x–y plane, where $p_y(K^+) > 0$. The three angles are defined as:

- θ_T, the angle between $\vec{p}(\mu^+)$ and the normal to the x–y plane, in the J/ψ meson rest frame,

- ϕ_T, the angle between the x-axis and $\vec{p}_{xy}(\mu^+)$, the projection of the μ^+ momentum in the x–y plane, in the J/ψ meson rest frame,

- ψ_T, the angle between $\vec{p}(K^+)$ and $-\vec{p}(J/\psi)$ in the ϕ meson rest frame.

The angular acceptance of the detector and the kinematic cuts on the angular distributions are included in the likelihood function through $A(\Omega_i, p_{Ti})$. This is calculated using a four-dimensional binned acceptance method, applying an event-by-event efficiency according to the transversity angles $(\theta_T, \psi_T, \phi_T)$ and the p_T of the candidate. The p_T binning is necessary, because the angular acceptance is influenced by the p_T of the B_s^0 candidate. The acceptance is calculated from the $B_s^0 \to J/\psi\phi$ MC events with additional weighting for p_T and η distributions. In the likelihood function, the acceptance is treated as an angular acceptance PDF, which is multiplied with the time- and angle-dependent PDF describing the $B_s^0 \to J/\psi(\mu^+\mu^-)\phi(K^+K^-)$ decays. As both the acceptance and time- and angle-dependent decay PDFs depend on the transversity angles they must be normalised together. This normalisation is done numerically during the likelihood fit. The PDF is normalised over the entire B_s^0 mass range, 5.150–5.650 GeV.

5.2 Background PDF

The background PDF has the following composition:

$$
\begin{aligned}
\mathcal{F}_{\text{bkg}}(m_i, t_i, \sigma_{t_i}, \Omega_i, P_i(B|Q_x), p_{Ti}) &= P_b(m_i) \cdot P_b(t_i|\sigma_{t_i}) \cdot P_b(P_i(B|Q_x)) \\
&\quad \cdot P_b(\Omega_i) \cdot P_b(\sigma_{m_i}|p_{Ti}) \cdot P_b(\sigma_{t_i}|p_{Ti}) \cdot P_b(p_{Ti}).
\end{aligned}
$$

The proper decay time function $P_b(t_i|\sigma_{t_i})$ is parameterised as a peak modelled by a Gaussian distribution, two positive-time exponential functions and two negative-time exponential functions. These functions are convolved with the same resolution function, defined in Eq. (4) as the signal decay time-dependence. The prompt peak models the combinatorial background events, which are expected to have reconstructed lifetimes distributed around zero. The two positive-time exponential functions represent a fraction of longer-lived backgrounds with non-prompt J/ψ, combined with hadrons from the primary vertex or from a B/D meson in the same event. The two negative-time exponential functions take into account events with poor vertex resolution. The probability terms $P_b(\sigma_{m_i}|p_{Ti})$, $P_b(\sigma_{t_i}|p_{Ti})$ and $P_b(p_{Ti})$ are described by gamma functions. They are unchanged from the analysis described in Ref. [41] and explained in detail there. The tagging probability term for background events $P_b(P_i(B|Q_x))$ is described in Section 4.4.

14

Table 4: The ten time-dependent functions, $O^{(k)}(t)$ and the functions of the transversity angles $g^{(k)}(\theta_T, \psi_T, \phi_T)$. The amplitudes $|A_0(0)|^2$ and $|A_\parallel(0)|^2$ are for the CP-even components of the $B_s^0 \to J/\psi\phi$ decay, $|A_\perp(0)|^2$ is the CP-odd amplitude; they have corresponding strong phases δ_0, $\delta_\parallel$ and $\delta_\perp$. By convention, δ_0 is set to be zero. The S-wave amplitude $|A_S(0)|^2$ gives the fraction of $B_s^0 \to J/\psi K^+ K^-$ (f_0) and has a related strong phase δ_S. The factor α is described in the text of Section 5.1. The $\pm$ and $\mp$ terms denote two cases: the upper sign describes the decay of a meson that was initially a B_s^0 meson, while the lower sign describes the decays of a meson that was initially $\bar{B}_s^0$.

k	$O^{(k)}(t)$	$g^{(k)}(\theta_T, \psi_T, \phi_T)$
1	$\frac{1}{2}\|A_0(0)\|^2 \left[(1+\cos\phi_s)\, e^{-\Gamma_L^{(s)} t} + (1-\cos\phi_s)\, e^{-\Gamma_H^{(s)} t} \pm 2e^{-\Gamma_s t} \sin(\Delta m_s t) \sin\phi_s \right]$	$2\cos^2\psi_T \left(1 - \sin^2\theta_T \cos^2\phi_T\right)$
2	$\frac{1}{2}\|A_\parallel(0)\|^2 \left[(1+\cos\phi_s)\, e^{-\Gamma_L^{(s)} t} + (1-\cos\phi_s)\, e^{-\Gamma_H^{(s)} t} \pm 2e^{-\Gamma_s t} \sin(\Delta m_s t) \sin\phi_s \right]$	$\sin^2\psi_T \left(1 - \sin^2\theta_T \sin^2\phi_T\right)$
3	$\frac{1}{2}\|A_\perp(0)\|^2 \left[(1-\cos\phi_s)\, e^{-\Gamma_L^{(s)} t} + (1+\cos\phi_s)\, e^{-\Gamma_H^{(s)} t} \mp 2e^{-\Gamma_s t} \sin(\Delta m_s t) \sin\phi_s \right]$	$\sin^2\psi_T \sin^2\theta_T$
4	$\frac{1}{2}\|A_0(0)\|\|A_\parallel(0)\| \cos\delta_\parallel \left[(1+\cos\phi_s)\, e^{-\Gamma_L^{(s)} t} + (1-\cos\phi_s)\, e^{-\Gamma_H^{(s)} t} \pm 2e^{-\Gamma_s t} \sin(\Delta m_s t) \sin\phi_s \right]$	$\frac{1}{\sqrt{2}} \sin 2\psi_T \sin^2\theta_T \sin 2\phi_T$
5	$\|A_\parallel(0)\|\|A_\perp(0)\| \left[\frac{1}{2}(e^{-\Gamma_L^{(s)} t} - e^{-\Gamma_H^{(s)} t}) \cos(\delta_\perp - \delta_\parallel) \sin\phi_s \pm e^{-\Gamma_s t} (\sin(\delta_\perp - \delta_\parallel) \cos(\Delta m_s t) - \cos(\delta_\perp - \delta_\parallel) \cos\phi_s \sin(\Delta m_s t)) \right]$	$-\sin^2\psi_T \sin 2\theta_T \sin\phi_T$
6	$\|A_0(0)\|\|A_\perp(0)\| \left[\frac{1}{2}(e^{-\Gamma_L^{(s)} t} - e^{-\Gamma_H^{(s)} t}) \cos\delta_\perp \sin\phi_s \pm e^{-\Gamma_s t} (\sin\delta_\perp \cos(\Delta m_s t) - \cos\delta_\perp \cos\phi_s \sin(\Delta m_s t)) \right]$	$\frac{1}{\sqrt{2}} \sin 2\psi_T \sin 2\theta_T \cos\phi_T$
7	$\frac{1}{2}\|A_S(0)\|^2 \left[(1-\cos\phi_s)\, e^{-\Gamma_L^{(s)} t} + (1+\cos\phi_s)\, e^{-\Gamma_H^{(s)} t} \mp 2e^{-\Gamma_s t} \sin(\Delta m_s t) \sin\phi_s \right]$	$\frac{2}{3}\left(1 - \sin^2\theta_T \cos^2\phi_T\right)$
8	$\alpha\|A_S(0)\|\|A_\parallel(0)\| \left[\frac{1}{2}(e^{-\Gamma_L^{(s)} t} - e^{-\Gamma_H^{(s)} t}) \sin(\delta_\parallel - \delta_S) \sin\phi_s \pm e^{-\Gamma_s t} (\cos(\delta_\parallel - \delta_S) \cos(\Delta m_s t) - \sin(\delta_\parallel - \delta_S) \cos\phi_s \sin(\Delta m_s t)) \right]$	$\frac{1}{3}\sqrt{6} \sin\psi_T \sin^2\theta_T \sin 2\phi_T$
9	$\frac{1}{2}\alpha\|A_S(0)\|\|A_\perp(0)\| \sin(\delta_\perp - \delta_S) \left[(1-\cos\phi_s)\, e^{-\Gamma_L^{(s)} t} + (1+\cos\phi_s)\, e^{-\Gamma_H^{(s)} t} \mp 2e^{-\Gamma_s t} \sin(\Delta m_s t) \sin\phi_s \right]$	$\frac{1}{3}\sqrt{6} \sin\psi_T \sin 2\theta_T \cos\phi_T$
10	$\alpha\|A_0(0)\|\|A_S(0)\| \left[\frac{1}{2}(e^{-\Gamma_H^{(s)} t} - e^{-\Gamma_L^{(s)} t}) \sin\delta_S \sin\phi_s \pm e^{-\Gamma_s t} (\cos\delta_S \cos(\Delta m_s t) + \sin\delta_S \cos\phi_s \sin(\Delta m_s t)) \right]$	$\frac{4}{3}\sqrt{3} \cos\psi_T \left(1 - \sin^2\theta_T \cos^2\phi_T\right)$

The shape of the background angular distribution, $P_{\rm b}(\Omega_i)$ arises primarily from detector and kinematic acceptance effects. The best description is achieved by Legendre polynomial functions:

$$
\begin{aligned}
Y_l^m(\theta_T) &= \sqrt{(2l+1)/(4\pi)}\sqrt{(l-m)!/(l+m)!}\, P_l^{|m|}(\cos\theta_T), \\
P_k(x) &= \frac{1}{2^k k!}\frac{{\rm d}^k}{{\rm d}x^k}(x^2-1)^k, \\
P_l^{|m|}(x) &= (-1)^{|m|}(1-x^2)^{|m|/2}\frac{{\rm d}^{|m|}}{{\rm d}x^{|m|}}(P_l(x)), \\
P_{\rm b}(\theta_T,\psi_T,\phi_T) &= \sum_{k=0}^{k_{max}}\sum_{l=0}^{l_{max}}\sum_{m=-l}^{l}
\begin{cases}
a_{k,l,m}\sqrt{2}Y_l^m(\theta_T)\cos(m\phi_T)P_k(\cos\psi_T) & \text{where } m>0 \\
a_{k,l,m}\sqrt{2}Y_l^{-m}(\theta_T)\sin(m\phi_T)P_k(\cos\psi_T) & \text{where } m<0 \\
a_{k,l,m}\sqrt{2}Y_l^0(\theta_T)P_k(\cos\psi_T) & \text{where } m=0
\end{cases}
\end{aligned}
$$

where $l_{max}=14$, $k_{max}=14$ and the coefficients $a_{k,l,m}$ are adjusted to give the best fit to the angular distributions for events in the sidebands of the B_s^0 mass distribution. These parameters are then fixed in the main fit, defined by Eq. (2). The B_s^0 mass interval used for the background fit is between 5.150 and 5.650 GeV excluding the signal mass region $|(m(B_s^0)-5.366|<0.110$ GeV. Higher-order Legendre polynomial functions were tested as a systematic check, described in Section 6.

The background mass model, $P_{\rm b}(m_i)$ is the sum of an exponential and a constant, with the exponential slope and the relative normalisation left as free parameters of the fit.

Contamination from $B_d\to J/\psi K^{0*}$ and $\Lambda_b\to J/\psi pK^-$ events misreconstructed as $B_s^0\to J/\psi\phi$ is accounted for in the fit through the $\mathcal{F}_{B^0}$ and $\mathcal{F}_{\Lambda_b}$ terms in the PDF described in Eq. (2). The PDFs are determined using MC simulation of these decays. The fractions of these contributions, $f_{B^0}=(4.3\pm0.5)\%$ and $f_{\Lambda_b}=(2.1\pm0.6)\%$, are defined relative to the number of the $B_s^0\to J/\psi\phi$ signal events and are evaluated from MC simulation using production cross sections and branching fractions from Refs. [33, 42–46].

MC simulated events are also used to determine the shape of the mass and transversity angle distributions. The 3D angular distributions of $B_d\to J/\psi K^{0*}$ and of the conjugate decay are modelled using input from Ref. [47], while angular distributions for $\Lambda_b\to J/\psi pK^-$ and the conjugate decay are considered flat. These distributions are sculpted for detector acceptance effects and then described by Legendre polynomial functions with $l_{max}=10$ and $k_{max}=10$, Eq. (5). These shapes are used as templates in the fit. The B_d and Λ_b lifetimes are accounted for in the fit by adding additional exponential terms, scaled by the ratio of B_d/B_s^0 or Λ_b/B_s^0 masses as appropriate, where the lifetimes and masses are taken from Ref. [33]. The PDF terms that describe each of the tagging, mass, decay time and p_T probability distributions are taken from the same PDFs used to describe the $B_s^0\to J/\psi\phi$ signal (described in Sections 4.4 and 5.1) to account for the fact that these dedicated background events are fully reconstructed b-hadron decays. Systematic uncertainties due to the background from $B_d\to J/\psi K^{0*}$ and $\Lambda_b\to J/\psi pK^-$ decays are described in Section 6. The contribution of the S-wave $B_d\to J/\psi K\pi$ decays as well as their interference with the P-wave $B_d\to J/\psi K^{0*}$ decays are included in the PDF of the fit, using the parameters measured in Ref. [47].

5.3 Proper decay time dependence of muon trigger efficiency

In the triggers used in this analysis, there is no minimum cut applied on the transverse impact parameter d_0 of muons. On the other side, trigger muons with values of $d_0>10$ mm are not accepted. This results in

inefficiency at large values of the proper decay time. This inefficiency is estimated using MC simulated events, by comparing the B_s^0 proper decay time distribution obtained before and after applying the trigger selection. To account for this inefficiency in the fit, the events are reweighted by a factor w, inversely proportional to the trigger efficiency:

$$1/w = p_0 \cdot [1 - p_1 \cdot (\text{Erf}((t - p_3)/p_2) + 1)], \tag{5}$$

where Erf denotes the error function and p_0, p_1, p_2 and p_3 are parameters determined in the fit to MC events. For more than 99% of the B_s^0 candidates the inefficiency is below 2%. For the most affected candidates the inefficiency reaches up to 50% at high decay time. No significant bias or inefficiency due to offline track reconstruction, vertex reconstruction, or track quality selection criteria is observed.

5.4 Summary of the fit parameters

The joint PDF of proper decay time and decay angles includes the main physics parameters of interest:

- the *CP*-violating phase ϕ_s,
- the average decay width Γ_s and the decay width difference $\Delta\Gamma_s$,
- the size of the *CP*-state amplitudes at $t = 0$: $|A_\parallel(0)|^2$, $|A_0(0)|^2$ and their corresponding strong phases $\delta_\perp$ and $\delta_\parallel$
- and the size of the *S*-wave amplitude at $t = 0$: $|A_S(0)|^2$ and corresponding strong phase δ_S.

The size of the remaining amplitude $|A_\perp(0)|^2$ is constrained by the normalisation condition, phase δ_0 is set to zero and Δm_s is fixed as mentioned above.

The likelihood function also includes other parameters referred to as "nuisance parameters" such as: the B_s^0 signal fraction f_s, parameters describing the invariant mass and decay time-angular distributions of combinatorial background events and scale factors of mass and decay time uncertainties. In addition, there are also other nuisance parameters describing: acceptance functions, parametrisations of the angles of dedicated backgrounds $B_d \rightarrow J/\psi K^{0*}$ and $\Lambda_b \rightarrow J/\psi pK^-$ and their fractions f_{B^0} and f_{Λ_b}, the probability density functions of time error distributions $P(\sigma_{t_i}|p_{T_i})$, mass error distributions $P(\sigma_{m_i}|p_{T_i})$, p_T distributions $P(p_{T_i})$ and tagging parameters and calibrations. These parameter values are mainly fixed in the fit to the values extracted from the B_s^0 mass signal and sideband regions or from MC simulations.

6 Systematic uncertainties

Systematic uncertainties are evaluated for effects that are described below.

- **Flavour tagging:** The effects on the main physics parameters from the fit, due to uncertainties introduced by the flavour tagging procedure, are assessed as follows: The statistical uncertainty due to the size of the sample of $B^\pm \rightarrow J/\psi K^\pm$ decays is included in the overall statistical uncertainty. The systematic uncertainty arising from the precision of the OST calibration, described in Section 4.2, is estimated by changing the models used to parameterise the probability distribution, $P(B|Q_x)$, as a function of the cone charge from the function used by default (a third-order polynomial for muons and a sinusoid for electrons) to one of several alternative functions: a linear function; a fifth-order

polynomial; or two third-order polynomials that describe the positive and negative regions and have common constant and linear terms, but independent quadratic and cubic terms. The B_s^0 fit is repeated using the alternative models and the largest deviation from the nominal fit is assigned as the systematic uncertainty. To validate the calibration procedure, calibration curves are derived from simulated samples of $B^{\pm}$ and B_s^0 signals. The variations between the curves from these two samples are propagated to the calibration curves derived from data. The differences in the parameter values between the nominal fit and that with the varied calibration curves are included in the systematic uncertainty.

An additional systematic uncertainty is assigned to account for potential dependencies on the pile-up distribution. The calibration data are split into subsets of approximately equal size, separated according to the estimated pile-up of the event, and separate calibrations are made for each subset. For the B_s^0 fit, the fit is repeated using the calibrations corresponding to the estimated pile-up of that event. Differences between the nominal and the modified fit for the parameters of interest are taken as the systematic uncertainty. For the terms $P_b(P(B|Q_x))$ and $P_s(P(B|Q_x))$, variations of the parameterisation are considered (including using histograms in place of a parameterisation). The resulting changes in the parameter values of the B_s^0 fit are similarly included in the systematic uncertainties.

- **ID alignment:** The changes of the fit parameters due to residual misalignments of the ID were studied and the observed deviations are included in the systematic uncertainties.

- **Angular acceptance method:** The angular acceptance of the detector and the kinematic cuts, $A(\Omega_i, p_{T_i})$, described in Section 5.1, is calculated from a binned fit to MC simulated data. In order to estimate the systematic uncertainty introduced by the choice of binning, different acceptance functions are calculated using different numbers of p_T bins as well as different widths and central values of the bins.

- **Time efficiency:** To correct for the proper decay time dependence of trigger inefficiencies, the events are reweighted according to Eq. (5). To estimate systematic uncertainties connected with this procedure, several alternative fits are performed. Firstly, using different sets of p_T binning in the MC sample used to determine the efficiency. Secondly, to assess the effects of mis-modelling of the B_s^0 vertex χ^2/ndof in simulated data, an alternative fit is done with MC χ^2/ndof reweighted according to data. Finally, the groups of similar triggers used to determine the efficiencies were subdivided further by their common features. These smaller groups allowed to address even more details of trigger varieties in time-efficiency determination. Deviations from the default fit result are included in the systematic uncertainties of the measurement.

- **Best candidate selection:** After applying all selection cuts for B_s^0 signal events, approximately 5% of the events are found to contain multiple candidates. In the default fit, the B_s^0 candidate with the lowest χ^2/ndof is selected. To assess the systematic uncertainty due to this selection, an equivalent sample is created where all candidates in the event are retained, each weighted by a factor of $1/N_{\text{cand}}$, where N_{cand} is number of B_s^0 candidates in the event. Deviations from the default fit are included in the systematic uncertainties of the measurement.

- **Background angles model:** The shape of the background angular distribution, $P_b(\theta_T, \varphi_T, \psi_T)$, is described by the fourteenth-order Legendre polynomial functions, given in Eq. (5). Alternatively, higher-order Legendre polynomial functions with $l_{max} = 16$ and $k_{max} = 16$ were tested, and the changes in the fit parameter values relative to the default fit are taken as systematic uncertainties.

The shapes are primarily determined by detector and kinematic acceptance effects and are sensitive to the p_T of the B_s^0 meson candidate. For this reason, the parameterisation using the Legendre polynomial functions is performed in six p_T intervals: 10–15 GeV, 15–20 GeV, 20–25 GeV, 25–30 GeV, 30–35 GeV and >35 GeV. The systematic uncertainties due to the choice of p_T intervals are estimated by repeating the fit, with these intervals enlarged and reduced by 1 GeV and by 2 GeV. The largest changes in the fit results are taken to represent the systematic uncertainties.

The sensitivity of the fit to the choice of the invariant mass window is tested by varying its size. The difference to the default fit results is assigned as a systematic uncertainty.

The parameters of the Legendre polynomial functions given in Eq. (5) are adjusted to give the best fit to the angular distributions for events in the B_s^0 mass sidebands. To test the sensitivity of the fit results to the choice of sideband regions, the fit is repeated with alternative choices for the excluded signal mass regions: $|(m(B_s^0) - 5.366 \text{ GeV}| > 0.085 \text{ GeV}$ and $|(m(B_s^0) - 5.366 \text{ GeV}| > 0.160 \text{ GeV}$ (instead of the default $|(m(B_s^0) - 5.366 \text{ GeV}| > 0.110 \text{ GeV}$). The changes in the fit results are assigned as systematic uncertainties.

- **B_d contribution:** The contamination from $B_d \to J/\psi K^{0*}$ events misreconstructed as $B_s^0 \to J/\psi \phi$ is accounted for in the final fit. Studies are performed to evaluate the systematic uncertainties due to trigger effects, the $B_d \to J/\psi K^{0*}$ fraction, and the distributions of the mass, transversity angles, and lifetime PDFs. In the MC events the angular distribution of the $B_d \to J/\psi K^{0*}$ decay is modelled using parameters taken from Ref. [47]. The contribution of the S-wave $B_d \to J/\psi K\pi$ decays as well as its interference with the P-wave $B_d \to J/\psi K^{0*}$ decays are also included in the PDF of the fit, following the parameters measured in Ref. [47]. The uncertainties of these parameters are taken into account in the estimation of the systematic uncertainty. After applying the B_s^0 signal selection cuts, the angular distributions are fitted using Legendre polynomial functions. The uncertainties of this fit are included in the systematic uncertainty.

- **Λ_b contribution:** The contamination from $\Lambda_b \to J/\psi p K^-$ events misreconstructed as $B_s^0 \to J/\psi \phi$ is accounted for in the final fit. Studies are performed to evaluate the effect of the uncertainties in the $\Lambda_b \to J/\psi p K^-$ fraction f_{Λ_b}, and the shapes of the distributions of the mass, transversity angles, and lifetime. Additional studies are performed to determine the effect of the uncertainties in the $\Lambda_b \to J/\psi \Lambda^*$ branching ratios used to reweight the generated MC sample.

- **Alternate Δm_s:** The systematics due to fixing the parameter Δm_s to the PDG value were estimated by running an alternative fit where the default model was altered by releasing Δm_s within a Gaussian constraint of which the width was taken from uncertainties assigned to Δm_s in [33]. The resulting changes to all the fit parameter values are found to be negligible except for $\delta_\perp$. The effects on the other variables are small for the parameters ϕ_s and $\delta_\parallel$.

- **Fit model mass and lifetime:** To estimate the systematic uncertainties due to the signal B_s^0 mass model, the default model was altered by adding a second Gaussian function in Eq. (3), which has the same structure as the first Gaussian function but a different scale factor, S_m^1, which is an additional free parameter of the fit. The resulting changes to other fit parameter values are found to be negligible.

To test the sensitivity of the part of the fit model describing the lifetime, two systematic tests are performed. The determination of signal and background lifetime errors is sensitive to the choice of p_T bins, in which the relative contributions of these two components are evaluated. To estimate the systematic uncertainty, the fit is repeated varying the intervals of the default p_T binning. The

determination of signal and background lifetime errors is also sensitive to the determination of the signal fraction. The fit is repeated by varying this fraction within one standard deviation of its uncertainty and differences are included in the systematic uncertainty.

- **Fit model S-wave phase**: As explained in Section 5.1, the model for the interference between $B_s^0 \to J/\psi\phi(K^+K^-)$ and S-wave $B_s^0 \to J/\psi K^+K^-$ is corrected by a factor α to account for the mass-dependent variations in absolute amplitude and phase of the two amplitudes within the interval 1.0085–1.0305 GeV in $m(K^+K^-)$. The value of α is 0.51 ± 0.08. The central value is obtained under the hypothesis of uniformity of the S-wave amplitude. The uncertainty is systematic and it is due to: detector mass resolution and mass scale uncertainties, uncertainties in the description of the ϕ resonance (mass, width, and shape descriptions as relativistic Breit-Wigner or Flatté parameterisation [48]), and to uncertainties in the description of the shape and phase variation of the S-wave amplitude. For the last effect, which is dominant, the S-wave amplitude is assumed to be due to the $f_0(980)$ resonance and it is described as in Ref. [49], similarly to what was done in Ref. [16]. The variation from the value of α obtained with the default assumption is taken as a systematic uncertainty. This procedure uses descriptions of the $f_0(980)$ based on other measurements [33]. To account for the uncertainty in α, the fit was repeated with $\alpha = 0.51 + 0.08$ and $\alpha = 0.51 - 0.08$ values. The variations of the parameter values relative to those from the default fit using the central value of α are included in the systematic uncertainties.

- **Fit bias:** Due to its complexity, the fit model can be sensitive to some nuisance parameters. This limited sensitivity could potentially lead to a bias in the measured physics parameters, even when the model describes the fitted data well. To test the stability of the results obtained from the chosen default fit model, a set of pseudo-experiments is conducted using the default model in both the generation and fit. The systematic uncertainties are determined from the mean of the pull distributions of the pseudo-experiments scaled according to the statistical uncertainty of that parameter in the fit to data. The observed deviations are included in the systematic uncertainties.

The systematic uncertainties are listed in Table 5. For each parameter, the total systematic uncertainty is obtained by adding all of the contributions in quadrature.

Table 5: Summary of systematic uncertainties assigned to the physical parameters of interest.

	ϕ_s [10^{-3} rad]	$\Delta\Gamma_s$ [10^{-3} ps^{-1}]	Γ_s [10^{-3} ps^{-1}]	$|A_\parallel(0)|^2$ [10^{-3}]	$|A_0(0)|^2$ [10^{-3}]	$|A_S(0)|^2$ [10^{-3}]	$\delta_\perp$ [10^{-3} rad]	$\delta_\parallel$ [10^{-3} rad]	$\delta_\perp - \delta_S$ [10^{-3} rad]
Tagging	19	0.4	0.3	0.2	0.2	1.1	17	19	2.3
ID alignment	0.8	0.2	0.5	< 0.1	< 0.1	< 0.1	11	7.2	< 0.1
Acceptance	0.5	0.3	< 0.1	1.0	0.9	2.9	37	64	8.6
Time efficiency	0.2	0.2	0.5	< 0.1	< 0.1	0.1	3.0	5.7	0.5
Best candidate selection	0.4	1.6	1.3	0.1	1.0	0.5	2.3	7.0	7.4
Background angles model:									
Choice of fit function	2.5	< 0.1	0.3	1.1	< 0.1	0.6	12	0.9	1.1
Choice of p_T bins	1.3	0.5	< 0.1	0.4	0.5	1.2	1.5	7.2	1.0
Choice of mass window	9.3	3.3	0.2	0.4	0.8	0.9	17	8.6	6.0
Choice of sidebands intervals	0.4	0.1	0.1	0.3	0.3	1.3	4.4	7.4	2.3
Dedicated backgrounds:									
B_d^0	2.6	1.1	< 0.1	0.2	3.1	1.5	10	23	2.1
Λ_b	1.6	0.3	0.2	0.5	1.2	1.8	14	30	0.8
Alternate Δm_s	1.0	< 0.1	< 0.1	< 0.1	< 0.1	< 0.1	15	4.0	< 0.1
Fit model:									
Time res. sig frac	1.4	1.1	0.5	0.5	0.6	0.8	12	30	0.4
Time res. p_T bins	0.7	0.5	0.8	0.1	0.1	0.1	2.2	14	0.7
S-wave phase	0.3	< 0.1	< 0.1	< 0.1	< 0.1	0.2	8.0	15	37
Fit bias	5.7	1.3	1.2	1.3	0.4	1.1	3.3	19	0.3
Total	22	4.3	2.2	2.3	3.8	4.6	55	88	39

7 Results

7.1 Fit results

The results of the likelihood fit are shown in Table 6. The total number of B_s^0 meson candidates is $453\,570 \pm 740$. The fitted value of the B_s^0 mass agrees well with the world average value [33]. Fit projections, including ratio plots, are shown in Figure 7 for the mass and proper decay time and in Figure 8 for the angles. The ratio plots show the difference between each data point and the total fit line divided by the statistical and systematic uncertainties summed in quadrature (σ) for that point. The deviations of ratio plots are within 2σ, which shows that the total uncertainties cover any discrepancy between data and fit model.

While for most of the physics parameters, including ϕ_s, $\Delta\Gamma_s$ and Γ_s, the fit determines a single solution with Gaussian behaviour of the projection of the log-likelihood (see Figure 10 in Section 7.2), for the strong-phases $\delta_\parallel$ and $\delta_\perp$ two well separated local maxima of the likelihood are found, and shown as solution (a) and (b) in Table 6. The difference in - $2\Delta\ln(L)$ between the two solutions is 0.03. As discussed in Section 7.2, the two-fold behaviour of the likelihood in the strong phases is the result of an approximate symmetry of the signal PDF. The effect is completely negligible for all other variables, for which the fit values and uncertainty ranges overlap accurately.

The correlation between statistical uncertainties of the parameters are also shown in Table 7 for solution (a) and in Table 8 for solution (b). The correlations do not change significantly between the physics variables which remain stable between the solutions (a) and (b). The correlations with the two strong phases: $\delta_\parallel$ and $\delta_\perp$ flip the sign, as expected, except for the correlations that are smaller than 0.01. The correlations between $\delta_\parallel$ and $\delta_\perp$ themselves keep the same sign in both solutions (a) and (b).

Releasing the direct *CP* related λ parameter (see Section 5.1) in the fit results in a λ value compatible within the statistical precision with unity as well as with results of other experiments. The effect on the values of the other parameters of interest is negligible, due to small correlations with λ.

Table 6: Fitted values for the physical parameters of interest with their statistical and systematic uncertainties. For variables $\delta_\perp$ and $\delta_\parallel$ the values are given for the two solutions (a) and (b). The difference in $- 2\Delta\ln(L)$ between solutions (b) and (a) is 0.03. For the rest of the variables the values for the two minima are consistent. The same is true for the statistical and systematic uncertainties of all the variables.

Parameter	Value	Statistical uncertainty	Systematic uncertainty
ϕ_s [rad]	-0.081	0.041	0.022
$\Delta\Gamma_s$ [ps^{-1}]	0.0607	0.0047	0.0043
Γ_s [ps^{-1}]	0.6687	0.0015	0.0022
$|A_\parallel(0)|^2$	0.2213	0.0019	0.0023
$|A_0(0)|^2$	0.5131	0.0013	0.0038
$|A_S(0)|^2$	0.0321	0.0033	0.0046
$\delta_\perp - \delta_S$ [rad]	-0.25	0.05	0.04
Solution (a)			
$\delta_\perp$ [rad]	3.12	0.11	0.06
$\delta_\parallel$ [rad]	3.35	0.05	0.09
Solution (b)			
$\delta_\perp$ [rad]	2.91	0.11	0.06
$\delta_\parallel$ [rad]	2.94	0.05	0.09

Table 7: Fit correlations between the physical parameters of interest, obtained from the fit for solution (a).

	$\Delta\Gamma$	Γ_s	$|A_\parallel(0)|^2$	$|A_0(0)|^2$	$|A_S(0)|^2$	$\delta_\parallel$	$\delta_\perp$	$\delta_\perp - \delta_S$
ϕ_s	-0.080	0.017	-0.003	-0.004	-0.007	0.007	0.004	-0.007
$\Delta\Gamma$	1	-0.586	0.090	0.095	0.051	0.032	0.005	0.020
Γ_s		1	-0.125	-0.045	0.080	-0.086	-0.023	0.015
$|A_\parallel(0)|^2$			1	-0.341	-0.172	0.522	0.133	-0.052
$|A_0(0)|^2$				1	0.276	-0.103	-0.034	0.070
$|A_S(0)|^2$					1	-0.362	-0.118	0.244
$\delta_\parallel$						1	0.254	-0.085
$\delta_\perp$							1	0.001

7.2 Fit to strong phases

As shown in Table 6, the likelihood fit has determined two solutions with well separated values for the strong phases $\delta_\parallel$ and $\delta_\perp$. Figure 9 shows results of the 2D log-likelihood scan in the $\delta_\parallel$, $\delta_\perp$ plane, revealing two minima, identified at ($\delta_\parallel = 3.35$, $\delta_\perp = 3.12$) and ($\delta_\parallel = 2.94$, $\delta_\perp = 2.91$). These minima are represented by two-dimensional contours at the level of $- 2\Delta\ln(L) = 2.30, 6.18$, and 11.83, where

Table 8: Fit correlations between the physical parameters of interest, obtained from the fit for solution (b).

	$\Delta\Gamma$	Γ_s	$|A_{||}(0)|^2$	$|A_0(0)|^2$	$|A_S(0)|^2$	$\delta_{||}$	$\delta_{\perp}$	$\delta_{\perp} - \delta_S$
ϕ_s	-0.084	0.019	-0.011	-0.003	-0.006	0.007	0.005	-0.006
$\Delta\Gamma$	1	-0.586	0.090	0.096	0.057	-0.029	-0.010	0.021
Γ_s		1	-0.116	-0.048	0.071	0.070	0.017	0.015
$|A_{||}(0)|^2$			1	-0.338	-0.110	-0.444	-0.106	-0.052
$|A_0(0)|^2$				1	0.269	0.080	0.017	0.070
$|A_S(0)|^2$					1	0.291	0.060	0.251
$\delta_{||}$						1	0.235	0.097
$\delta_{\perp}$							1	0.056

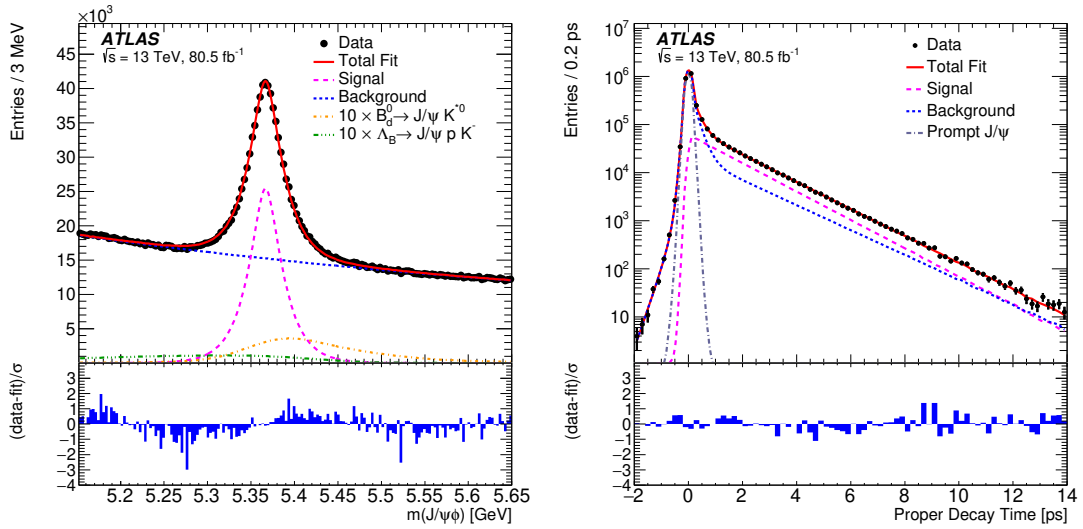Figure 7: (Left) Mass fit projection for the $B_s^0 \to J/\psi\phi$ sample. The red line shows the total fit, the short-dashed magenta line shows the $B_s^0 \to J/\psi\phi$ signal component, the combinatorial background is shown as a blue dotted line, the orange dash-dotted line shows the $B_d^0 \to J/\psi K^{0*}$ component, and the green dash-dot-dot line shows the contribution from $\Lambda_b \to J/\psi p K^-$ events. (Right) Proper decay time fit projection for the $B_s^0 \to J/\psi\phi$ sample. The red line shows the total fit while the short-dashed magenta line shows the total signal. The total background is shown as a blue dotted line, and a long-dashed grey line shows the prompt J/ψ background component. Below each figure is a ratio plot that shows the difference between each data point and the total fit line divided by the statistical and systematic uncertainties summed in quadrature (σ) of that point.
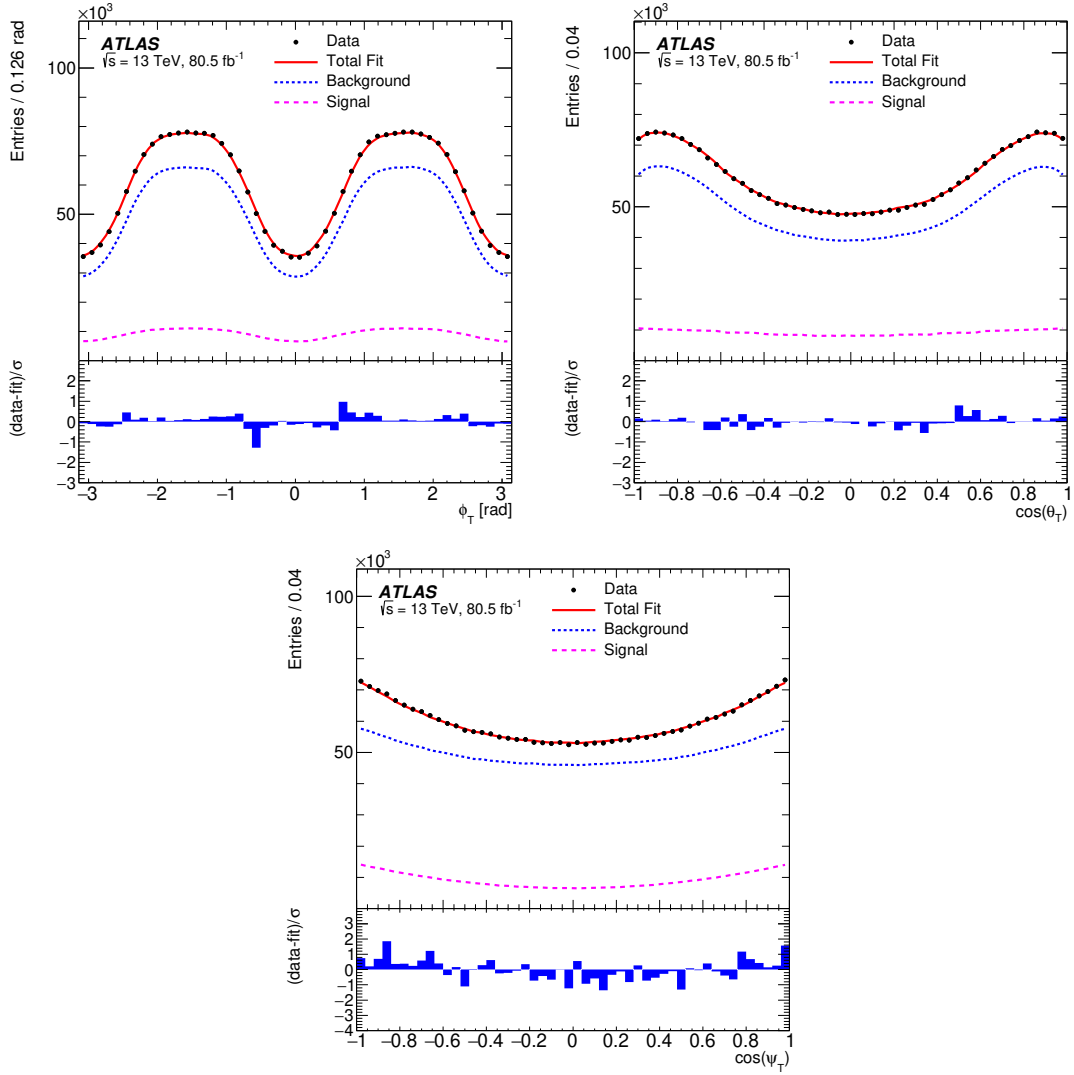
Figure 8: Fit projections for the transversity angles ϕ_T (top left), $\cos(\theta_T)$ (top right), and $\cos(\psi_T)$ (bottom). In all three plots the red solid line shows the total fit, the $B_s^0 \to J/\psi\phi$ signal component is shown by the magenta dashed line and the blue dotted line shows the contribution of all background components. Below each figure is a ratio plot that shows the difference between each data point and the total fit line divided by the statistical and systematic uncertainties summed in quadrature (σ) of that point.

$-2\Delta\ln(L) = 2(\ln(L^i) - \ln(L^a))$ is the difference between the likelihood values (L^i) of the fit in which the two strong phases are fixed to the values shown on the horizontal and vertical axis, and L^a which is the likelihood value for solution (a) of the fit.

An approximate symmetry in the signal PDF is at the origin of this duality. The strong phases are determined by the six interference terms 4) − 6) and 8) − 10) in Table 4. Four of them, namely terms 4), 5), 8) and 9), are invariant under the transformation

$$\{\delta_{\parallel}, \ \delta_{\perp}, \ \delta_S\} \rightarrow \{2\pi - \delta_{\parallel}, \ \delta_{\perp} + 2(\pi - \delta_{\parallel}), \ \delta_S + 2(\pi - \delta_{\parallel})\}. \tag{6}$$

This transformation is proportional to $\pi - \delta_{\parallel}$, which from our data is equal to 0.21. The two local maxima of the likelihood determined in this analysis satisfy the relation of Eq. (6) very accurately for $\delta_{\parallel}$ and ($\delta_{\perp}$ - δ_S), and within the statistical uncertainty in the transformation for $\delta_{\perp}$. The difference in the log-likelihoods, $-2\Delta\ln(L)$, between the two solutions is equal to 0.03, favouring (a) but without ruling out (b).

As discussed in Section 7.1, the two-fold nature of the likelihood maxima for the strong phases has a negligible effect on all the other variables. Figure 10 shows the one-dimensional likelihood scans for all other physics parameters, separately for the two solutions (a) and (b). For each scan, the other physics parameters and all nuisance parameters are optimised in a profile-likelihood fit. The 1D scans are almost identical for the two solutions.
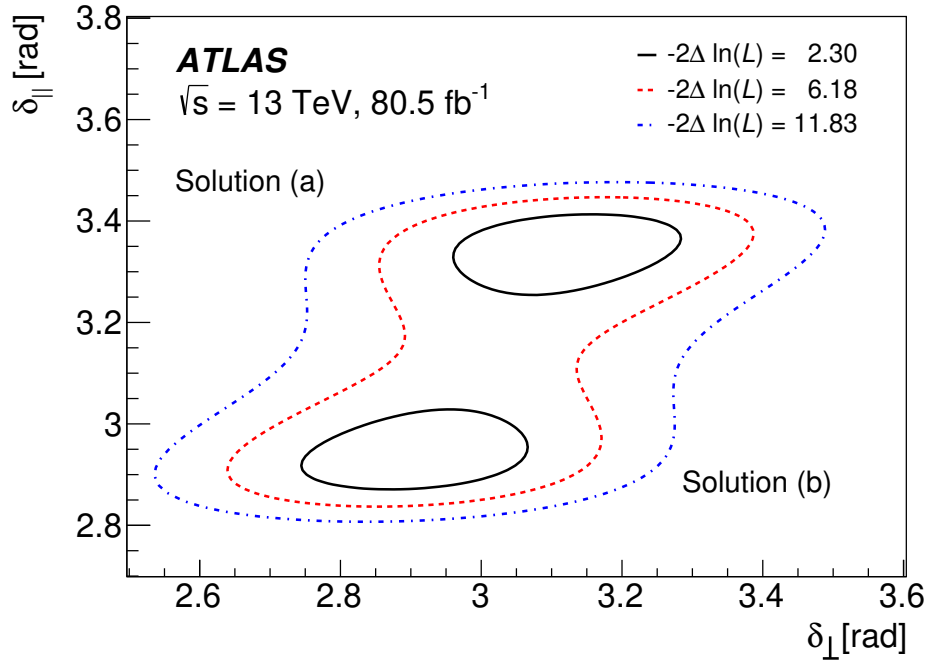

Figure 9: Two-dimensional constraints on the values of $\delta_{\parallel}$ and $\delta_{\perp}$ for solutions (a) and (b) at the level of $-2\Delta\ln(L) = 2.30, 6.18$, and 11.83 respectively created using a full 2D scan. The minimum of the solution (b) is $-2\Delta\ln(L) = 0.03$ higher than the minimum of the solution (a).
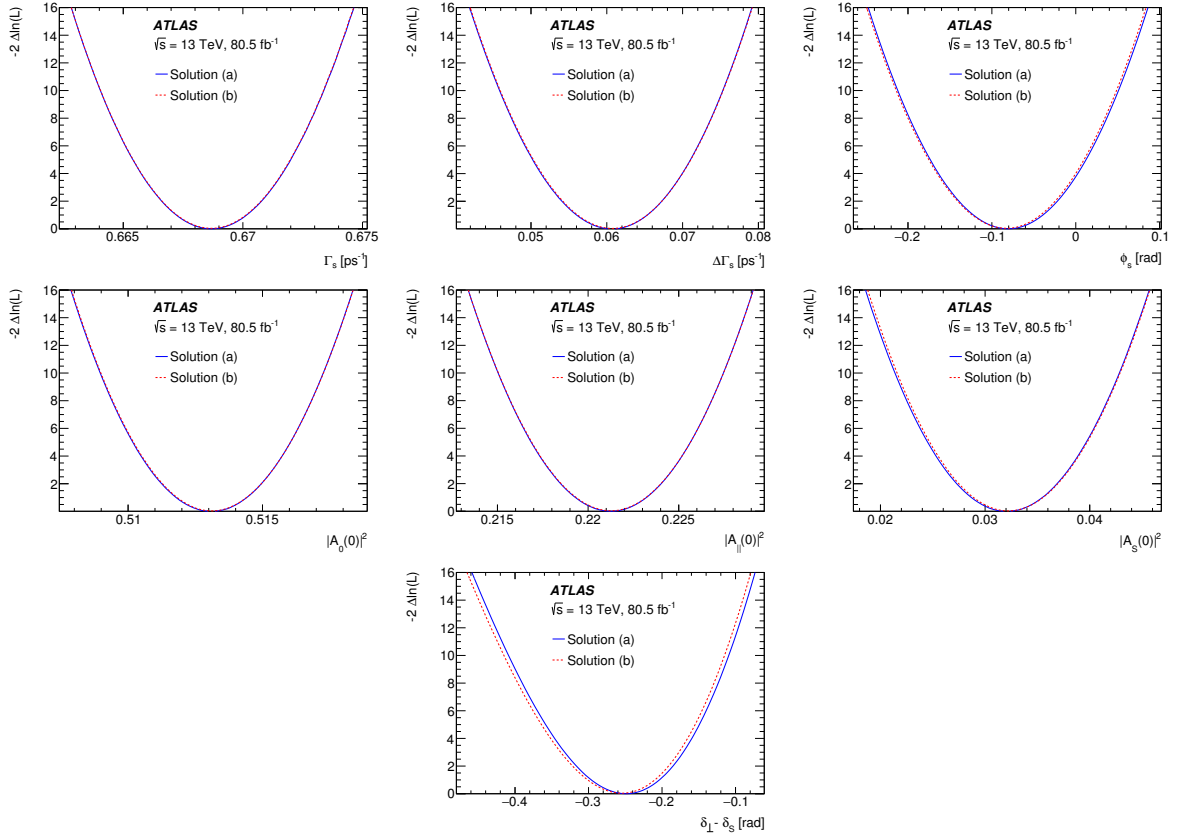
Figure 10: 1D log-likelihood scans of all other variables of the fit for the solution (a) (blue) and the solution (b) (dashed red). The variable on the vertical axis, $-2\Delta\ln(L) = 2(\ln(L^a) - \ln(L^i))$, is the difference between the likelihood values of the default fit, (L^a), and of the fit in which the physical parameter is fixed to values shown on the horizontal axis.

8 Combination with 7 TeV and 8 TeV results

The measured values of solution (a) and solution (b) are consistent with those obtained in the previous analysis [13] using 19.2 fb^{-1} of data collected at $\sqrt{s}$ = 7 TeV and 8 TeV. A best linear unbiased estimator (BLUE) [50, 51] is used to combine the current results with those from the previous analysis. The measured values, uncertainties, and correlations are taken from the measurements performed at each centre-of-mass energy. The statistical correlation between these three measurements is zero as the events are different. The correlations of the systematic uncertainties between the three measurements are estimated and tested in several categories depending on whether the given systematic effect changed significantly between the measurements. Solution (a) and solution (b) are treated separately, leading to the two sets of combined results as shown in Table 9. The correlation matrices of these two combinations are shown in Table 10 and Table 11.

The two-dimensional likelihood contours in the ϕ_s–$\Delta\Gamma_s$ plane for the ATLAS result based on 7 TeV and 8 TeV data, the solution (a) of the 13 TeV measurement, and the combined result for the solution (a) are shown in Figure 11. The statistical and systematic uncertainties are combined in quadrature and correlations

are taken into account in the construction of Gaussian contours. Because there is no significant difference in the ϕ_s and $\Delta\Gamma_s$ values between solution (a) and solution (b), only contours for solution (a) are shown.

Table 9: Values of the physical parameters extracted in the combination of solution (a) and solution (b) of 13 TeV results with those obtained from 7 TeV and 8 TeV data.

Parameter	Solution (a)			Solution (b)		
	Value	Statistical uncertainty	Systematic uncertainty	Value	Statistical uncertainty	Systematic uncertainty
ϕ_s [rad]	−0.087	0.036	0.021	−0.087	0.036	0.021
$\Delta\Gamma_s$ [ps^{-1}]	0.0657	0.0043	0.0037	0.0657	0.0043	0.0037
Γ_s [ps^{-1}]	0.6703	0.0014	0.0018	0.6704	0.0014	0.0018
$|A_\parallel(0)|^2$	0.2220	0.0017	0.0021	0.2218	0.0017	0.0021
$|A_0(0)|^2$	0.5152	0.0012	0.0034	0.5152	0.0012	0.0034
$|A_S|^2$	0.0343	0.0031	0.0045	0.0348	0.0031	0.0045
$\delta_\perp$ [rad]	3.22	0.10	0.05	3.03	0.10	0.05
$\delta_\parallel$ [rad]	3.36	0.05	0.09	2.95	0.05	0.09
$\delta_\perp - \delta_S$ [rad]	−0.24	0.05	0.04	−0.24	0.05	0.04

Table 10: Correlation matrix of the BLUE combination of the 7 TeV and 8 TeV results and the solution (a) of the 13 TeV result.

	$\Delta\Gamma$	Γ_s	$|A_\parallel(0)|^2$	$|A_0(0)|^2$	$|A_S(0)|^2$	$\delta_\perp$	$\delta_\parallel$	$\delta_\perp - \delta_S$
ϕ_s	−0.025	0.001	0.001	0.000	−0.001	0.003	0.003	−0.004
$\Delta\Gamma$	1	−0.259	0.043	0.027	0.020	0.003	0.011	0.010
Γ_s		1	−0.045	−0.009	0.025	−0.010	−0.021	0.006
$|A_\parallel(0)|^2$			1	−0.071	−0.056	0.068	0.155	−0.024
$|A_0(0)|^2$				1	0.048	−0.009	−0.015	0.016
$|A_S(0)|^2$					1	−0.056	−0.099	0.108
$\delta_\perp$						1	0.106	0.001
$\delta_\parallel$							1	−0.032

Two-dimensional likelihood contours in the ϕ_s−$\Delta\Gamma_s$ plane are shown in Figure 12 for this ATLAS result, the result from CMS [17] using the $B_s^0 \to J/\psi\phi$ decay, the result from LHCb [16] using the $B_s^0 \to J/\psi K^+K^-$ decay and finally the LHCb result including all B_s^0 channels [16, 18–21]. The contours are obtained by interpreting each result as a two-dimensional Gaussian probability distribution in the ϕ_s−$\Delta\Gamma_s$ plane. All results are consistent with each other and with the SM [5, 52].

Table 11: Correlation matrix of the BLUE combination of the 7 TeV and 8 TeV results and the solution (b) of the 13 TeV result.

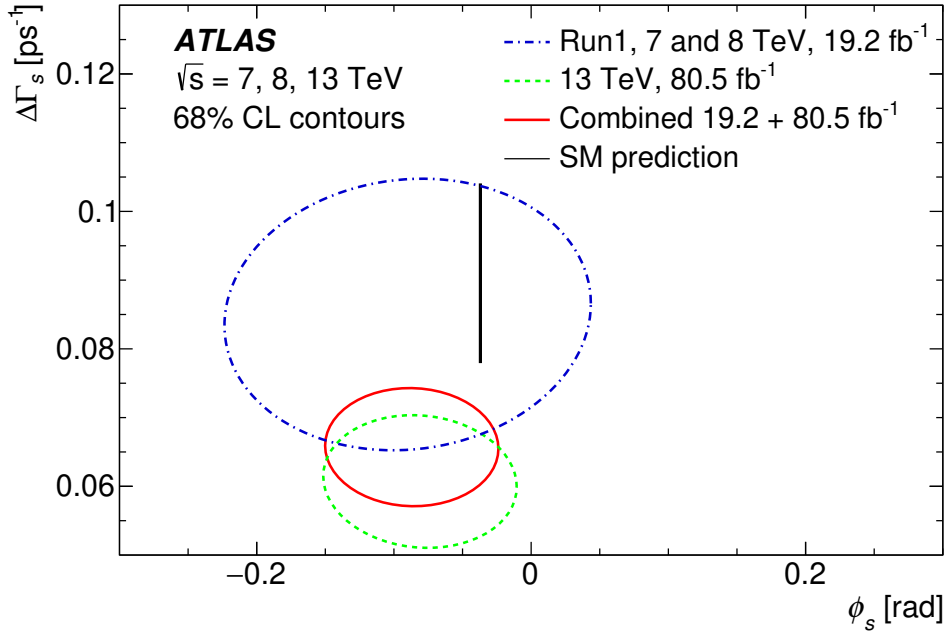|	$\Delta\Gamma$	Γ_s	$|A_\parallel(0)|^2$	$|A_0(0)|^2$	$|A_S(0)|^2$	$\delta_\perp$	$\delta_\parallel$	$\delta_\perp - \delta_S$
ϕ_s	-0.027	0.002	-0.003	0.001	-0.001	0.004	0.002	-0.003
$\Delta\Gamma$	1	-0.259	0.043	0.027	0.023	-0.006	-0.010	0.011
Γ_s		1	-0.042	-0.010	0.023	0.007	0.018	0.006
$|A_\parallel(0)|^2$			1	-0.071	-0.035	-0.053	-0.132	-0.024
$|A_0(0)|^2$				1	0.046	0.004	0.012	0.016
$|A_S(0)|^2$					1	0.027	0.080	0.111
$\delta_\perp$						1	0.098	0.037
$\delta_\parallel$							1	0.036

Figure 11: Contours of 68% confidence level in the ϕ_s–$\Delta\Gamma_s$ plane, showing ATLAS results for 7 TeV and 8 TeV data (blue dashed-dotted curve), for 13 TeV data (green dashed curve) and for 13 TeV data combined with 7 TeV and 8 TeV (red solid curve) data. The Standard Model prediction [5, 52] is shown as a very thin black rectangle. In all contours the statistical and systematic uncertainties are combined in quadrature and correlations are taken into account.
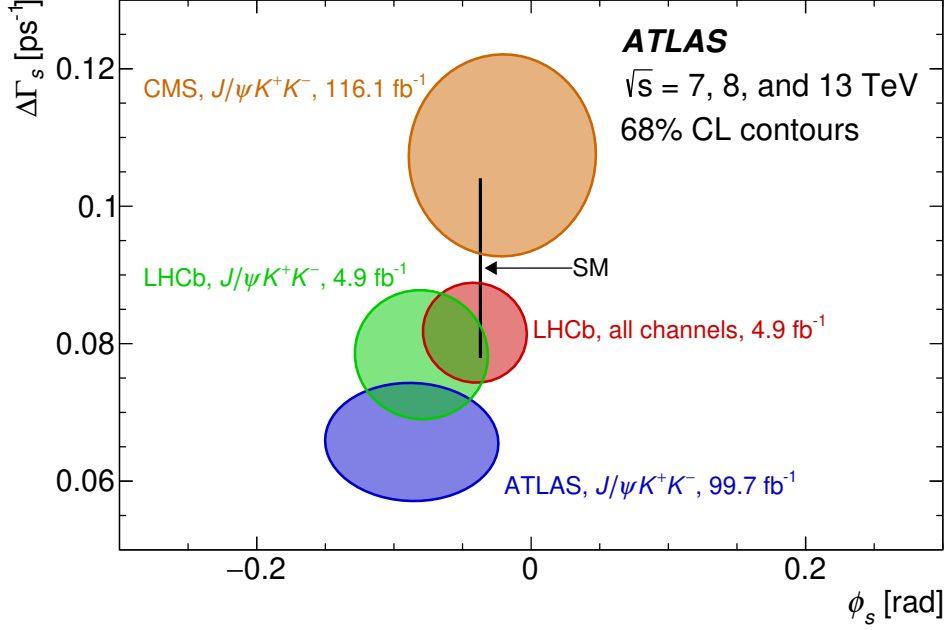
Figure 12: Contours of 68% confidence level in the ϕ_s–$\Delta\Gamma_s$ plane, including results from CMS (orange) and LHCb (green) using the $B_s^0 \to J/\psi K^+K^-$ decay only and LHCb (red) for all the channels. The blue contour shows the ATLAS result for 13 TeV combined with 7 TeV and 8 TeV. The Standard Model prediction [5, 52] is shown as a very thin black rectangle. In all contours the statistical and systematic uncertainties are combined in quadrature.

9 Summary

This paper presents a measurement of the time-dependent *CP* asymmetry parameters in $B_s^0 \to J/\psi\phi$ decays from an 80.5 fb^{-1} data sample of pp collisions collected with the ATLAS detector during the 13 TeV LHC run. The values from the 13 TeV analysis are consistent with those obtained in the previous ATLAS analysis using 7 TeV and 8 TeV data. The two measurements are statistically combined.

The *CP*-violating phase ϕ_s is measured to be -0.087 ± 0.036 (stat.) ± 0.021 (syst.) rad, the decay width difference between heavy and light B_s^0 mass eigenstates, $\Delta\Gamma_s = 0.0657 \pm 0.0043$ (stat.) ± 0.0037 (syst.) ps^{-1} and the measurement for their average decay width, $\Gamma_s = 0.6703 \pm 0.0014$ (stat.) ± 0.0018 (syst.) ps^{-1}. The measurement of the *CP*-violating phase ϕ_s is consistent with the Standard Model prediction, and it improves on the precision of previous ATLAS measurements, while for the average decay width, Γ_s, the comparison of the 13 TeV analysis with the current world combined value reveals a tension at the level of 3σ.

Acknowledgements

References

[1] F. J. Botella, G. C. Branco and M. Nebot,
CP violation and limits on New Physics including recent B_s measurements,
Nucl. Phys. B **768** (2007) 1, arXiv: 0608100 [hep-ph].

[2] CKMfitter group, Charles, J. et al.,
Current status of the Standard Model CKM fit and constraints on $\Delta F = 2$ New Physics,
Phys. Rev. D **91** (2015) 073007, Numbers updated using the results from the 2019 values in https://ckmfitter.in2p3.fr/www/results/plots_summer19/ckm_res_summer19.html,
arXiv: 1501.05013 [hep-ph].

[3] UTfit Collaboration, M. Bona et al., *The unitarity triangle fit in the standard model and hadronic parameters from lattice QCD: A reappraisal after the measurements of Δm_s and BR($B \to \tau \nu_\tau$)*,
JHEP **10** (2006) 081, Numbers updated to the 2018 results from https://www.utfit.org/UTfit/ResultsSummer2018SM,
arXiv: hep-ph/0606167 [hep-ph].

[4] LHCb Collaboration,
Precision measurement of the $B_s^0 - \bar{B}_s^0$ oscillation frequency with the decay $B_s^0 \to D_s^- \pi^+$,
New J. Phys. **15** (2013) 053021, arXiv: `1304.4741 [hep-ex]`.

[5] A. Lenz and G. Tetlalmatzi-Xolocotzi,
Model-independent bounds on new physics effects in non-leptonic tree-level decays of B-mesons,
JHEP **07** (2020) 177, arXiv: `1912.07621 [hep-ph]`.

[6] C. T. Davies et al.,
Lattice QCD matrix elements for the $B_s^0 - \bar{B}_s^0$ width difference beyond leading order,
Phys. Rev. Lett. **124** (2020) 082001, arXiv: `1910.00970 [hep-lat]`.

[7] A. Lenz and U. Nierste, *Theoretical update of $B_s - \bar{B}_s$ mixing*, JHEP **06** (2007) 072,
arXiv: `hep-ph/0612167`.

[8] A. Lenz, M. L. Piscopo and A. V. Rusov,
Contribution of the Darwin operator to non-leptonic decays of heavy quarks, JHEP **12** (2020) 199,
arXiv: `2004.09527 [hep-ph]`.

[9] P. Zyla et al., *Review of Particle Physics*, PTEP **2020** (2020) 083C01.

[10] D0 Collaboration, *Measurement of the CP-violating phase $\phi_s^{J/\psi\phi}$ using the flavor-tagged decay $B_s^0 \to J/\psi\phi$ in 8 fb^{-1} of $p\bar{p}$ collisions*, Phys. Rev. D **85** (2012) 032006,
arXiv: `1109.3166 [hep-ex]`.

[11] CDF Collaboration,
Measurement of the Bottom-Strange Meson Mixing Phase in the Full CDF Data Set,
Phys. Rev. Lett. **109** (2012) 171802, arXiv: `1208.2967 [hep-ex]`.

[12] LHCb Collaboration, *Precision Measurement of CP violation in $B_s^0 \to J/\psi K^+ K^-$ Decays*,
Phys. Rev. Lett. **114** (2015) 041801, arXiv: `1411.3104 [hep-ex]`.

[13] ATLAS Collaboration, *Measurement of the CP-violating phase ϕ_s and the B_s^0 meson decay width difference with $B_s^0 \to J/\psi\phi$ decays in ATLAS*, JHEP **08** (2016) 147,
arXiv: `1601.03297 [hep-ex]`.

[14] CMS Collaboration, *Measurement of the CP-violating weak phase ϕ_s and the decay width difference $\Delta\Gamma_s$ using the $B_s^0 \to J/\psi\phi(1020)$ decay channel in pp collisions at $\sqrt{s} = 8$ TeV*,
Phys. Lett. B **757** (2016) 97, arXiv: `1507.07527 [hep-ex]`.

[15] LHCb Collaboration, *Resonances and CP violation in B_s^0 and $\overline{B}_s^0 \to J/\psi K^+ K^-$ decays in the mass region above the $\phi(1020)$*, JHEP **08** (2017) 037, arXiv: `1704.08217 [hep-ex]`.

[16] LHCb Collaboration,
Updated measurement of time-dependent CP-violating observables in $B_s^0 \to J/\psi K^+ K^-$ decays,
Eur. Phys. J. **C79** (2019) 706, arXiv: `1906.08356 [hep-ex]`,
Erratum: Eur. Phys. J. **C80** (2020) 601.

[17] CMS Collaboration, *Measurement of the CP-violating phase ϕ_s in the $B_s^0 \to J/\psi \phi(1020) \to \mu^+\mu^- K^+ K^-$ channel in proton-proton collisions at $\sqrt{s} = 13$ TeV*,
Phys. Lett. B **816** (2021) 136188, arXiv: `2007.02434 [hep-ex]`.

[18] LHCb Collaboration,
First study of the CP -violating phase and decay-width difference in $B_s^0 \to \psi(2S)\phi$ decays,
Phys. Lett. B **762** (2016) 253, arXiv: `1608.04855 [hep-ex]`.

[19] LHCb Collaboration, *Measurement of the CP-violating phase ϕ_s in $\bar{B}^0_s \to D^+_s D^-_s$ decays*, Phys. Rev. Lett. **113** (2014) 211801, arXiv: 1409.4619 [hep-ex].

[20] LHCb Collaboration, *Measurement of the CP-violating phase ϕ_s in $\overline{B}^0_s \to J/\psi\pi^+\pi^-$ decays*, Phys. Lett. **B736** (2014) 186, arXiv: 1405.4140 [hep-ex].

[21] LHCb Collaboration, *Measurement of the CP-violating phase ϕ_s from $B^0_s \to J/\psi\pi^+\pi^-$ decays in 13 TeV pp collisions*, Phys. Lett. **B797** (2019) 134789, arXiv: 1903.05530 [hep-ex].

[22] ATLAS Collaboration, *The ATLAS Experiment at the CERN Large Hadron Collider*, JINST **3** (2008) S08003.

[23] ATLAS Collaboration, *ATLAS Insertable B-Layer Technical Design Report*, ATLAS-TDR-19; CERN-LHCC-2010-013, 2010, URL: https://cds.cern.ch/record/1291633.

[24] B. Abbott et al., *Production and Integration of the ATLAS Insertable B-Layer*, JINST **13** (2018) T05008, arXiv: 1803.00844 [physics.ins-det].

[25] ATLAS Collaboration, *Luminosity determination in pp collisions at $\sqrt{s} = 13$ TeV using the ATLAS detector at the LHC*, ATLAS-CONF-2019-021, 2019, URL: https://cds.cern.ch/record/2677054.

[26] G. Avoni et al., *The new LUCID-2 detector for luminosity measurement and monitoring in ATLAS*, JINST **13** (2018) P07017.

[27] T. Sjöstrand et al., *An Introduction to PYTHIA 8.2*, Comput. Phys. Commun. **191** (2015) 159, arXiv: 1410.3012 [hep-ph].

[28] ATLAS Collaboration, *ATLAS Pythia 8 tunes to 7 TeV data*, ATL-PHYS-PUB-2014-021, 2014, URL: https://cds.cern.ch/record/1966419.

[29] J. Pumplin et al., *New generation of parton distributions with uncertainties from global QCD analysis*, JHEP **07** (2002) 012, arXiv: hep-ph/0201195.

[30] ATLAS Collaboration, *The ATLAS Simulation Infrastructure*, Eur. Phys. J. C **70** (2010) 823, arXiv: 1005.4568 [physics.ins-det].

[31] S. Agostinelli et al., *Geant4—a simulation toolkit*, Nucl. Instrum. Meth. A **506** (2003) 250.

[32] ATLAS Collaboration, *Muon reconstruction performance of the ATLAS detector in proton–proton collision data at $\sqrt{s} = 13$ TeV*, Eur. Phys. J. C **76** (2016) 292, arXiv: 1603.05598 [hep-ex].

[33] M. Tanabashi et al., *Review of Particle Physics*, Phys. Rev. D **98** (2018) 030001.

[34] ATLAS Collaboration, *Electron and photon performance measurements with the ATLAS detector using the 2015–2017 LHC proton–proton collision data*, JINST **14** (2019) P12006, arXiv: 1908.00005 [hep-ex].

[35] ATLAS Collaboration, *Topological cell clustering in the ATLAS calorimeters and its performance in LHC Run 1*, Eur. Phys. J. C **77** (2017) 490, arXiv: 1603.02934 [hep-ex].

[36] M. Cacciari, G. P. Salam and G. Soyez, *The anti-k_t jet clustering algorithm*, JHEP **04** (2008) 063, arXiv: 0802.1189 [hep-ph].

[37] M. Cacciari, G. P. Salam and G. Soyez, *FastJet user manual*, Eur. Phys. J. C **72** (2012) 1896, arXiv: 1111.6097 [hep-ph].

[38] ATLAS Collaboration, *ATLAS b-jet identification performance and efficiency measurement with $t\bar{t}$ events in pp collisions at $\sqrt{s}$ = 13 TeV*, Eur. Phys. J. C **79** (2019) 970, arXiv: 1907.05120 [hep-ex].

[39] A. S. Dighe, I. Dunietz and R. Fleischer, *Extracting CKM phases and $B_s - \bar{B}_s$ mixing parameters from angular distributions of non-leptonic B decays*, Eur. Phys. J. C **6** (1999) 647, arXiv: hep-ph/9804253.

[40] S. Stone and L. Zhang, *S-waves and the Measurement of CP Violating Phases in B_s Decays*, Phys. Rev. **D79** (2009) 074024, arXiv: 0812.2832 [hep-ph].

[41] ATLAS Collaboration, *Time-dependent angular analysis of the decay $B_s^0 \to J/\psi\phi$ and extraction of $\Delta\Gamma_s$ and the CP-violating weak phase ϕ_s by ATLAS*, JHEP **12** (2012) 072, arXiv: 1208.0572 [hep-ex].

[42] LHCb Collaboration,
Updated average f_s/f_d b-hadron production fraction ratio for 7 TeV pp collisions,
LHCb-CONF-2013-011, 2013, URL: https://cds.cern.ch/record/1559262.

[43] BaBar Collaboration, *Search for the $Z(4430)^-$ at BABAR*, Phys. Rev. D **79** (2009) 112001, arXiv: 0811.0564 [hep-ex].

[44] LHCb Collaboration, *Study of the kinematic dependences of Λ_b^0 production in pp collisions and a measurement of the $\Lambda_b^0 \to \Lambda_c^+ \pi^-$ branching fraction*, JHEP **08** (2014) 143, arXiv: 1405.6842 [hep-ex].

[45] LHCb Collaboration, *Study of the production of Λ_b^0 and $\overline{B}^0$ hadrons in pp collisions and first measurement of the $\Lambda_b^0 \to J/\psi pK^-$ branching fraction*, Chin. Phys. C **40** (2016) 011001, arXiv: 1509.00292 [hep-ex].

[46] LHCb Collaboration,
Observation of $J/\psi p$ Resonances Consistent with Pentaquark States in $\Lambda_b^0 \to J/\psi K^- p$ Decays,
Phys. Rev. Lett. **115** (2015) 072001, arXiv: 1507.03414 [hep-ex].

[47] LHCb Collaboration, *Measurement of the polarization amplitudes in $B^0 \to J/\psi K^*(892)^0$ decays*, Phys. Rev. D **88** (2013) 052002, arXiv: 1307.2782 [hep-ex].

[48] S. M. Flatté, *Coupled - Channel Analysis of the $\pi\eta$ and $K\bar{K}$ Systems Near $K\bar{K}$ Threshold*, Phys. Lett. B **63** (1976) 224.

[49] LHCb Collaboration, *Measurement of resonant and CP components in $\bar{B}_s^0 \to J/\psi\pi^+\pi^-$ decays*, Phys.Rev. D **89** (2014) 092006, arXiv: 1402.6248 [hep-ex].

[50] L. Lyons, D. Gibaut and P. Clifford,
How to Combine Correlated Estimates of a Single Physical Quantity,
Nucl. Instrum. Meth. **A270** (1988) 110.

[51] A. Valassi, *Combining correlated measurements of several different physical quantities*, Nucl. Instrum. Meth. **A500** (2003) 391.

[52] J. Charles et al.,
Current status of the Standard Model CKM fit and constraints on $\Delta F = 2$ New Physics,
Phys. Rev. **D91** (2015) 073007, arXiv: 1501.05013 [hep-ph].

[53]   ATLAS Collaboration, *ATLAS Computing Acknowledgements*, ATL-SOFT-PUB-2020-001,
          URL: https://cds.cern.ch/record/2717821.

The ATLAS Collaboration

G. Aad[102], B. Abbott[129], D.C. Abbott[103], O. Abdinov[13,*], A. Abed Abud[71a,71b], K. Abeling[53],
D.K. Abhayasinghe[94], S.H. Abidi[168], O.S. AbouZeid[40], N.L. Abraham[157], H. Abramowicz[162],
H. Abreu[161], Y. Abulaiti[6], B.S. Acharya[67a,67b,q], B. Achkar[53], S. Adachi[164], L. Adam[100],
C. Adam Bourdarios[65], L. Adamczyk[84a], L. Adamek[168], J. Adelman[121], M. Adersberger[114],
A. Adiguzel[12c,an], S. Adorni[54], T. Adye[144], A.A. Affolder[146], Y. Afik[161], C. Agapopoulou[65],
M.N. Agaras[38], A. Aggarwal[119], C. Agheorghiesei[27c], J.A. Aguilar-Saavedra[140f,140a,am], F. Ahmadov[80],
W.S. Ahmed[104], X. Ai[18], G. Aielli[74a,74b], S. Akatsuka[86], T.P.A. Åkesson[97], E. Akilli[54], A.V. Akimov[111],
K. Al Khoury[65], G.L. Alberghi[23b,23a], J. Albert[177], M.J. Alconada Verzini[162], S. Alderweireldt[36],
M. Aleksa[36], I.N. Aleksandrov[80], C. Alexa[27b], D. Alexandre[19], T. Alexopoulos[10], A. Alfonsi[120],
M. Alhroob[129], B. Ali[142], G. Alimonti[69a], J. Alison[37], S.P. Alkire[149], C. Allaire[65], B.M.M. Allbrooke[157],
B.W. Allen[132], P.P. Allport[21], A. Aloisio[70a,70b], A. Alonso[40], F. Alonso[89], C. Alpigiani[149],
A.A. Alshehri[57], M. Alvarez Estevez[99], D. Álvarez Piqueras[175], M.G. Alviggi[70a,70b],
Y. Amaral Coutinho[81b], A. Ambler[104], L. Ambroz[135], C. Amelung[26], D. Amidei[106],
S.P. Amor Dos Santos[140a], S. Amoroso[46], C.S. Amrouche[54], F. An[79], C. Anastopoulos[150], N. Andari[145],
T. Andeen[11], C.F. Anders[61b], J.K. Anders[20], A. Andreazza[69a,69b], V. Andrei[61a], C.R. Anelli[177],
S. Angelidakis[38], A. Angerami[39], A.V. Anisenkov[122b,122a], A. Annovi[72a], C. Antel[61a], M.T. Anthony[150],
M. Antonelli[51], D.J.A. Antrim[172], F. Anulli[73a], M. Aoki[82], J.A. Aparisi Pozo[175], L. Aperio Bella[36],
G. Arabidze[107], J.P. Araque[140a], V. Araujo Ferraz[81b], R. Araujo Pereira[81b], C. Arcangeletti[51],
A.T.H. Arce[49], F.A. Arduh[89], J-F. Arguin[110], S. Argyropoulos[78], J.-H. Arling[46], A.J. Armbruster[36],
L.J. Armitage[93], A. Armstrong[172], O. Arnaez[168], H. Arnold[120], A. Artamonov[124,*], G. Artoni[135],
S. Artz[100], S. Asai[164], N. Asbah[59], E.M. Asimakopoulou[173], L. Asquith[157], K. Assamagan[29], R. Astalos[28a],
R.J. Atkin[33a], M. Atkinson[174], N.B. Atlay[152], H. Atmani[65], K. Augsten[142], G. Avolio[36], R. Avramidou[60a],
M.K. Ayoub[15a], A.M. Azoulay[169b], G. Azuelos[110,ba], M.J. Baca[21], H. Bachacou[145], K. Bachas[68a,68b],
M. Backes[135], F. Backman[45a,45b], P. Bagnaia[73a,73b], M. Bahmani[85], H. Bahrasemani[153], A.J. Bailey[175],
V.R. Bailey[174], J.T. Baines[144], M. Bajic[40], C. Bakalis[10], O.K. Baker[184], P.J. Bakker[120], D. Bakshi Gupta[8],
S. Balaji[158], E.M. Baldin[122b,122a], P. Balek[181], F. Balli[145], W.K. Balunas[135], J. Balz[100], E. Banas[85],
A. Bandyopadhyay[24], Sw. Banerjee[182,k], A.A.E. Bannoura[183], L. Barak[162], W.M. Barbe[38],
E.L. Barberio[105], D. Barberis[55b,55a], M. Barbero[102], T. Barillari[115], M-S. Barisits[36], J. Barkeloo[132],
T. Barklow[154], R. Barnea[161], S.L. Barnes[60c], B.M. Barnett[144], R.M. Barnett[18], Z. Barnovska-Blenessy[60a],
A. Baroncelli[60a], G. Barone[29], A.J. Barr[135], L. Barranco Navarro[45a,45b], F. Barreiro[99],
J. Barreiro Guimarães da Costa[15a], S. Barsov[138], R. Bartoldus[154], G. Bartolini[102], A.E. Barton[90],
P. Bartos[28a], A. Basalaev[46], A. Bassalat[65,au], R.L. Bates[57], S.J. Batista[168], S. Batlamous[35f], J.R. Batley[32],
B. Batool[152], M. Battaglia[146], M. Bauce[73a,73b], F. Bauer[145,*], K.T. Bauer[172], H.S. Bawa[31,o],
J.B. Beacham[49], T. Beau[136], P.H. Beauchemin[171], F. Becherer[52], P. Bechtle[24], H.C. Beck[53], H.P. Beck[20,u],
K. Becker[52], M. Becker[100], C. Becot[46], A. Beddall[12d], A.J. Beddall[12a], V.A. Bednyakov[80],
M. Bedognetti[120], C.P. Bee[156], T.A. Beermann[77], M. Begalli[81b], M. Begel[29], A. Behera[156], J.K. Behr[46],
F. Beisiegel[24], A.S. Bell[95], G. Bella[162], L. Bellagamba[23b], A. Bellerive[34], P. Bellos[9],
K. Beloborodov[122b,122a], K. Belotskiy[112], N.L. Belyaev[112], D. Benchekroun[35a], N. Benekos[10],
Y. Benhammou[162], D.P. Benjamin[6], M. Benoit[54], J.R. Bensinger[26], S. Bentvelsen[120], L. Beresford[135],
M. Beretta[51], D. Berge[46], E. Bergeaas Kuutmann[173], N. Berger[5], B. Bergmann[142], L.J. Bergsten[26],
J. Beringer[18], S. Berlendis[7], N.R. Bernard[103], G. Bernardi[136], C. Bernius[154], F.U. Bernlochner[24],
T. Berry[94], P. Berta[100], C. Bertella[15a], I.A. Bertram[90], G.J. Besjes[40], O. Bessidskaia Bylund[183],
N. Besson[145], A. Bethani[101], S. Bethke[115], A. Betti[24], A.J. Bevan[93], J. Beyer[115], R. Bi[139], R.M. Bianchi[139],
O. Biebel[114], D. Biedermann[19], R. Bielski[36], K. Bierwagen[100], N.V. Biesuz[72a,72b], M. Biglietti[75a],

T.R.V. Billoud[110], M. Bindi[53], A. Bingul[12d], C. Bini[73a,73b], S. Biondi[23b,23a], M. Birman[181], T. Bisanz[53],
J.P. Biswal[162], A. Bitadze[101], C. Bittrich[48], K. Bjørke[134], K.M. Black[25], T. Blazek[28a], I. Bloch[46],
C. Blocker[26], A. Blue[57], U. Blumenschein[93], G.J. Bobbink[120], V.S. Bobrovnikov[122b,122a], S.S. Bocchetta[97],
A. Bocci[49], D. Bogavac[14], A.G. Bogdanchikov[122b,122a], C. Bohm[45a], V. Boisvert[94], P. Bokan[53], T. Bold[84a],
A.S. Boldyrev[113], A.E. Bolz[61b], M. Bomben[136], M. Bona[93], J.S. Bonilla[132], M. Boonekamp[145],
H.M. Borecka-Bielska[91], A. Borisov[123], G. Borissov[90], J. Bortfeldt[36], D. Bortoletto[135],
V. Bortolotto[74a,74b], D. Boscherini[23b], M. Bosman[14], J.D. Bossio Sola[104], K. Bouaouda[35a], J. Boudreau[139],
E.V. Bouhova-Thacker[90], D. Boumediene[38], S.K. Boutle[57], A. Boveia[127], J. Boyd[36], D. Boye[33c,av],
I.R. Boyko[80], A.J. Bozson[94], J. Bracinik[21], N. Brahimi[102], G. Brandt[183], O. Brandt[61a], F. Braren[46],
B. Brau[103], J.E. Brau[132], W.D. Breaden Madden[57], K. Brendlinger[46], L. Brenner[46], R. Brenner[173],
S. Bressler[181], B. Brickwedde[100], D.L. Briglin[21], D. Britton[57], D. Britzger[115], I. Brock[24], R. Brock[107],
G. Brooijmans[39], W.K. Brooks[147d], E. Brost[121], J.H Broughton[21], P.A. Bruckman de Renstrom[85],
D. Bruncko[28b], A. Bruni[23b], G. Bruni[23b], L.S. Bruni[120], S. Bruno[74a,74b], B.H. Brunt[32], M. Bruschi[23b],
N. Bruscino[139], P. Bryant[37], L. Bryngemark[97], T. Buanes[17], Q. Buat[36], P. Buchholz[152], A.G. Buckley[57],
I.A. Budagov[80], M.K. Bugge[134], F. Bührer[52], O. Bulekov[112], T.J. Burch[121], S. Burdin[91], C.D. Burgard[120],
A.M. Burger[130], B. Burghgrave[8], J.T.P. Burr[46], J.C. Burzynski[103], V. Büscher[100], E. Buschmann[53],
P.J. Bussey[57], J.M. Butler[25], C.M. Buttar[57], J.M. Butterworth[95], P. Butti[36], W. Buttinger[36], A. Buzatu[159],
A.R. Buzykaev[122b,122a], G. Cabras[23b,23a], S. Cabrera Urbán[175], D. Caforio[56], H. Cai[174], V.M.M. Cairo[154],
O. Cakir[4a], N. Calace[36], P. Calafiura[18], A. Calandri[102], G. Calderini[136], P. Calfayan[66], G. Callea[57],
L.P. Caloba[81b], S. Calvente Lopez[99], D. Calvet[38], S. Calvet[38], T.P. Calvet[156], M. Calvetti[72a,72b],
R. Camacho Toro[136], S. Camarda[36], D. Camarero Munoz[99], P. Camarri[74a,74b], D. Cameron[134],
R. Caminal Armadans[103], C. Camincher[36], S. Campana[36], M. Campanelli[95], A. Camplani[40],
A. Campoverde[152], V. Canale[70a,70b], A. Canesse[104], M. Cano Bret[60c], J. Cantero[130], T. Cao[162], Y. Cao[12b],
M.D.M. Capeans Garrido[36], M. Capua[41b,41a], R. Cardarelli[74a], F. Cardillo[150], G. Carducci[41b,41a],
I. Carli[143], T. Carli[36], G. Carlino[70a], B.T. Carlson[139], L. Carminati[69a,69b], R.M.D. Carney[45a,45b],
S. Caron[119], E. Carquin[147d], S. Carrá[46], J.W.S. Carter[168], M.P. Casado[14,f], A.F. Casha[168], D.W. Casper[172],
R. Castelijn[120], F.L. Castillo[175], V. Castillo Gimenez[175], N.F. Castro[140a,140e], A. Catinaccio[36],
J.R. Catmore[134], A. Cattai[36], J. Caudron[24], V. Cavaliere[29], E. Cavallaro[14], M. Cavalli-Sforza[14],
V. Cavasinni[72a,72b], E. Celebi[12b], F. Ceradini[75a,75b], L. Cerda Alberich[175], K. Cerny[131], A.S. Cerqueira[81a],
A. Cerri[157], L. Cerrito[74a,74b], F. Cerutti[18], A. Cervelli[23b,23a], S.A. Cetin[12b], Z. Chadi[35a], D. Chakraborty[121],
S.K. Chan[59], W.S. Chan[120], W.Y. Chan[91], J.D. Chapman[32], B. Chargeishvili[160b], D.G. Charlton[21],
T.P. Charman[93], C.C. Chau[34], S. Che[127], A. Chegwidden[107], S. Chekanov[6], S.V. Chekulaev[169a],
G.A. Chelkov[80,as], M.A. Chelstowska[36], B. Chen[79], C. Chen[60a], C.H. Chen[79], H. Chen[29], J. Chen[60a],
J. Chen[39], S. Chen[137], S.J. Chen[15c], X. Chen[15b,az], Y. Chen[83], Y-H. Chen[46], H.C. Cheng[63a], H.J. Cheng[15a],
A. Cheplakov[80], E. Cheremushkina[123], R. Cherkaoui El Moursli[35f], E. Cheu[7], K. Cheung[64],
T.J.A. Chevalérias[145], L. Chevalier[145], V. Chiarella[51], G. Chiarelli[72a], G. Chiodini[68a], A.S. Chisholm[36,21],
A. Chitan[27b], I. Chiu[164], Y.H. Chiu[177], M.V. Chizhov[80], K. Choi[66], A.R. Chomont[73a,73b], S. Chouridou[163],
Y.S. Chow[120], M.C. Chu[63a], X. Chu[15a,15d], J. Chudoba[141], A.J. Chuinard[104], J.J. Chwastowski[85],
L. Chytka[131], K.M. Ciesla[85], D. Cinca[47], V. Cindro[92], I.A. Cioară[27b], A. Ciocio[18], F. Cirotto[70a,70b],
Z.H. Citron[181,m], M. Citterio[69a], D.A. Ciubotaru[27b], B.M. Ciungu[168], A. Clark[54], M.R. Clark[39],
P.J. Clark[50], C. Clement[45a,45b], Y. Coadou[102], M. Cobal[67a,67c], A. Coccaro[55b], J. Cochran[79], H. Cohen[162],
A.E.C. Coimbra[36], L. Colasurdo[119], B. Cole[39], A.P. Colijn[120], J. Collot[58], P. Conde Muiño[140a,g],
E. Coniavitis[52], S.H. Connell[33c], I.A. Connelly[57], S. Constantinescu[27b], F. Conventi[70a,bb],
A.M. Cooper-Sarkar[135], F. Cormier[176], K.J.R. Cormier[168], L.D. Corpe[95], M. Corradi[73a,73b],
E.E. Corrigan[97], F. Corriveau[104,ai], M.J. Costa[175], F. Costanza[5], D. Costanzo[150], G. Cowan[94],
J.W. Cowley[32], J. Crane[101], K. Cranmer[125], S.J. Crawley[57], R.A. Creager[137], S. Crépé-Renaudin[58],
F. Crescioli[136], M. Cristinziani[24], V. Croft[120], G. Crosetti[41b,41a], A. Cueto[5], T. Cuhadar Donszelmann[150],

A.R. Cukierman[154], S. Czekierda[85], P. Czodrowski[36], M.J. Da Cunha Sargedas De Sousa[60b],
J.V. Da Fonseca Pinto[81b], C. Da Via[101], W. Dabrowski[84a], T. Dado[28a], S. Dahbi[35f], T. Dai[106],
C. Dallapiccola[103], M. Dam[40], G. D'amen[23b,23a], V. D'Amico[75a,75b], J. Damp[100], J.R. Dandoy[137],
M.F. Daneri[30], N.P. Dang[182,k], N.S. Dann[101], M. Danninger[176], V. Dao[36], G. Darbo[55b], O. Dartsi[5],
A. Dattagupta[132], T. Daubney[46], S. D'Auria[69a,69b], W. Davey[24], C. David[46], T. Davidek[143], D.R. Davis[49],
I. Dawson[150], K. De[8], R. De Asmundis[70a], M. De Beurs[120], S. De Castro[23b,23a], S. De Cecco[73a,73b],
N. De Groot[119], P. de Jong[120], H. De la Torre[107], A. De Maria[15c], D. De Pedis[73a], A. De Salvo[73a],
U. De Sanctis[74a,74b], M. De Santis[74a,74b], A. De Santo[157], K. De Vasconcelos Corga[102],
J.B. De Vivie De Regie[65], C. Debenedetti[146], D.V. Dedovich[80], A.M. Deiana[42], M. Del Gaudio[41b,41a],
J. Del Peso[99], Y. Delabat Diaz[46], D. Delgove[65], F. Deliot[145,t], C.M. Delitzsch[7], M. Della Pietra[70a,70b],
D. Della Volpe[54], A. Dell'Acqua[36], L. Dell'Asta[74a,74b], M. Delmastro[5], C. Delporte[65], P.A. Delsart[58],
D.A. DeMarco[168], S. Demers[184], M. Demichev[80], G. Demontigny[110], S.P. Denisov[123], D. Denysiuk[120],
L. D'Eramo[136], D. Derendarz[85], J.E. Derkaoui[35e], F. Derue[136], P. Dervan[91], K. Desch[24], C. Deterre[46],
K. Dette[168], C. Deutsch[24], M.R. Devesa[30], P.O. Deviveiros[36], A. Dewhurst[144], S. Dhaliwal[26],
F.A. Di Bello[54], A. Di Ciaccio[74a,74b], L. Di Ciaccio[5], W.K. Di Clemente[137], C. Di Donato[70a,70b],
A. Di Girolamo[36], G. Di Gregorio[72a,72b], B. Di Micco[75a,75b], R. Di Nardo[103], K.F. Di Petrillo[59],
R. Di Sipio[168], D. Di Valentino[34], C. Diaconu[102], F.A. Dias[40], T. Dias Do Vale[140a], M.A. Diaz[147a],
J. Dickinson[18], E.B. Diehl[106], J. Dietrich[19], A. Dimitrievska[18], W. Ding[15b],
J. Dingfelder[24], F. Dittus[36], F. Djama[102], T. Djobava[160b], J.I. Djuvsland[17], M.A.B. Do Vale[148],
M. Dobre[27b], D. Dodsworth[26], C. Doglioni[97], J. Dolejsi[143], Z. Dolezal[143], M. Donadelli[81c], B. Dong[60c],
J. Donini[38], A. D'onofrio[93], M. D'Onofrio[91], J. Dopke[144], A. Doria[70a], M.T. Dova[89], A.T. Doyle[57],
E. Drechsler[153], E. Dreyer[153], T. Dreyer[53], A.S. Drobac[171], Y. Duan[60b], F. Dubinin[111], M. Dubovsky[28a],
A. Dubreuil[54], E. Duchovni[181], G. Duckeck[114], A. Ducourthial[136], O.A. Ducu[110], D. Duda[115],
A. Dudarev[36], A.C. Dudder[100], E.M. Duffield[18], L. Duflot[65], M. Dührssen[36], C. Dülsen[183],
M. Dumancic[181], A.E. Dumitriu[27b], A.K. Duncan[57], M. Dunford[61a], A. Duperrin[102], H. Duran Yildiz[4a],
M. Düren[56], A. Durglishvili[160b], D. Duschinger[48], B. Dutta[46], D. Duvnjak[1], G.I. Dyckes[137], M. Dyndal[36],
S. Dysch[101], B.S. Dziedzic[85], K.M. Ecker[115], R.C. Edgar[106], T. Eifert[36], G. Eigen[17], K. Einsweiler[18],
T. Ekelof[173], H. El Jarrari[35f], M. El Kacimi[35c], R. El Kosseifi[102], V. Ellajosyula[173], M. Ellert[173],
F. Ellinghaus[183], A.A. Elliot[93], N. Ellis[36], J. Elmsheuser[29], M. Elsing[36], D. Emeliyanov[144], A. Emerman[39],
Y. Enari[164], M.B. Epland[49], J. Erdmann[47], A. Ereditato[20], M. Errenst[36], M. Escalier[65], C. Escobar[175],
O. Estrada Pastor[175], E. Etzion[162], H. Evans[66], A. Ezhilov[138], F. Fabbri[57], L. Fabbri[23b,23a], V. Fabiani[119],
G. Facini[95], R.M. Faisca Rodrigues Pereira[140a], R.M. Fakhrutdinov[123], S. Falciano[73a], P.J. Falke[5],
S. Falke[5], J. Faltova[143], Y. Fang[15a], Y. Fang[15a], G. Fanourakis[44], M. Fanti[69a,69b], M. Faraj[67a,67c,w],
A. Farbin[8], A. Farilla[75a], E.M. Farina[71a,71b], T. Farooque[107], S. Farrell[18], S.M. Farrington[50], P. Farthouat[36],
F. Fassi[35f], P. Fassnacht[36], D. Fassouliotis[9], M. Faucci Giannelli[50], W.J. Fawcett[32], L. Fayard[65],
O.L. Fedin[138,r], W. Fedorko[176], M. Feickert[42], S. Feigl[134], L. Feligioni[102], A. Fell[150], C. Feng[60b],
E.J. Feng[36], M. Feng[49], M.J. Fenton[57], A.B. Fenyuk[123], J. Ferrando[46], A. Ferrante[174], A. Ferrari[173],
P. Ferrari[120], R. Ferrari[71a], D.E. Ferreira de Lima[61b], A. Ferrer[175], D. Ferrere[54], C. Ferretti[106], F. Fiedler[100],
A. Filipčič[92], F. Filthaut[119], K.D. Finelli[25], M.C.N. Fiolhais[140a,140c,a], L. Fiorini[175], F. Fischer[114],
W.C. Fisher[107], I. Fleck[152], P. Fleischmann[106], R.R.M. Fletcher[137], T. Flick[183], B.M. Flierl[114], L. Flores[137],
L.R. Flores Castillo[63a], F.M. Follega[76a,76b], N. Fomin[17], J.H. Foo[168], G.T. Forcolin[76a,76b], A. Formica[145],
F.A. Förster[14], A.C. Forti[101], A.G. Foster[21], M.G. Foti[135], D. Fournier[65], H. Fox[90], P. Francavilla[72a,72b],
S. Francescato[73a,73b], M. Franchini[23b,23a], S. Franchino[61a], D. Francis[36], L. Franconi[20], M. Franklin[59],
A.N. Fray[93], B. Freund[110], W.S. Freund[81b], E.M. Freundlich[47], D.C. Frizzell[129], D. Froidevaux[36],
J.A. Frost[135], C. Fukunaga[165], E. Fullana Torregrosa[175], E. Fumagalli[55b,55a], T. Fusayasu[116], J. Fuster[175],
A. Gabrielli[23b,23a], A. Gabrielli[18], G.P. Gach[84a], S. Gadatsch[54], P. Gadow[115], G. Gagliardi[55b,55a],
L.G. Gagnon[110], C. Galea[27b], B. Galhardo[140a], G.E. Gallardo[135], E.J. Gallas[135], B.J. Gallop[144],

G. Galster[40], R. Gamboa Goni[93], K.K. Gan[127], S. Ganguly[181], J. Gao[60a], Y. Gao[50], Y.S. Gao[31,o],
C. García[175], J.E. García Navarro[175], J.A. García Pascual[15a], C. Garcia-Argos[52], M. Garcia-Sciveres[18],
R.W. Gardner[37], N. Garelli[154], S. Gargiulo[52], V. Garonne[134], A. Gaudiello[55b,55a], G. Gaudio[71a],
I.L. Gavrilenko[111], A. Gavrilyuk[124], C. Gay[176], G. Gaycken[46], E.N. Gazis[10], A.A. Geanta[27b],
C.N.P. Gee[144], J. Geisen[53], M. Geisen[100], M.P. Geisler[61a], C. Gemme[55b], M.H. Genest[58], C. Geng[106],
S. Gentile[73a,73b], S. George[94], T. Geralis[44], L.O. Gerlach[53], P. Gessinger-Befurt[100], G. Gessner[47],
S. Ghasemi[152], M. Ghasemi Bostanabad[177], A. Ghosh[65], A. Ghosh[78], B. Giacobbe[23b], S. Giagu[73a,73b],
N. Giangiacomi[23b,23a], P. Giannetti[72a], A. Giannini[70a,70b], S.M. Gibson[94], M. Gignac[146], D. Gillberg[34],
G. Gilles[183], D.M. Gingrich[3,ba], M.P. Giordani[67a,67c], F.M. Giorgi[23b], P.F. Giraud[145], G. Giugliarelli[67a,67c],
D. Giugni[69a], F. Giuli[74a,74b], S. Gkaitatzis[163], I. Gkialas[9,i], E.L. Gkougkousis[14], P. Gkountoumis[10],
L.K. Gladilin[113], C. Glasman[99], J. Glatzer[14], P.C.F. Glaysher[46], A. Glazov[46], M. Goblirsch-Kolb[26],
S. Goldfarb[105], T. Golling[54], D. Golubkov[123], A. Gomes[140a,140b], R. Goncalves Gama[53], R. Gonçalo[140a],
G. Gonella[52], L. Gonella[21], A. Gongadze[80], F. Gonnella[21], J.L. Gonski[59], S. González de la Hoz[175],
S. Gonzalez-Sevilla[54], G.R. Gonzalvo Rodriguez[175], L. Goossens[36], P.A. Gorbounov[124], H.A. Gordon[29],
B. Gorini[36], E. Gorini[68a,68b], A. Gorišek[92], A.T. Goshaw[49], M.I. Gostkin[80], C.A. Gottardo[119],
M. Gouighri[35b], D. Goujdami[35c], A.G. Goussiou[149], N. Govender[33c,b], C. Goy[5], E. Gozani[161],
I. Grabowska-Bold[84a], E.C. Graham[91], J. Gramling[172], E. Gramstad[134], S. Grancagnolo[19], M. Grandi[157],
V. Gratchev[138], P.M. Gravila[27f], F.G. Gravili[68a,68b], C. Gray[57], H.M. Gray[18], C. Grefe[24], K. Gregersen[97],
I.M. Gregor[46], P. Grenier[154], K. Grevtsov[46], C. Grieco[14], N.A. Grieser[129], J. Griffiths[8], A.A. Grillo[146],
K. Grimm[31,n], S. Grinstein[14,ac], J.-F. Grivaz[65], S. Groh[100], E. Gross[181], J. Grosse-Knetter[53], Z.J. Grout[95],
C. Grud[106], A. Grummer[118], L. Guan[106], W. Guan[182], J. Guenther[36], A. Guerguichon[65],
J.G.R. Guerrero Rojas[175], F. Guescini[115], D. Guest[172], R. Gugel[52], T. Guillemin[5], S. Guindon[36], U. Gul[57],
J. Guo[60c], W. Guo[106], Y. Guo[60a,v], Z. Guo[102], R. Gupta[46], S. Gurbuz[12c], G. Gustavino[129], P. Gutierrez[129],
C. Gutschow[95], C. Guyot[145], C. Gwenlan[135], C.B. Gwilliam[91], A. Haas[125], C. Haber[18], H.K. Hadavand[8],
N. Haddad[35f], A. Hadef[60a], S. Hageböck[36], M. Hagihara[170], M. Haleem[178], J. Haley[130], G. Halladjian[107],
G.D. Hallewell[102], K. Hamacher[183], P. Hamal[131], K. Hamano[177], H. Hamdaoui[35f], G.N. Hamity[150],
K. Han[60a,ab], L. Han[60a], S. Han[15a], K. Hanagaki[82,z], M. Hance[146], D.M. Handl[114], B. Haney[137],
R. Hankache[136], E. Hansen[97], J.B. Hansen[40], J.D. Hansen[40], M.C. Hansen[24], P.H. Hansen[40],
E.C. Hanson[101], K. Hara[170], A.S. Hard[182], T. Harenberg[183], S. Harkusha[108], P.F. Harrison[179],
N.M. Hartmann[114], Y. Hasegawa[151], A. Hasib[50], S. Hassani[145], S. Haug[20], R. Hauser[107], L.B. Havener[39],
M. Havranek[142], C.M. Hawkes[21], R.J. Hawkings[36], D. Hayden[107], C. Hayes[156], R.L. Hayes[176],
C.P. Hays[135], J.M. Hays[93], H.S. Hayward[91], S.J. Haywood[144], F. He[60a], M.P. Heath[50], V. Hedberg[97],
L. Heelan[8], S. Heer[24], K.K. Heidegger[52], W.D. Heidorn[79], J. Heilman[34], S. Heim[46], T. Heim[18],
B. Heinemann[46,aw], J.J. Heinrich[132], L. Heinrich[36], C. Heinz[56], J. Hejbal[141], L. Helary[61b], A. Held[176],
S. Hellesund[134], C.M. Helling[146], S. Hellman[45a,45b], C. Helsens[36], R.C.W. Henderson[90], Y. Heng[182],
S. Henkelmann[176], A.M. Henriques Correia[36], G.H. Herbert[19], H. Herde[26], V. Herget[178],
Y. Hernández Jiménez[33e], H. Herr[100], M.G. Herrmann[114], T. Herrmann[48], G. Herten[52], R. Hertenberger[114],
L. Hervas[36], T.C. Herwig[137], G.G. Hesketh[95], N.P. Hessey[169a], A. Higashida[164], S. Higashino[82],
E. Higón-Rodriguez[175], K. Hildebrand[37], E. Hill[177], J.C. Hill[32], K.K. Hill[29], K.H. Hiller[46], S.J. Hillier[21],
M. Hils[48], I. Hinchliffe[18], F. Hinterkeuser[24], M. Hirose[133], S. Hirose[52], D. Hirschbuehl[183], B. Hiti[92],
O. Hladik[141], D.R. Hlaluku[33e], X. Hoad[50], J. Hobbs[156], N. Hod[181], M.C. Hodgkinson[150], A. Hoecker[36],
F. Hoenig[114], D. Hohn[52], D. Hohov[65], T.R. Holmes[37], M. Holzbock[114], L.B.A.H. Hommels[32], S. Honda[170],
T. Honda[82], T.M. Hong[139], A. Hönle[115], B.H. Hooberman[174], W.H. Hopkins[6], Y. Horii[117], P. Horn[48],
L.A. Horyn[37], A. Hostiuc[149], S. Hou[159], A. Hoummada[35a], J. Howarth[101], J. Hoya[89], M. Hrabovsky[131],
J. Hrdinka[77], I. Hristova[19], J. Hrivnac[65], A. Hrynevich[109], T. Hryn'ova[5], P.J. Hsu[64], S.-C. Hsu[149], Q. Hu[29],
S. Hu[60c], Y. Huang[15a], Z. Hubacek[142], F. Hubaut[102], M. Huebner[24], F. Huegging[24], T.B. Huffman[135],
M. Huhtinen[36], R.F.H. Hunter[34], P. Huo[156], A.M. Hupe[34], N. Huseynov[80,ak], J. Huston[107], J. Huth[59],

38

R. Hyneman[106], S. Hyrych[28a], G. Iacobucci[54], G. Iakovidis[29], I. Ibragimov[152], L. Iconomidou-Fayard[65],
Z. Idrissi[35f], P. Iengo[36], R. Ignazzi[40], O. Igonkina[120,ae,*], R. Iguchi[164], T. Iizawa[54], Y. Ikegami[82],
M. Ikeno[82], D. Iliadis[163], N. Ilic[119,168,ai], F. Iltzsche[48], G. Introzzi[71a,71b], M. Iodice[75a], K. Iordanidou[169a],
V. Ippolito[73a,73b], M.F. Isacson[173], M. Ishino[164], M. Ishitsuka[166], W. Islam[130], C. Issever[135], S. Istin[161],
F. Ito[170], J.M. Iturbe Ponce[63a], R. Iuppa[76a,76b], A. Ivina[181], H. Iwasaki[82], J.M. Izen[43], V. Izzo[70a],
P. Jacka[141], P. Jackson[1], R.M. Jacobs[24], B.P. Jaeger[153], V. Jain[2], G. Jäkel[183], K.B. Jakobi[100], K. Jakobs[52],
S. Jakobsen[77], T. Jakoubek[141], J. Jamieson[57], K.W. Janas[84a], R. Jansky[54], J. Janssen[24], M. Janus[53],
P.A. Janus[84a], G. Jarlskog[97], N. Javadov[80,ak], T. Javůrek[36], M. Javurkova[52], F. Jeanneau[145], L. Jeanty[132],
J. Jejelava[160a,al], A. Jelinskas[179], P. Jenni[52,c], J. Jeong[46], N. Jeong[46], S. Jézéquel[5], H. Ji[182], J. Jia[156],
H. Jiang[79], Y. Jiang[60a], Z. Jiang[154,s], S. Jiggins[52], F.A. Jimenez Morales[38], J. Jimenez Pena[115], S. Jin[15c],
A. Jinaru[27b], O. Jinnouchi[166], H. Jivan[33e], P. Johansson[150], K.A. Johns[7], C.A. Johnson[66],
K. Jon-And[45a,45b], R.W.L. Jones[90], S.D. Jones[157], S. Jones[7], T.J. Jones[91], J. Jongmanns[61a], P.M. Jorge[140a],
J. Jovicevic[36], X. Ju[18], J.J. Junggeburth[115], A. Juste Rozas[14,ac], A. Kaczmarska[85], M. Kado[73a,73b],
H. Kagan[127], M. Kagan[154], C. Kahra[100], T. Kaji[180], E. Kajomovitz[161], C.W. Kalderon[97], A. Kaluza[100],
A. Kamenshchikov[123], L. Kanjir[92], Y. Kano[164], V.A. Kantserov[112], J. Kanzaki[82], L.S. Kaplan[182],
D. Kar[33e], M.J. Kareem[169b], S.N. Karpov[80], Z.M. Karpova[80], V. Kartvelishvili[90], A.N. Karyukhin[123],
L. Kashif[182], R.D. Kass[127], A. Kastanas[45a,45b], Y. Kataoka[164], C. Kato[60d,60c], J. Katzy[46], K. Kawade[83],
K. Kawagoe[88], T. Kawaguchi[117], T. Kawamoto[164], G. Kawamura[53], E.F. Kay[177], V.F. Kazanin[122b,122a],
R. Keeler[177], R. Kehoe[42], J.S. Keller[34], E. Kellermann[97], D. Kelsey[157], J.J. Kempster[21], J. Kendrick[21],
O. Kepka[141], S. Kersten[183], B.P. Kerševan[92], S. Ketabchi Haghighat[168], M. Khader[174], F. Khalil-Zada[13],
M. Khandoga[145], A. Khanov[130], A.G. Kharlamov[122b,122a], T. Kharlamova[122b,122a], E.E. Khoda[176],
A. Khodinov[167], T.J. Khoo[54], E. Khramov[80], J. Khubua[160b], S. Kido[83], M. Kiehn[54], C.R. Kilby[94],
Y.K. Kim[37], N. Kimura[95], O.M. Kind[19], B.T. King[91,*], D. Kirchmeier[48], J. Kirk[144], A.E. Kiryunin[115],
T. Kishimoto[164], D.P. Kisliuk[168], V. Kitali[46], O. Kivernyk[5], E. Kladiva[28b,*], T. Klapdor-Kleingrothaus[52],
M. Klassen[61a], M.H. Klein[106], M. Klein[91], U. Klein[91], K. Kleinknecht[100], P. Klimek[121], A. Klimentov[29],
T. Klingl[24], T. Klioutchnikova[36], F.F. Klitzner[114], P. Kluit[120], S. Kluth[115], E. Kneringer[77],
E.B.F.G. Knoops[102], A. Knue[52], D. Kobayashi[88], T. Kobayashi[164], M. Kobel[48], M. Kocian[154], P. Kodys[143],
P.T. Koenig[24], T. Koffas[34], N.M. Köhler[36], T. Koi[154], M. Kolb[61b], I. Koletsou[5], T. Komarek[131], T. Kondo[82],
N. Kondrashova[60c], K. Köneke[52], A.C. König[119], T. Kono[126], R. Konoplich[125,ar], V. Konstantinides[95],
N. Konstantinidis[95], B. Konya[97], R. Kopeliansky[66], S. Koperny[84a], K. Korcyl[85], K. Kordas[163],
G. Koren[162], A. Korn[95], I. Korolkov[14], E.V. Korolkova[150], N. Korotkova[113], O. Kortner[115], S. Kortner[115],
T. Kosek[143], V.V. Kostyukhin[24], A. Kotwal[49], A. Koulouris[10], A. Kourkoumeli-Charalampidi[71a,71b],
C. Kourkoumelis[9], E. Kourlitis[150], V. Kouskoura[29], A.B. Kowalewska[85], R. Kowalewski[177], C. Kozakai[164],
W. Kozanecki[145], A.S. Kozhin[123], V.A. Kramarenko[113], G. Kramberger[92], D. Krasnopevtsev[60a],
M.W. Krasny[136], A. Krasznahorkay[36], D. Krauss[115], J.A. Kremer[84a], J. Kretzschmar[91], P. Krieger[168],
F. Krieter[114], A. Krishnan[61b], K. Krizka[18], K. Kroeninger[47], H. Kroha[115], J. Kroll[141], J. Kroll[137],
J. Krstic[16], U. Kruchonak[80], H. Krüger[24], N. Krumnack[79], M.C. Kruse[49], J.A. Krzysiak[85], T. Kubota[105],
O. Kuchinskaia[167], S. Kuday[4b], D. Kuechler[46], J.T. Kuechler[46], S. Kuehn[36], A. Kugel[61a], T. Kuhl[46],
V. Kukhtin[80], R. Kukla[102], Y. Kulchitsky[108,ao], S. Kuleshov[147d], Y.P. Kulinich[174], M. Kuna[58], T. Kunigo[86],
A. Kupco[141], T. Kupfer[47], O. Kuprash[52], H. Kurashige[83], L.L. Kurchaninov[169a], Y.A. Kurochkin[108],
A. Kurova[112], M.G. Kurth[15a,15d], E.S. Kuwertz[36], M. Kuze[166], A.K. Kvam[149], J. Kvita[131], T. Kwan[104],
A. La Rosa[115], L. La Rotonda[41b,41a], F. La Ruffa[41b,41a], C. Lacasta[175], F. Lacava[73a,73b], D.P.J. Lack[101],
H. Lacker[19], D. Lacour[136], E. Ladygin[80], R. Lafaye[5], B. Laforge[136], T. Lagouri[33e], S. Lai[53], S. Lammers[66],
W. Lampl[7], C. Lampoudis[163], E. Lançon[29], U. Landgraf[52], M.P.J. Landon[93], M.C. Lanfermann[54],
V.S. Lang[46], J.C. Lange[53], R.J. Langenberg[36], A.J. Lankford[172], F. Lanni[29], K. Lantzsch[24], A. Lanza[71a],
A. Lapertosa[55b,55a], S. Laplace[136], J.F. Laporte[145], T. Lari[69a], F. Lasagni Manghi[23b,23a], M. Lassnig[36],
T.S. Lau[63a], A. Laudrain[65], A. Laurier[34], M. Lavorgna[70a,70b], M. Lazzaroni[69a,69b], B. Le[105],

E. Le Guirriec[102], M. LeBlanc[7], T. LeCompte[6], F. Ledroit-Guillon[58], C.A. Lee[29], G.R. Lee[17], L. Lee[59], S.C. Lee[159], S.J. Lee[34], B. Lefebvre[169a], M. Lefebvre[177], F. Legger[114], C. Leggett[18], K. Lehmann[153], N. Lehmann[183], G. Lehmann Miotto[36], W.A. Leight[46], A. Leisos[163,aa], M.A.L. Leite[81c], C.E. Leitgeb[114], R. Leitner[143], D. Lellouch[181,*], K.J.C. Leney[42], T. Lenz[24], B. Lenzi[36], R. Leone[7], S. Leone[72a], C. Leonidopoulos[50], A. Leopold[136], G. Lerner[157], C. Leroy[110], R. Les[168], C.G. Lester[32], M. Levchenko[138], J. Levêque[5], D. Levin[106], L.J. Levinson[181], D.J. Lewis[21], B. Li[15b], B. Li[106], C-Q. Li[60a], F. Li[60c], H. Li[60a], H. Li[60b], J. Li[60c], K. Li[154], L. Li[60c], M. Li[15a,15d], Q. Li[15a,15d], Q.Y. Li[60a], S. Li[60d,60c], X. Li[46], Y. Li[46], Z. Li[60b], Z. Liang[15a], B. Liberti[74a], A. Liblong[168], K. Lie[63c], S. Liem[120], C.Y. Lin[32], K. Lin[107], T.H. Lin[100], R.A. Linck[66], J.H. Lindon[21], A.L. Lionti[54], E. Lipeles[137], A. Lipniacka[17], M. Lisovyi[61b], T.M. Liss[174,ay], A. Lister[176], A.M. Litke[146], J.D. Little[8], B. Liu[79,ah], B.X. Liu[6], H.B. Liu[29], H. Liu[106], J.B. Liu[60a], J.K.K. Liu[135], K. Liu[136], M. Liu[60a], P. Liu[18], Y. Liu[15a,15d], Y.L. Liu[106], Y.W. Liu[60a], M. Livan[71a,71b], A. Lleres[58], J. Llorente Merino[15a], S.L. Lloyd[93], C.Y. Lo[63b], F. Lo Sterzo[42], E.M. Lobodzinska[46], P. Loch[7], S. Loffredo[74a,74b], T. Lohse[19], K. Lohwasser[150], M. Lokajicek[141], J.D. Long[174], R.E. Long[90], L. Longo[36], K.A. Looper[127], J.A. Lopez[147d], I. Lopez Paz[101], A. Lopez Solis[150], J. Lorenz[114], N. Lorenzo Martinez[5], M. Losada[22a], P.J. Lösel[114], A. Lösle[52], X. Lou[46], X. Lou[15a], A. Lounis[65], J. Love[6], P.A. Love[90], J.J. Lozano Bahilo[175], M. Lu[60a], Y.J. Lu[64], H.J. Lubatti[149], C. Luci[73a,73b], A. Lucotte[58], C. Luedtke[52], F. Luehring[66], I. Luise[136], L. Luminari[73a], B. Lund-Jensen[155], M.S. Lutz[103], D. Lynn[29], R. Lysak[141], E. Lytken[97], F. Lyu[15a], V. Lyubushkin[80], T. Lyubushkina[80], H. Ma[29], L.L. Ma[60b], Y. Ma[60b], G. Maccarrone[51], A. Macchiolo[115], C.M. Macdonald[150], J. Machado Miguens[137], D. Madaffari[175], R. Madar[38], W.F. Mader[48], N. Madysa[48], J. Maeda[83], K. Maekawa[164], S. Maeland[17], T. Maeno[29], M. Maerker[48], A.S. Maevskiy[113], V. Magerl[52], N. Magini[79], D.J. Mahon[39], C. Maidantchik[81b], T. Maier[114], A. Maio[140a,140b,140d], K. Maj[85], O. Majersky[28a], S. Majewski[132], Y. Makida[82], N. Makovec[65], B. Malaescu[136], Pa. Malecki[85], V.P. Maleev[138], F. Malek[58], U. Mallik[78], D. Malon[6], C. Malone[32], S. Maltezos[10], S. Malyukov[80], J. Mamuzic[175], G. Mancini[51], I. Mandić[92], L. Manhaes de Andrade Filho[81a], I.M. Maniatis[163], J. Manjarres Ramos[48], K.H. Mankinen[97], A. Mann[114], A. Manousos[77], B. Mansoulie[145], I. Manthos[163], S. Manzoni[120], A. Marantis[163], G. Marceca[30], L. Marchese[135], G. Marchiori[136], M. Marcisovsky[141], C. Marcon[97], C.A. Marin Tobon[36], M. Marjanovic[38], Z. Marshall[18], M.U.F. Martensson[173], S. Marti-Garcia[175], C.B. Martin[127], T.A. Martin[179], V.J. Martin[50], B. Martin dit Latour[17], L. Martinelli[75a,75b], M. Martinez[14,ac], V.I. Martinez Outschoorn[103], S. Martin-Haugh[144], V.S. Martoiu[27b], A.C. Martyniuk[95], A. Marzin[36], S.R. Maschek[115], L. Masetti[100], T. Mashimo[164], R. Mashinistov[111], J. Masik[101], A.L. Maslennikov[122b,122a], L.H. Mason[105], L. Massa[74a,74b], P. Massarotti[70a,70b], P. Mastrandrea[72a,72b], A. Mastroberardino[41b,41a], T. Masubuchi[164], D. Matakias[10], A. Matic[114], P. Mättig[24], J. Maurer[27b], B. Maček[92], D.A. Maximov[122b,122a], R. Mazini[159], I. Maznas[163], S.M. Mazza[146], S.P. Mc Kee[106], T.G. McCarthy[115], L.I. McClymont[95], W.P. McCormack[18], E.F. McDonald[105], J.A. Mcfayden[36], M.A. McKay[42], K.D. McLean[177], S.J. McMahon[144], P.C. McNamara[105], C.J. McNicol[179], R.A. McPherson[177,ai], J.E. Mdhluli[33e], Z.A. Meadows[103], S. Meehan[149], T. Megy[52], S. Mehlhase[114], A. Mehta[91], T. Meideck[58], B. Meirose[43], D. Melini[175], B.R. Mellado Garcia[33e], J.D. Mellenthin[53], M. Melo[28a], F. Meloni[46], A. Melzer[24], S.B. Menary[101], E.D. Mendes Gouveia[140a,140e], L. Meng[36], X.T. Meng[106], S. Menke[115], E. Meoni[41b,41a], S. Mergelmeyer[19], S.A.M. Merkt[139], C. Merlassino[20], P. Mermod[54], L. Merola[70a,70b], C. Meroni[69a], O. Meshkov[113,111], J.K.R. Meshreki[152], A. Messina[73a,73b], J. Metcalfe[6], A.S. Mete[172], C. Meyer[66], J. Meyer[161], J-P. Meyer[145], H. Meyer Zu Theenhausen[61a], F. Miano[157], M. Michetti[19], R.P. Middleton[144], L. Mijović[50], G. Mikenberg[181], M. Mikestikova[141], M. Mikuž[92], H. Mildner[150], M. Milesi[105], A. Milic[168], D.A. Millar[93], D.W. Miller[37], A. Milov[181], D.A. Milstead[45a,45b], R.A. Mina[154,s], A.A. Minaenko[123], M. Miñano Moya[175], I.A. Minashvili[160b], A.I. Mincer[125], B. Mindur[84a], M. Mineev[80], Y. Minegishi[164], Y. Ming[182], L.M. Mir[14], A. Mirto[68a,68b], K.P. Mistry[137], T. Mitani[180], J. Mitrevski[114], V.A. Mitsou[175], M. Mittal[60c], A. Miucci[20], P.S. Miyagawa[150], A. Mizukami[82], J.U. Mjörnmark[97],

T. Mkrtchyan[185], M. Mlynarikova[143], T. Moa[45a,45b], K. Mochizuki[110], P. Mogg[52], S. Mohapatra[39], R. Moles-Valls[24], M.C. Mondragon[107], K. Mönig[46], J. Monk[40], E. Monnier[102], A. Montalbano[153], J. Montejo Berlingen[36], M. Montella[95], F. Monticelli[89], S. Monzani[69a], N. Morange[65], D. Moreno[22a], M. Moreno Llácer[36], C. Moreno Martinez[14], P. Morettini[55b], M. Morgenstern[120], S. Morgenstern[48], D. Mori[153], M. Morii[59], M. Morinaga[180], V. Morisbak[134], A.K. Morley[36], G. Mornacchi[36], A.P. Morris[95], L. Morvaj[156], P. Moschovakos[36], B. Moser[120], M. Mosidze[160b], T. Moskalets[145], H.J. Moss[150], J. Moss[31,p], K. Motohashi[166], E. Mountricha[36], E.J.W. Moyse[103], S. Muanza[102], J. Mueller[139], R.S.P. Mueller[114], D. Muenstermann[90], G.A. Mullier[97], J.L. Munoz Martinez[14], F.J. Munoz Sanchez[101], P. Murin[28b], W.J. Murray[179,144], A. Murrone[69a,69b], M. Muškinja[18], C. Mwewa[33a], A.G. Myagkov[123,as], J. Myers[132], M. Myska[142], B.P. Nachman[18], O. Nackenhorst[47], A.Nag Nag[48], K. Nagai[135], K. Nagano[82], Y. Nagasaka[62], M. Nagel[52], E. Nagy[102], A.M. Nairz[36], Y. Nakahama[117], K. Nakamura[82], T. Nakamura[164], I. Nakano[128], H. Nanjo[133], F. Napolitano[61a], R.F. Naranjo Garcia[46], R. Narayan[42], I. Naryshkin[138], T. Naumann[46], G. Navarro[22a], H.A. Neal[106,*], P.Y. Nechaeva[111], F. Nechansky[46], T.J. Neep[21], A. Negri[71a,71b], M. Negrini[23b], C. Nellist[53], M.E. Nelson[135], S. Nemecek[141], P. Nemethy[125], M. Nessi[36,e], M.S. Neubauer[174], M. Neumann[183], P.R. Newman[21], Y.S. Ng[19], Y.W.Y. Ng[172], H.D.N. Nguyen[102], T. Nguyen Manh[110], E. Nibigira[38], R.B. Nickerson[135], R. Nicolaidou[145], D.S. Nielsen[40], J. Nielsen[146], N. Nikiforou[11], V. Nikolaenko[123,as], I. Nikolic-Audit[136], K. Nikolopoulos[21], P. Nilsson[29], H.R. Nindhito[54], Y. Ninomiya[82], A. Nisati[73a], N. Nishu[60c], R. Nisius[115], I. Nitsche[47], T. Nitta[180], T. Nobe[164], Y. Noguchi[86], I. Nomidis[136], M.A. Nomura[29], M. Nordberg[36], N. Norjoharuddeen[135], T. Novak[92], O. Novgorodova[48], L. Novotny[142], R. Novotny[142], L. Nozka[131], K. Ntekas[172], E. Nurse[95], F.G. Oakham[34,ba], H. Oberlack[115], J. Ocariz[136], A. Ochi[83], I. Ochoa[39], J.P. Ochoa-Ricoux[147a], K. O'Connor[26], S. Oda[88], S. Odaka[82], S. Oerdek[53], A. Ogrodnik[84a], A. Oh[101], S.H. Oh[49], C.C. Ohm[155], H. Oide[55b,55a], M.L. Ojeda[168], H. Okawa[170], Y. Okazaki[86], Y. Okumura[164], T. Okuyama[82], A. Olariu[27b], L.F. Oleiro Seabra[140a], S.A. Olivares Pino[147a], D. Oliveira Damazio[29], J.L. Oliver[1], M.J.R. Olsson[172], A. Olszewski[85], J. Olszowska[85], D.C. O'Neil[153], A. Onofre[140a,140e], K. Onogi[117], P.U.E. Onyisi[11], H. Oppen[134], M.J. Oreglia[37], G.E. Orellana[89], D. Orestano[75a,75b], N. Orlando[14], R.S. Orr[168], V. O'Shea[57], R. Ospanov[60a], G. Otero y Garzon[30], H. Otono[88], P.S. Ott[61a], M. Ouchrif[35e], J. Ouellette[29], F. Ould-Saada[134], A. Ouraou[145,*], Q. Ouyang[15a], M. Owen[57], R.E. Owen[21], V.E. Ozcan[12c], N. Ozturk[8], J. Pacalt[131], H.A. Pacey[32], K. Pachal[49], A. Pacheco Pages[14], C. Padilla Aranda[14], S. Pagan Griso[18], M. Paganini[184], G. Palacino[66], S. Palazzo[50], S. Palestini[36], M. Palka[84b], D. Pallin[38], I. Panagoulias[10], C.E. Pandini[36], J.G. Panduro Vazquez[94], P. Pani[46], G. Panizzo[67a,67c], L. Paolozzi[54], C. Papadatos[110], K. Papageorgiou[9,i], A. Paramonov[6], D. Paredes Hernandez[63b], S.R. Paredes Saenz[135], B. Parida[167], T.H. Park[168], A.J. Parker[90], M.A. Parker[32], F. Parodi[55b,55a], E.W. Parrish[121], J.A. Parsons[39], U. Parzefall[52], L. Pascual Dominguez[136], V.R. Pascuzzi[168], J.M.P. Pasner[146], E. Pasqualucci[73a], S. Passaggio[55b], F. Pastore[94], P. Pasuwan[45a,45b], S. Pataraia[100], J.R. Pater[101], A. Pathak[182], T. Pauly[36], B. Pearson[115], M. Pedersen[134], L. Pedraza Diaz[119], R. Pedro[140a], T. Peiffer[53], S.V. Peleganchuk[122b,122a], O. Penc[141], H. Peng[60a], B.S. Peralva[81a], M.M. Perego[65], A.P. Pereira Peixoto[140a], D.V. Perepelitsa[29], F. Peri[19], L. Perini[69a,69b], H. Pernegger[36], S. Perrella[70a,70b], K. Peters[46], R.F.Y. Peters[101], B.A. Petersen[36], T.C. Petersen[40], E. Petit[102], A. Petridis[1], C. Petridou[163], M. Petrov[135], F. Petrucci[75a,75b], M. Pettee[184], N.E. Pettersson[103], K. Petukhova[143], A. Peyaud[145], R. Pezoa[147d], L. Pezzotti[71a,71b], T. Pham[105], F.H. Phillips[107], P.W. Phillips[144], M.W. Phipps[174], G. Piacquadio[156], E. Pianori[18], A. Picazio[103], R.H. Pickles[101], R. Piegaia[30], D. Pietreanu[27b], J.E. Pilcher[37], A.D. Pilkington[101], M. Pinamonti[74a,74b], J.L. Pinfold[3], M. Pitt[181], L. Pizzimento[74a,74b], M.-A. Pleier[29], V. Pleskot[143], E. Plotnikova[80], P. Podberezko[122b,122a], R. Poettgen[97], R. Poggi[54], L. Poggioli[65], I. Pogrebnyak[107], D. Pohl[24], I. Pokharel[53], G. Polesello[71a], A. Poley[18], A. Policicchio[73a,73b], R. Polifka[143], A. Polini[23b], C.S. Pollard[46], V. Polychronakos[29], D. Ponomarenko[112], L. Pontecorvo[36], S. Popa[27a], G.A. Popeneciu[27d], D.M. Portillo Quintero[58], S. Pospisil[142], K. Potamianos[46], I.N. Potrap[80], C.J. Potter[32], H. Potti[11],

T. Poulsen[97], J. Poveda[36], T.D. Powell[150], G. Pownall[46], M.E. Pozo Astigarraga[36], P. Pralavorio[102], S. Prell[79], D. Price[101], M. Primavera[68a], S. Prince[104], M.L. Proffitt[149], N. Proklova[112], K. Prokofiev[63c], F. Prokoshin[80], S. Protopopescu[29], J. Proudfoot[6], M. Przybycien[84a], D. Pudzha[138], A. Puri[174], P. Puzo[65], J. Qian[106], Y. Qin[101], A. Quadt[53], M. Queitsch-Maitland[46], A. Qureshi[1], P. Rados[105], F. Ragusa[69a,69b], G. Rahal[98], J.A. Raine[54], S. Rajagopalan[29], A. Ramirez Morales[93], K. Ran[15a,15d], T. Rashid[65], S. Raspopov[5], D.M. Rauch[46], F. Rauscher[114], S. Rave[100], B. Ravina[150], I. Ravinovich[181], J.H. Rawling[101], M. Raymond[36], A.L. Read[134], N.P. Readioff[58], M. Reale[68a,68b], D.M. Rebuzzi[71a,71b], A. Redelbach[178], G. Redlinger[29], K. Reeves[43], L. Rehnisch[19], J. Reichert[137], D. Reikher[162], A. Reiss[100], A. Rej[152], C. Rembser[36], M. Renda[27b], M. Rescigno[73a], S. Resconi[69a], E.D. Resseguie[137], S. Rettie[176], E. Reynolds[21], O.L. Rezanova[122b,122a], P. Reznicek[143], E. Ricci[76a,76b], R. Richter[115], S. Richter[46], E. Richter-Was[84b], O. Ricken[24], M. Ridel[136], P. Rieck[115], C.J. Riegel[183], O. Rifki[46], M. Rijssenbeek[156], A. Rimoldi[71a,71b], M. Rimoldi[46], L. Rinaldi[23b], G. Ripellino[155], B. Ristić[90], I. Riu[14], J.C. Rivera Vergara[177], F. Rizatdinova[130], E. Rizvi[93], C. Rizzi[36], R.T. Roberts[101], S.H. Robertson[104,ai], M. Robin[46], D. Robinson[32], J.E.M. Robinson[46], C.M. Robles Gajardo[147d], A. Robson[57], E. Rocco[100], C. Roda[72a,72b], S. Rodriguez Bosca[175], A. Rodriguez Perez[14], D. Rodriguez Rodriguez[175], A.M. Rodríguez Vera[169b], S. Roe[36], O. Røhne[134], R. Röhrig[115], C.P.A. Roland[66], J. Roloff[59], A. Romaniouk[112], M. Romano[23b,23a], N. Rompotis[91], M. Ronzani[125], L. Roos[136], S. Rosati[73a], K. Rosbach[52], G. Rosin[103], B.J. Rosser[137], E. Rossi[46], E. Rossi[75a,75b], E. Rossi[70a,70b], L.P. Rossi[55b], L. Rossini[69a,69b], R. Rosten[14], M. Rotaru[27b], J. Rothberg[149], D. Rousseau[65], G. Rovelli[71a,71b], A. Roy[11], D. Roy[33e], A. Rozanov[102], Y. Rozen[161], X. Ruan[33e], F. Rubbo[154], F. Rühr[52], A. Ruiz-Martinez[175], A. Rummler[36], Z. Rurikova[52], N.A. Rusakovich[80], H.L. Russell[104], L. Rustige[38,47], J.P. Rutherfoord[7], E.M. Rüttinger[46,l], M. Rybar[39], G. Rybkin[65], E.B. Rye[134], A. Ryzhov[123], G.F. Rzehorz[53], P. Sabatini[53], G. Sabato[120], S. Sacerdoti[65], H.F-W. Sadrozinski[146], R. Sadykov[80], F. Safai Tehrani[73a], B. Safarzadeh Samani[157], P. Saha[121], S. Saha[104], M. Sahinsoy[61a], A. Sahu[183], M. Saimpert[46], M. Saito[164], T. Saito[164], H. Sakamoto[164], A. Sakharov[125,ar], D. Salamani[54], G. Salamanna[75a,75b], J.E. Salazar Loyola[147d], P.H. Sales De Bruin[173], A. Salnikov[154], J. Salt[175], D. Salvatore[41b,41a], F. Salvatore[157], A. Salvucci[63a,63b,63c], A. Salzburger[36], J. Samarati[36], D. Sammel[52], D. Sampsonidis[163], D. Sampsonidou[163], J. Sánchez[175], A. Sanchez Pineda[67a,67c], H. Sandaker[134], C.O. Sander[46], I.G. Sanderswood[90], M. Sandhoff[183], C. Sandoval[22a], D.P.C. Sankey[144], M. Sannino[55b,55a], Y. Sano[117], A. Sansoni[51], C. Santoni[38], H. Santos[140a,140b], S.N. Santpur[18], A. Santra[175], A. Sapronov[80], J.G. Saraiva[140a,140d], O. Sasaki[82], K. Sato[170], E. Sauvan[5], P. Savard[168,ba], N. Savic[115], R. Sawada[164], C. Sawyer[144], L. Sawyer[96,ap], C. Sbarra[23b], A. Sbrizzi[23a], T. Scanlon[95], J. Schaarschmidt[149], P. Schacht[115], B.M. Schachtner[114], D. Schaefer[37], L. Schaefer[137], J. Schaeffer[100], S. Schaepe[36], U. Schäfer[100], A.C. Schaffer[65], D. Schaile[114], R.D. Schamberger[156], N. Scharmberg[101], V.A. Schegelsky[138], D. Scheirich[143], F. Schenck[19], M. Schernau[172], C. Schiavi[55b,55a], S. Schier[146], L.K. Schildgen[24], Z.M. Schillaci[26], E.J. Schioppa[36], M. Schioppa[41b,41a], K.E. Schleicher[52], S. Schlenker[36], K.R. Schmidt-Sommerfeld[115], K. Schmieden[36], C. Schmitt[100], S. Schmitt[46], S. Schmitz[100], J.C. Schmoeckel[46], U. Schnoor[52], L. Schoeffel[145], A. Schoening[61b], P.G. Scholer[52], E. Schopf[135], M. Schott[100], J.F.P. Schouwenberg[119], J. Schovancova[36], S. Schramm[54], F. Schroeder[183], A. Schulte[100], H-C. Schultz-Coulon[61a], M. Schumacher[52], B.A. Schumm[146], Ph. Schune[145], A. Schwartzman[154], T.A. Schwarz[106], Ph. Schwemling[145], R. Schwienhorst[107], A. Sciandra[146], G. Sciolla[26], M. Scodeggio[46], M. Scornajenghi[41b,41a], F. Scuri[72a], F. Scutti[105], L.M. Scyboz[115], C.D. Sebastiani[73a,73b], P. Seema[19], S.C. Seidel[118], A. Seiden[146], T. Seiss[37], J.M. Seixas[81b], G. Sekhniaidze[70a], K. Sekhon[106], S.J. Sekula[42], N. Semprini-Cesari[23b,23a], S. Sen[49], S. Senkin[38], C. Serfon[77], L. Serin[65], L. Serkin[67a,67b], M. Sessa[60a], H. Severini[129], T. Šfiligoj[92], F. Sforza[171], A. Sfyrla[54], E. Shabalina[53], J.D. Shahinian[146], N.W. Shaikh[45a,45b], D. Shaked Renous[181], L.Y. Shan[15a], R. Shang[174], J.T. Shank[25], M. Shapiro[18], A. Sharma[135], A.S. Sharma[1], P.B. Shatalov[124], K. Shaw[157], S.M. Shaw[101], A. Shcherbakova[138], Y. Shen[129], N. Sherafati[34], A.D. Sherman[25], P. Sherwood[95], L. Shi[159,ax], S. Shimizu[82], C.O. Shimmin[184],

Y. Shimogama[180], M. Shimojima[116], I.P.J. Shipsey[135], S. Shirabe[88], M. Shiyakova[80,af], J. Shlomi[181], A. Shmeleva[111], M.J. Shochet[37], J. Shojaii[105], D.R. Shope[129], S. Shrestha[127], E.M. Shrif[33e], E. Shulga[181], P. Sicho[141], A.M. Sickles[174], P.E. Sidebo[155], E. Sideras Haddad[33e], O. Sidiropoulou[36], A. Sidoti[23b,23a], F. Siegert[48], Dj. Sijacki[16], M.Jr. Silva[182], M.V. Silva Oliveira[81a], S.B. Silverstein[45a], S. Simion[65], E. Simioni[100], R. Simoniello[100], S. Simsek[12b], P. Sinervo[168], V. Sinetckii[113,111], N.B. Sinev[132], M. Sioli[23b,23a], I. Siral[106], S.Yu. Sivoklokov[113], J. Sjölin[45a,45b], E. Skorda[97], P. Skubic[129], M. Slawinska[85], K. Sliwa[171], R. Slovak[143], V. Smakhtin[181], B.H. Smart[144], J. Smiesko[28a], N. Smirnov[112], S.Yu. Smirnov[112], Y. Smirnov[112], L.N. Smirnova[113,x], O. Smirnova[97], J.W. Smith[53], M. Smizanska[90], K. Smolek[142], A. Smykiewicz[85], A.A. Snesarev[111], H.L. Snoek[120], I.M. Snyder[132], S. Snyder[29], R. Sobie[177,ai], A.M. Soffa[172], A. Soffer[162], A. Søgaard[50], F. Sohns[53], C.A. Solans Sanchez[36], E.Yu. Soldatov[112], U. Soldevila[175], A.A. Solodkov[123], A. Soloshenko[80], O.V. Solovyanov[123], V. Solovyev[138], P. Sommer[150], H. Son[171], W. Song[144], W.Y. Song[169b], A. Sopczak[142], F. Sopkova[28b], C.L. Sotiropoulou[72a,72b], S. Sottocornola[71a,71b], R. Soualah[67a,67c,h], A.M. Soukharev[122b,122a], D. South[46], S. Spagnolo[68a,68b], M. Spalla[115], M. Spangenberg[179], F. Spanò[94], D. Sperlich[52], T.M. Spieker[61a], R. Spighi[23b], G. Spigo[36], M. Spina[157], D.P. Spiteri[57], M. Spousta[143], A. Stabile[69a,69b], B.L. Stamas[121], R. Stamen[61a], M. Stamenkovic[120], E. Stanecka[85], R.W. Stanek[6], B. Stanislaus[135], M.M. Stanitzki[46], M. Stankaityte[135], B. Stapf[120], E.A. Starchenko[123], G.H. Stark[146], J. Stark[58], S.H. Stark[40], P. Staroba[141], P. Starovoitov[61a], S. Stärz[104], R. Staszewski[85], G. Stavropoulos[44], M. Stegler[46], P. Steinberg[29], A.L. Steinhebel[132], B. Stelzer[153], H.J. Stelzer[139], O. Stelzer-Chilton[169a], H. Stenzel[56], T.J. Stevenson[157], G.A. Stewart[36], M.C. Stockton[36], G. Stoicea[27b], M. Stolarski[140a], P. Stolte[53], S. Stonjek[115], A. Straessner[48], J. Strandberg[155], S. Strandberg[45a,45b], M. Strauss[129], P. Strizenec[28b], R. Ströhmer[178], D.M. Strom[132], R. Stroynowski[42], A. Strubig[50], S.A. Stucci[29], B. Stugu[17], J. Stupak[129], N.A. Styles[46], D. Su[154], S. Suchek[61a], V.V. Sulin[111], M.J. Sullivan[91], D.M.S. Sultan[54], S. Sultansoy[4c], T. Sumida[86], S. Sun[106], X. Sun[3], K. Suruliz[157], C.J.E. Suster[158], M.R. Sutton[157], S. Suzuki[82], M. Svatos[141], M. Swiatlowski[37], S.P. Swift[2], T. Swirski[178], A. Sydorenko[100], I. Sykora[28a], M. Sykora[143], T. Sykora[143], D. Ta[100], K. Tackmann[46,ad], J. Taenzer[162], A. Taffard[172], R. Tafirout[169a], H. Takai[29], R. Takashima[87], K. Takeda[83], T. Takeshita[151], E.P. Takeva[50], Y. Takubo[82], M. Talby[102], A.A. Talyshev[122b,122a], N.M. Tamir[162], J. Tanaka[164], M. Tanaka[166], R. Tanaka[65], S. Tapia Araya[174], S. Tapprogge[100], A. Tarek Abouelfadl Mohamed[136], S. Tarem[161], G. Tarna[27b,d], G.F. Tartarelli[69a], P. Tas[143], M. Tasevsky[141], T. Tashiro[86], E. Tassi[41b,41a], A. Tavares Delgado[140a,140b], Y. Tayalati[35f], A.J. Taylor[50], G.N. Taylor[105], W. Taylor[169b], A.S. Tee[90], R. Teixeira De Lima[154], P. Teixeira-Dias[94], H. Ten Kate[36], J.J. Teoh[120], S. Terada[82], K. Terashi[164], J. Terron[99], S. Terzo[14], M. Testa[51], R.J. Teuscher[168,ai], S.J. Thais[184], T. Theveneaux-Pelzer[46], F. Thiele[40], D.W. Thomas[94], J.O. Thomas[42], J.P. Thomas[21], A.S. Thompson[57], P.D. Thompson[21], L.A. Thomsen[184], E. Thomson[137], E.J. Thorpe[93], Y. Tian[39], R.E. Ticse Torres[53], V.O. Tikhomirov[111,at], Yu.A. Tikhonov[122b,122a], S. Timoshenko[112], P. Tipton[184], S. Tisserant[102], K. Todome[23b,23a], S. Todorova-Nova[5], S. Todt[48], J. Tojo[88], S. Tokár[28a], K. Tokushuku[82], E. Tolley[127], K.G. Tomiwa[33e], M. Tomoto[117], L. Tompkins[154,s], B. Tong[59], P. Tornambe[103], E. Torrence[132], H. Torres[48], E. Torró Pastor[149], C. Tosciri[135], J. Toth[102,ag], D.R. Tovey[150], A. Traeet[17], C.J. Treado[125], T. Trefzger[178], F. Tresoldi[157], A. Tricoli[29], I.M. Trigger[169a], S. Trincaz-Duvoid[136], W. Trischuk[168], B. Trocmé[58], A. Trofymov[145], C. Troncon[69a], M. Trovatelli[177], F. Trovato[157], L. Truong[33c], M. Trzebinski[85], A. Trzupek[85], F. Tsai[46], J.C-L. Tseng[135], P.V. Tsiareshka[108,ao], A. Tsirigotis[163], N. Tsirintanis[9], V. Tsiskaridze[156], E.G. Tskhadadze[160a], M. Tsopoulou[163], I.I. Tsukerman[124], V. Tsulaia[18], S. Tsuno[82], D. Tsybychev[156], Y. Tu[63b], A. Tudorache[27b], V. Tudorache[27b], T.T. Tulbure[27a], A.N. Tuna[59], S. Turchikhin[80], D. Turgeman[181], I. Turk Cakir[4b,y], R.J. Turner[21], R. Turra[69a], P.M. Tuts[39], S. Tzamarias[163], E. Tzovara[100], G. Ucchielli[47], K. Uchida[164], I. Ueda[82], M. Ughetto[45a,45b], F. Ukegawa[170], G. Unal[36], A. Undrus[29], G. Unel[172], F.C. Ungaro[105], Y. Unno[82], K. Uno[164], J. Urban[28b], P. Urquijo[105], G. Usai[8], J. Usui[82], Z. Uysal[12d], L. Vacavant[102], V. Vacek[142], B. Vachon[104], K.O.H. Vadla[134], A. Vaidya[95],

C. Valderanis[114], E. Valdes Santurio[45a,45b], M. Valente[54], S. Valentinetti[23b,23a], A. Valero[175], L. Valéry[46], R.A. Vallance[21], A. Vallier[36], J.A. Valls Ferrer[175], T.R. Van Daalen[14], P. Van Gemmeren[6], I. Van Vulpen[120], M. Vanadia[74a,74b], W. Vandelli[36], A. Vaniachine[167], D. Vannicola[73a,73b], R. Vari[73a], E.W. Varnes[7], C. Varni[55b,55a], T. Varol[42], D. Varouchas[65], K.E. Varvell[158], M.E. Vasile[27b], G.A. Vasquez[177], J.G. Vasquez[184], F. Vazeille[38], D. Vazquez Furelos[14], T. Vazquez Schroeder[36], J. Veatch[53], V. Vecchio[75a,75b], M.J. Veen[120], L.M. Veloce[168], F. Veloso[140a,140c], S. Veneziano[73a], A. Ventura[68a,68b], N. Venturi[36], A. Verbytskyi[115], V. Vercesi[71a], M. Verducci[72a,72b], C.M. Vergel Infante[79], C. Vergis[24], W. Verkerke[120], A.T. Vermeulen[120], J.C. Vermeulen[120], M.C. Vetterli[153,ba], N. Viaux Maira[147d], M. Vicente Barreto Pinto[54], T. Vickey[150], O.E. Vickey Boeriu[150], G.H.A. Viehhauser[135], L. Vigani[61b], M. Villa[23b,23a], M. Villaplana Perez[69a,69b], E. Vilucchi[51], M.G. Vincter[34], V.B. Vinogradov[80], A. Vishwakarma[46], C. Vittori[23b,23a], I. Vivarelli[157], M. Vogel[183], P. Vokac[142], S.E. von Buddenbrock[33e], E. Von Toerne[24], V. Vorobel[143], K. Vorobev[112], M. Vos[175], J.H. Vossebeld[91], M. Vozak[101], N. Vranjes[16], M. Vranjes Milosavljevic[16], V. Vrba[142,*], M. Vreeswijk[120], R. Vuillermet[36], I. Vukotic[37], P. Wagner[24], W. Wagner[183], J. Wagner-Kuhr[114], S. Wahdan[183], H. Wahlberg[89], K. Wakamiya[83], V.M. Walbrecht[115], J. Walder[90], R. Walker[114], S.D. Walker[94], W. Walkowiak[152], V. Wallangen[45a,45b], A.M. Wang[59], C. Wang[60c], C. Wang[60b], F. Wang[182], H. Wang[18], H. Wang[3], J. Wang[158], J. Wang[61b], P. Wang[42], Q. Wang[129], R.-J. Wang[100], R. Wang[60a], R. Wang[6], S.M. Wang[159], W.T. Wang[60a], W. Wang[15c,aj], W.X. Wang[60a,aj], Y. Wang[60a,aq], Z. Wang[60c], C. Wanotayaroj[46], A. Warburton[104], C.P. Ward[32], D.R. Wardrope[95], N. Warrack[57], A. Washbrook[50], A.T. Watson[21], M.F. Watson[21], G. Watts[149], B.M. Waugh[95], A.F. Webb[11], S. Webb[100], C. Weber[184], M.S. Weber[20], S.A. Weber[34], S.M. Weber[61a], A.R. Weidberg[135], J. Weingarten[47], M. Weirich[100], C. Weiser[52], P.S. Wells[36], T. Wenaus[29], T. Wengler[36], S. Wenig[36], N. Wermes[24], M.D. Werner[79], M. Wessels[61a], T.D. Weston[20], K. Whalen[132], N.L. Whallon[149], A.M. Wharton[90], A.S. White[106], A. White[8], M.J. White[1], D. Whiteson[172], B.W. Whitmore[90], W. Wiedenmann[182], M. Wielers[144], N. Wieseotte[100], C. Wiglesworth[40], L.A.M. Wiik-Fuchs[52], F. Wilk[101], H.G. Wilkens[36], L.J. Wilkins[94], H.H. Williams[137], S. Williams[32], C. Willis[107], S. Willocq[103], J.A. Wilson[21], I. Wingerter-Seez[5], E. Winkels[157], F. Winklmeier[132], O.J. Winston[157], B.T. Winter[52], M. Wittgen[154], M. Wobisch[96], A. Wolf[100], T.M.H. Wolf[120], R. Wolff[102], R. Wölker[135], J. Wollrath[52], M.W. Wolter[85], H. Wolters[140a,140c], V.W.S. Wong[176], N.L. Woods[146], S.D. Worm[21], B.K. Wosiek[85], K.W. Woźniak[85], K. Wraight[57], S.L. Wu[182], X. Wu[54], Y. Wu[60a], T.R. Wyatt[101], B.M. Wynne[50], S. Xella[40], Z. Xi[106], D. Xu[15a], H. Xu[60a,d], L. Xu[29], T. Xu[145], W. Xu[106], Z. Xu[60b], Z. Xu[154], B. Yabsley[158], S. Yacoob[33a], K. Yajima[133], D.P. Yallup[95], D. Yamaguchi[166], Y. Yamaguchi[166], A. Yamamoto[82], F. Yamane[83], M. Yamatani[164], T. Yamazaki[164], Y. Yamazaki[83], Z. Yan[25], H.J. Yang[60c,60d], H.T. Yang[18], S. Yang[78], X. Yang[60b,58], Y. Yang[164], W-M. Yao[18], Y.C. Yap[46], Y. Yasu[82], E. Yatsenko[60c,60d], J. Ye[42], S. Ye[29], I. Yeletskikh[80], M.R. Yexley[90], E. Yigitbasi[25], K. Yorita[180], K. Yoshihara[137], C.J.S. Young[36], C. Young[154], J. Yu[79], R. Yuan[60b,j], X. Yue[61a], S.P.Y. Yuen[24], B. Zabinski[85], G. Zacharis[10], E. Zaffaroni[54], J. Zahreddine[136], A.M. Zaitsev[123,as], T. Zakareishvili[160b], N. Zakharchuk[34], S. Zambito[59], D. Zanzi[36], D.R. Zaripovas[57], S.V. Zeißner[47], C. Zeitnitz[183], G. Zemaityte[135], J.C. Zeng[174], O. Zenin[123], T. Ženiš[28a], D. Zerwas[65], M. Zgubič[135], D.F. Zhang[15b], F. Zhang[182], G. Zhang[60a], G. Zhang[15b], H. Zhang[15c], J. Zhang[6], L. Zhang[15c], L. Zhang[60a], M. Zhang[174], R. Zhang[60a], R. Zhang[24], X. Zhang[60b], Y. Zhang[15a,15d], Z. Zhang[63a], Z. Zhang[65], P. Zhao[49], Y. Zhao[60b], Z. Zhao[60a], A. Zhemchugov[80], Z. Zheng[106], D. Zhong[174], B. Zhou[106], C. Zhou[182], M.S. Zhou[15a,15d], M. Zhou[156], N. Zhou[60c], Y. Zhou[7], C.G. Zhu[60b], H.L. Zhu[60a], H. Zhu[15a], J. Zhu[106], Y. Zhu[60a], X. Zhuang[15a], K. Zhukov[111], V. Zhulanov[122b,122a], D. Zieminska[66], N.I. Zimine[80], S. Zimmermann[52,*], Z. Zinonos[115], M. Ziolkowski[152], L. Živković[16], G. Zobernig[182], A. Zoccoli[23b,23a], K. Zoch[53], T.G. Zorbas[150], R. Zou[37], L. Zwalinski[36].

[1]Department of Physics, University of Adelaide, Adelaide; Australia.

[2]Physics Department, SUNY Albany, Albany NY; United States of America.

[3]Department of Physics, University of Alberta, Edmonton AB; Canada.

[4][a]Department of Physics, Ankara University, Ankara;[b]Istanbul Aydin University, Application and Research Center for Advanced Studies, Istanbul;[c]Division of Physics, TOBB University of Economics and Technology, Ankara; Turkey.

[5]LAPP, Université Grenoble Alpes, Université Savoie Mont Blanc, CNRS/IN2P3, Annecy; France.

[6]High Energy Physics Division, Argonne National Laboratory, Argonne IL; United States of America.

[7]Department of Physics, University of Arizona, Tucson AZ; United States of America.

[8]Department of Physics, University of Texas at Arlington, Arlington TX; United States of America.

[9]Physics Department, National and Kapodistrian University of Athens, Athens; Greece.

[10]Physics Department, National Technical University of Athens, Zografou; Greece.

[11]Department of Physics, University of Texas at Austin, Austin TX; United States of America.

[12][a]Bahcesehir University, Faculty of Engineering and Natural Sciences, Istanbul;[b]Istanbul Bilgi University, Faculty of Engineering and Natural Sciences, Istanbul;[c]Department of Physics, Bogazici University, Istanbul;[d]Department of Physics Engineering, Gaziantep University, Gaziantep; Turkey.

[13]Institute of Physics, Azerbaijan Academy of Sciences, Baku; Azerbaijan.

[14]Institut de Física d'Altes Energies (IFAE), Barcelona Institute of Science and Technology, Barcelona; Spain.

[15][a]Institute of High Energy Physics, Chinese Academy of Sciences, Beijing;[b]Physics Department, Tsinghua University, Beijing;[c]Department of Physics, Nanjing University, Nanjing;[d]University of Chinese Academy of Science (UCAS), Beijing; China.

[16]Institute of Physics, University of Belgrade, Belgrade; Serbia.

[17]Department for Physics and Technology, University of Bergen, Bergen; Norway.

[18]Physics Division, Lawrence Berkeley National Laboratory and University of California, Berkeley CA; United States of America.

[19]Institut für Physik, Humboldt Universität zu Berlin, Berlin; Germany.

[20]Albert Einstein Center for Fundamental Physics and Laboratory for High Energy Physics, University of Bern, Bern; Switzerland.

[21]School of Physics and Astronomy, University of Birmingham, Birmingham; United Kingdom.

[22][a]Facultad de Ciencias y Centro de Investigaciónes, Universidad Antonio Nariño, Bogotá;[b]Departamento de Física, Universidad Nacional de Colombia, Bogotá, Colombia; Colombia.

[23][a]INFN Bologna and Universita' di Bologna, Dipartimento di Fisica;[b]INFN Sezione di Bologna; Italy.

[24]Physikalisches Institut, Universität Bonn, Bonn; Germany.

[25]Department of Physics, Boston University, Boston MA; United States of America.

[26]Department of Physics, Brandeis University, Waltham MA; United States of America.

[27][a]Transilvania University of Brasov, Brasov;[b]Horia Hulubei National Institute of Physics and Nuclear Engineering, Bucharest;[c]Department of Physics, Alexandru Ioan Cuza University of Iasi, Iasi;[d]National Institute for Research and Development of Isotopic and Molecular Technologies, Physics Department, Cluj-Napoca;[e]University Politehnica Bucharest, Bucharest;[f]West University in Timisoara, Timisoara; Romania.

[28][a]Faculty of Mathematics, Physics and Informatics, Comenius University, Bratislava;[b]Department of Subnuclear Physics, Institute of Experimental Physics of the Slovak Academy of Sciences, Kosice; Slovak Republic.

[29]Physics Department, Brookhaven National Laboratory, Upton NY; United States of America.

[30]Departamento de Física, Universidad de Buenos Aires, Buenos Aires; Argentina.

[31]California State University, CA; United States of America.

[32]Cavendish Laboratory, University of Cambridge, Cambridge; United Kingdom.

[33] [(a)]Department of Physics, University of Cape Town, Cape Town;[(b)]iThemba Labs, Western Cape;[(c)]Department of Mechanical Engineering Science, University of Johannesburg, Johannesburg;[(d)]University of South Africa, Department of Physics, Pretoria;[(e)]School of Physics, University of the Witwatersrand, Johannesburg; South Africa.

[34]Department of Physics, Carleton University, Ottawa ON; Canada.

[35] [(a)]Faculté des Sciences Ain Chock, Réseau Universitaire de Physique des Hautes Energies - Université Hassan II, Casablanca;[(b)]Faculté des Sciences, Université Ibn-Tofail, Kénitra;[(c)]Faculté des Sciences Semlalia, Université Cadi Ayyad, LPHEA-Marrakech;[(d)]Moroccan Foundation for Advanced Science Innovation and Research (MAScIR), Rabat;[(e)]LPMR, Faculté des Sciences, Université Mohamed Premier, Oujda;[(f)]Faculté des sciences, Université Mohammed V, Rabat; Morocco.

[36]CERN, Geneva; Switzerland.

[37]Enrico Fermi Institute, University of Chicago, Chicago IL; United States of America.

[38]LPC, Université Clermont Auvergne, CNRS/IN2P3, Clermont-Ferrand; France.

[39]Nevis Laboratory, Columbia University, Irvington NY; United States of America.

[40]Niels Bohr Institute, University of Copenhagen, Copenhagen; Denmark.

[41] [(a)]Dipartimento di Fisica, Università della Calabria, Rende;[(b)]INFN Gruppo Collegato di Cosenza, Laboratori Nazionali di Frascati; Italy.

[42]Physics Department, Southern Methodist University, Dallas TX; United States of America.

[43]Physics Department, University of Texas at Dallas, Richardson TX; United States of America.

[44]National Centre for Scientific Research "Demokritos", Agia Paraskevi; Greece.

[45] [(a)]Department of Physics, Stockholm University;[(b)]Oskar Klein Centre, Stockholm; Sweden.

[46]Deutsches Elektronen-Synchrotron DESY, Hamburg and Zeuthen; Germany.

[47]Lehrstuhl für Experimentelle Physik IV, Technische Universität Dortmund, Dortmund; Germany.

[48]Institut für Kern- und Teilchenphysik, Technische Universität Dresden, Dresden; Germany.

[49]Department of Physics, Duke University, Durham NC; United States of America.

[50]SUPA - School of Physics and Astronomy, University of Edinburgh, Edinburgh; United Kingdom.

[51]INFN e Laboratori Nazionali di Frascati, Frascati; Italy.

[52]Physikalisches Institut, Albert-Ludwigs-Universität Freiburg, Freiburg; Germany.

[53]II. Physikalisches Institut, Georg-August-Universität Göttingen, Göttingen; Germany.

[54]Département de Physique Nucléaire et Corpusculaire, Université de Genève, Genève; Switzerland.

[55] [(a)]Dipartimento di Fisica, Università di Genova, Genova;[(b)]INFN Sezione di Genova; Italy.

[56]II. Physikalisches Institut, Justus-Liebig-Universität Giessen, Giessen; Germany.

[57]SUPA - School of Physics and Astronomy, University of Glasgow, Glasgow; United Kingdom.

[58]LPSC, Université Grenoble Alpes, CNRS/IN2P3, Grenoble INP, Grenoble; France.

[59]Laboratory for Particle Physics and Cosmology, Harvard University, Cambridge MA; United States of America.

[60] [(a)]Department of Modern Physics and State Key Laboratory of Particle Detection and Electronics, University of Science and Technology of China, Hefei;[(b)]Institute of Frontier and Interdisciplinary Science and Key Laboratory of Particle Physics and Particle Irradiation (MOE), Shandong University, Qingdao;[(c)]School of Physics and Astronomy, Shanghai Jiao Tong University, Key Laboratory for Particle Astrophysics and Cosmology (MOE), SKLPPC, Shanghai;[(d)]Tsung-Dao Lee Institute, Shanghai; China.

[61] [(a)]Kirchhoff-Institut für Physik, Ruprecht-Karls-Universität Heidelberg, Heidelberg;[(b)]Physikalisches Institut, Ruprecht-Karls-Universität Heidelberg, Heidelberg; Germany.

[62]Faculty of Applied Information Science, Hiroshima Institute of Technology, Hiroshima; Japan.

[63] [(a)]Department of Physics, Chinese University of Hong Kong, Shatin, N.T., Hong Kong;[(b)]Department of Physics, University of Hong Kong, Hong Kong;[(c)]Department of Physics and Institute for Advanced Study, Hong Kong University of Science and Technology, Clear Water Bay, Kowloon, Hong Kong; China.

[64]Department of Physics, National Tsing Hua University, Hsinchu; Taiwan.

[65]IJCLab, Université Paris-Saclay, CNRS/IN2P3, 91405, Orsay; France.

[66]Department of Physics, Indiana University, Bloomington IN; United States of America.

[67][a]INFN Gruppo Collegato di Udine, Sezione di Trieste, Udine;[b]ICTP, Trieste;[c]Dipartimento Politecnico di Ingegneria e Architettura, Università di Udine, Udine; Italy.

[68][a]INFN Sezione di Lecce;[b]Dipartimento di Matematica e Fisica, Università del Salento, Lecce; Italy.

[69][a]INFN Sezione di Milano;[b]Dipartimento di Fisica, Università di Milano, Milano; Italy.

[70][a]INFN Sezione di Napoli;[b]Dipartimento di Fisica, Università di Napoli, Napoli; Italy.

[71][a]INFN Sezione di Pavia;[b]Dipartimento di Fisica, Università di Pavia, Pavia; Italy.

[72][a]INFN Sezione di Pisa;[b]Dipartimento di Fisica E. Fermi, Università di Pisa, Pisa; Italy.

[73][a]INFN Sezione di Roma;[b]Dipartimento di Fisica, Sapienza Università di Roma, Roma; Italy.

[74][a]INFN Sezione di Roma Tor Vergata;[b]Dipartimento di Fisica, Università di Roma Tor Vergata, Roma; Italy.

[75][a]INFN Sezione di Roma Tre;[b]Dipartimento di Matematica e Fisica, Università Roma Tre, Roma; Italy.

[76][a]INFN-TIFPA;[b]Università degli Studi di Trento, Trento; Italy.

[77]Institut für Astro- und Teilchenphysik, Leopold-Franzens-Universität, Innsbruck; Austria.

[78]University of Iowa, Iowa City IA; United States of America.

[79]Department of Physics and Astronomy, Iowa State University, Ames IA; United States of America.

[80]Joint Institute for Nuclear Research, Dubna; Russia.

[81][a]Departamento de Engenharia Elétrica, Universidade Federal de Juiz de Fora (UFJF), Juiz de Fora;[b]Universidade Federal do Rio De Janeiro COPPE/EE/IF, Rio de Janeiro;[c]Instituto de Física, Universidade de São Paulo, São Paulo; Brazil.

[82]KEK, High Energy Accelerator Research Organization, Tsukuba; Japan.

[83]Graduate School of Science, Kobe University, Kobe; Japan.

[84][a]AGH University of Science and Technology, Faculty of Physics and Applied Computer Science, Krakow;[b]Marian Smoluchowski Institute of Physics, Jagiellonian University, Krakow; Poland.

[85]Institute of Nuclear Physics Polish Academy of Sciences, Krakow; Poland.

[86]Faculty of Science, Kyoto University, Kyoto; Japan.

[87]Kyoto University of Education, Kyoto; Japan.

[88]Research Center for Advanced Particle Physics and Department of Physics, Kyushu University, Fukuoka ; Japan.

[89]Instituto de Física La Plata, Universidad Nacional de La Plata and CONICET, La Plata; Argentina.

[90]Physics Department, Lancaster University, Lancaster; United Kingdom.

[91]Oliver Lodge Laboratory, University of Liverpool, Liverpool; United Kingdom.

[92]Department of Experimental Particle Physics, Jožef Stefan Institute and Department of Physics, University of Ljubljana, Ljubljana; Slovenia.

[93]School of Physics and Astronomy, Queen Mary University of London, London; United Kingdom.

[94]Department of Physics, Royal Holloway University of London, Egham; United Kingdom.

[95]Department of Physics and Astronomy, University College London, London; United Kingdom.

[96]Louisiana Tech University, Ruston LA; United States of America.

[97]Fysiska institutionen, Lunds universitet, Lund; Sweden.

[98]Centre de Calcul de l'Institut National de Physique Nucléaire et de Physique des Particules (IN2P3), Villeurbanne; France.

[99]Departamento de Física Teorica C-15 and CIAFF, Universidad Autónoma de Madrid, Madrid; Spain.

[100]Institut für Physik, Universität Mainz, Mainz; Germany.

[101]School of Physics and Astronomy, University of Manchester, Manchester; United Kingdom.

[102]CPPM, Aix-Marseille Université, CNRS/IN2P3, Marseille; France.

[103]Department of Physics, University of Massachusetts, Amherst MA; United States of America.

[104]Department of Physics, McGill University, Montreal QC; Canada.

[105]School of Physics, University of Melbourne, Victoria; Australia.

[106]Department of Physics, University of Michigan, Ann Arbor MI; United States of America.

[107]Department of Physics and Astronomy, Michigan State University, East Lansing MI; United States of America.

[108]B.I. Stepanov Institute of Physics, National Academy of Sciences of Belarus, Minsk; Belarus.

[109]Research Institute for Nuclear Problems of Byelorussian State University, Minsk; Belarus.

[110]Group of Particle Physics, University of Montreal, Montreal QC; Canada.

[111]P.N. Lebedev Physical Institute of the Russian Academy of Sciences, Moscow; Russia.

[112]National Research Nuclear University MEPhI, Moscow; Russia.

[113]D.V. Skobeltsyn Institute of Nuclear Physics, M.V. Lomonosov Moscow State University, Moscow; Russia.

[114]Fakultät für Physik, Ludwig-Maximilians-Universität München, München; Germany.

[115]Max-Planck-Institut für Physik (Werner-Heisenberg-Institut), München; Germany.

[116]Nagasaki Institute of Applied Science, Nagasaki; Japan.

[117]Graduate School of Science and Kobayashi-Maskawa Institute, Nagoya University, Nagoya; Japan.

[118]Department of Physics and Astronomy, University of New Mexico, Albuquerque NM; United States of America.

[119]Institute for Mathematics, Astrophysics and Particle Physics, Radboud University/Nikhef, Nijmegen; Netherlands.

[120]Nikhef National Institute for Subatomic Physics and University of Amsterdam, Amsterdam; Netherlands.

[121]Department of Physics, Northern Illinois University, DeKalb IL; United States of America.

[122][(a)]Budker Institute of Nuclear Physics and NSU, SB RAS, Novosibirsk;[(b)]Novosibirsk State University Novosibirsk; Russia.

[123]Institute for High Energy Physics of the National Research Centre Kurchatov Institute, Protvino; Russia.

[124]Institute for Theoretical and Experimental Physics named by A.I. Alikhanov of National Research Centre "Kurchatov Institute", Moscow; Russia.

[125]Department of Physics, New York University, New York NY; United States of America.

[126]Ochanomizu University, Otsuka, Bunkyo-ku, Tokyo; Japan.

[127]Ohio State University, Columbus OH; United States of America.

[128]Faculty of Science, Okayama University, Okayama; Japan.

[129]Homer L. Dodge Department of Physics and Astronomy, University of Oklahoma, Norman OK; United States of America.

[130]Department of Physics, Oklahoma State University, Stillwater OK; United States of America.

[131]Palacký University, RCPTM, Joint Laboratory of Optics, Olomouc; Czech Republic.

[132]Institute for Fundamental Science, University of Oregon, Eugene, OR; United States of America.

[133]Graduate School of Science, Osaka University, Osaka; Japan.

[134]Department of Physics, University of Oslo, Oslo; Norway.

[135]Department of Physics, Oxford University, Oxford; United Kingdom.

[136]LPNHE, Sorbonne Université, Université de Paris, CNRS/IN2P3, Paris; France.

[137]Department of Physics, University of Pennsylvania, Philadelphia PA; United States of America.

[138]Konstantinov Nuclear Physics Institute of National Research Centre "Kurchatov Institute", PNPI, St. Petersburg; Russia.

[139]Department of Physics and Astronomy, University of Pittsburgh, Pittsburgh PA; United States of

America.

[140] [a]Laboratório de Instrumentação e Física Experimental de Partículas - LIP, Lisboa; [b]Departamento de Física, Faculdade de Ciências, Universidade de Lisboa, Lisboa; [c]Departamento de Física, Universidade de Coimbra, Coimbra; [d]Centro de Física Nuclear da Universidade de Lisboa, Lisboa; [e]Departamento de Física, Universidade do Minho, Braga; [f]Departamento de Física Teórica y del Cosmos, Universidad de Granada, Granada (Spain); [g]Dep Física and CEFITEC of Faculdade de Ciências e Tecnologia, Universidade Nova de Lisboa, Caparica; [h]Instituto Superior Técnico, Universidade de Lisboa, Lisboa; Portugal.

[141] Institute of Physics of the Czech Academy of Sciences, Prague; Czech Republic.

[142] Czech Technical University in Prague, Prague; Czech Republic.

[143] Charles University, Faculty of Mathematics and Physics, Prague; Czech Republic.

[144] Particle Physics Department, Rutherford Appleton Laboratory, Didcot; United Kingdom.

[145] IRFU, CEA, Université Paris-Saclay, Gif-sur-Yvette; France.

[146] Santa Cruz Institute for Particle Physics, University of California Santa Cruz, Santa Cruz CA; United States of America.

[147] [a]Departamento de Física, Pontificia Universidad Católica de Chile, Santiago; [b]Universidad Andres Bello, Department of Physics, Santiago; [c]Instituto de Alta Investigación, Universidad de Tarapacá; [d]Departamento de Física, Universidad Técnica Federico Santa María, Valparaíso; Chile.

[148] Universidade Federal de São João del Rei (UFSJ), São João del Rei; Brazil.

[149] Department of Physics, University of Washington, Seattle WA; United States of America.

[150] Department of Physics and Astronomy, University of Sheffield, Sheffield; United Kingdom.

[151] Department of Physics, Shinshu University, Nagano; Japan.

[152] Department Physik, Universität Siegen, Siegen; Germany.

[153] Department of Physics, Simon Fraser University, Burnaby BC; Canada.

[154] SLAC National Accelerator Laboratory, Stanford CA; United States of America.

[155] Physics Department, Royal Institute of Technology, Stockholm; Sweden.

[156] Departments of Physics and Astronomy, Stony Brook University, Stony Brook NY; United States of America.

[157] Department of Physics and Astronomy, University of Sussex, Brighton; United Kingdom.

[158] School of Physics, University of Sydney, Sydney; Australia.

[159] Institute of Physics, Academia Sinica, Taipei; Taiwan.

[160] [a]E. Andronikashvili Institute of Physics, Iv. Javakhishvili Tbilisi State University, Tbilisi; [b]High Energy Physics Institute, Tbilisi State University, Tbilisi; Georgia.

[161] Department of Physics, Technion, Israel Institute of Technology, Haifa; Israel.

[162] Raymond and Beverly Sackler School of Physics and Astronomy, Tel Aviv University, Tel Aviv; Israel.

[163] Department of Physics, Aristotle University of Thessaloniki, Thessaloniki; Greece.

[164] International Center for Elementary Particle Physics and Department of Physics, University of Tokyo, Tokyo; Japan.

[165] Graduate School of Science and Technology, Tokyo Metropolitan University, Tokyo; Japan.

[166] Department of Physics, Tokyo Institute of Technology, Tokyo; Japan.

[167] Tomsk State University, Tomsk; Russia.

[168] Department of Physics, University of Toronto, Toronto ON; Canada.

[169] [a]TRIUMF, Vancouver BC; [b]Department of Physics and Astronomy, York University, Toronto ON; Canada.

[170] Division of Physics and Tomonaga Center for the History of the Universe, Faculty of Pure and Applied Sciences, University of Tsukuba, Tsukuba; Japan.

[171] Department of Physics and Astronomy, Tufts University, Medford MA; United States of America.

[172]Department of Physics and Astronomy, University of California Irvine, Irvine CA; United States of America.

[173]Department of Physics and Astronomy, University of Uppsala, Uppsala; Sweden.

[174]Department of Physics, University of Illinois, Urbana IL; United States of America.

[175]Instituto de Física Corpuscular (IFIC), Centro Mixto Universidad de Valencia - CSIC, Valencia; Spain.

[176]Department of Physics, University of British Columbia, Vancouver BC; Canada.

[177]Department of Physics and Astronomy, University of Victoria, Victoria BC; Canada.

[178]Fakultät für Physik und Astronomie, Julius-Maximilians-Universität Würzburg, Würzburg; Germany.

[179]Department of Physics, University of Warwick, Coventry; United Kingdom.

[180]Waseda University, Tokyo; Japan.

[181]Department of Particle Physics and Astrophysics, Weizmann Institute of Science, Rehovot; Israel.

[182]Department of Physics, University of Wisconsin, Madison WI; United States of America.

[183]Fakultät für Mathematik und Naturwissenschaften, Fachgruppe Physik, Bergische Universität Wuppertal, Wuppertal; Germany.

[184]Department of Physics, Yale University, New Haven CT; United States of America.

[185]Yerevan Physics Institute, Yerevan; Armenia.

[a] Also at Borough of Manhattan Community College, City University of New York, New York NY; United States of America.

[b] Also at Centre for High Performance Computing, CSIR Campus, Rosebank, Cape Town; South Africa.

[c] Also at CERN, Geneva; Switzerland.

[d] Also at CPPM, Aix-Marseille Université, CNRS/IN2P3, Marseille; France.

[e] Also at Département de Physique Nucléaire et Corpusculaire, Université de Genève, Genève; Switzerland.

[f] Also at Departament de Fisica de la Universitat Autonoma de Barcelona, Barcelona; Spain.

[g] Also at Departamento de Física, Instituto Superior Técnico, Universidade de Lisboa, Lisboa; Portugal.

[h] Also at Department of Applied Physics and Astronomy, University of Sharjah, Sharjah; United Arab Emirates.

[i] Also at Department of Financial and Management Engineering, University of the Aegean, Chios; Greece.

[j] Also at Department of Physics and Astronomy, Michigan State University, East Lansing MI; United States of America.

[k] Also at Department of Physics and Astronomy, University of Louisville, Louisville, KY; United States of America.

[l] Also at Department of Physics and Astronomy, University of Sheffield, Sheffield; United Kingdom.

[m] Also at Department of Physics, Ben Gurion University of the Negev, Beer Sheva; Israel.

[n] Also at Department of Physics, California State University, East Bay; United States of America.

[o] Also at Department of Physics, California State University, Fresno; United States of America.

[p] Also at Department of Physics, California State University, Sacramento; United States of America.

[q] Also at Department of Physics, King's College London, London; United Kingdom.

[r] Also at Department of Physics, St. Petersburg State Polytechnical University, St. Petersburg; Russia.

[s] Also at Department of Physics, Stanford University, Stanford CA; United States of America.

[t] Also at Department of Physics, University of Adelaide, Adelaide; Australia.

[u] Also at Department of Physics, University of Fribourg, Fribourg; Switzerland.

[v] Also at Department of Physics, University of Michigan, Ann Arbor MI; United States of America.

[w] Also at Dipartimento di Matematica, Informatica e Fisica, Università di Udine, Udine; Italy.

[x] Also at Faculty of Physics, M.V. Lomonosov Moscow State University, Moscow; Russia.

[y] Also at Giresun University, Faculty of Engineering, Giresun; Turkey.

[z] Also at Graduate School of Science, Osaka University, Osaka; Japan.

[aa] Also at Hellenic Open University, Patras; Greece.

[ab] Also at IJCLab, Université Paris-Saclay, CNRS/IN2P3, 91405, Orsay; France.

[ac] Also at Institucio Catalana de Recerca i Estudis Avancats, ICREA, Barcelona; Spain.

[ad] Also at Institut für Experimentalphysik, Universität Hamburg, Hamburg; Germany.

[ae] Also at Institute for Mathematics, Astrophysics and Particle Physics, Radboud University/Nikhef, Nijmegen; Netherlands.

[af] Also at Institute for Nuclear Research and Nuclear Energy (INRNE) of the Bulgarian Academy of Sciences, Sofia; Bulgaria.

[ag] Also at Institute for Particle and Nuclear Physics, Wigner Research Centre for Physics, Budapest; Hungary.

[ah] Also at Institute of High Energy Physics, Chinese Academy of Sciences, Beijing; China.

[ai] Also at Institute of Particle Physics (IPP); Canada.

[aj] Also at Institute of Physics, Academia Sinica, Taipei; Taiwan.

[ak] Also at Institute of Physics, Azerbaijan Academy of Sciences, Baku; Azerbaijan.

[al] Also at Institute of Theoretical Physics, Ilia State University, Tbilisi; Georgia.

[am] Also at Instituto de Fisica Teorica, IFT-UAM/CSIC, Madrid; Spain.

[an] Also at Istanbul University, Dept. of Physics, Istanbul; Turkey.

[ao] Also at Joint Institute for Nuclear Research, Dubna; Russia.

[ap] Also at Louisiana Tech University, Ruston LA; United States of America.

[aq] Also at LPNHE, Sorbonne Université, Université de Paris, CNRS/IN2P3, Paris; France.

[ar] Also at Manhattan College, New York NY; United States of America.

[as] Also at Moscow Institute of Physics and Technology State University, Dolgoprudny; Russia.

[at] Also at National Research Nuclear University MEPhI, Moscow; Russia.

[au] Also at Physics Department, An-Najah National University, Nablus; Palestine.

[av] Also at Physics Dept, University of South Africa, Pretoria; South Africa.

[aw] Also at Physikalisches Institut, Albert-Ludwigs-Universität Freiburg, Freiburg; Germany.

[ax] Also at School of Physics, Sun Yat-sen University, Guangzhou; China.

[ay] Also at The City College of New York, New York NY; United States of America.

[az] Also at The Collaborative Innovation Center of Quantum Matter (CICQM), Beijing; China.

[ba] Also at TRIUMF, Vancouver BC; Canada.

[bb] Also at Universita di Napoli Parthenope, Napoli; Italy.

* Deceased